ABSTRACT

Title of Thesis: IDENTIFYING SMOKE DETECTION BIASES WITHIN DIFFERING ROOM CONFIGURATIONS FOR ZONE AND COMPUTATIONAL FLUID DYNAMIC MODELS

Adam D. Lee

Master of Science, 2022

Thesis Directed By: Professor and Chair, Dr. James Milke
Department of Fire Protection Engineering

This research project aims to identify room configuration conditions in which FDS, a CFD model, and CFAST, a zone model, may differ in detector activation time. A total of four configurations, with varying aspect ratios, were explored. Additionally, a range of four ceiling heights were also modeled. Furthermore, a total of three statistically significant models were developed to relate the differences between detection times within CFAST and FDS. It was found that FDS and CFAST discrepancies were a result of the compartment volume to doorway area ratios. Larger volumes compared to the doorway area resulted in better agreement between FDS and CFAST. Additionally, for larger ceilings in FDS, larger variability in activation times were present. Furthermore, for higher ceilings, FDSs' ability to account for thermal buoyancy within the smoke plume resulted in quicker activation within FDS.

IDENTIFYING SMOKE DETECTION BIASES WITHIN DIFFERING ROOM
CONFIGURATIONS FOR ZONE AND COMPUTATIONAL FLUID DYNAMIC
MODELS

by

Adam Doon-Aut Lee

Thesis submitted to the Faculty of the Graduate School of the
University of Maryland, College Park, in partial fulfillment
of the requirements for the degree of
Master of Science
2022

Advisory Committee:
 James A. Milke, Professor, Chair
 Arnaud Trouvé, Professor
 Fernando Raffan Montoya, Professor

Acknowledgements

I would like to initially thank the faculty and graduate students at the University of Maryland, Department of Fire Protection Engineering for providing overall support and community that helped me persevere through this project. I would like to personally acknowledge and thank my advisor, Dr. Milke, for taking me on as an advisee as well as supporting this project. His continued encouragement and belief in me, despite having my own doubts about the project, gave me confidence to see this project through the end. Additionally, I would like to thank Dr. Trouve for setting time aside for any last minute questions I may have had.

I would also like to thank my co-workers at NRC for their continued support in me throughout my entire undergraduate senior and graduate year. I would like to specifically thank MarkHenry Salley, Kenneth A. Hamburger, David Stroup, and Gabe Taylor for making themselves available and being there for me when I had questions or needed guidance. Additionally, I would like to thank the folks at NIST for their help in steering me in the right direction and explaining any questions I had. Specifically, I would like to thank Tom Cleary and Kevin McGratten for their help in initially identifying research projects that could be applicable and contribute to the fire community.

Lastly, I would like to give a huge thanks to my friends and family that have supported and believed in me throughout the entire research process. Personally, I would like to thank my friends Jesse Hearn, Shuvam Roy, Matthew Perez, Anu P., Candice Lee, and Sara Pohland for supporting me throughout my entire graduate career, editing my work, and consistently assuring me that I would not fail.

Table of Contents

List of Figures

List of Tables

Chapter 1: Introduction

Performance-based design is becoming an increasingly popular practice within the fire protection community [1]. In 2001, the National American Fire Protection Association (NFPA) introduced NFPA 805, the *Performance-Based Standard for Fire Protection for Light Water Reactor Electric Generating Plants* [2]. In July of 2004, the United States Nuclear Regulatory Commission (NRC) adopted NFPA 805 into the fire protection requirements of Title 10, Section 50.48, of the *Code of Federal Regulations* (10 CFR 50.48) [3]. This revision allows reactor licensees to voluntarily adopt fire protection requirements contained within NFPA 805, and can be used as an alternative to the existing deterministic fire protection requirements [4].

In the context of fire scenarios in nuclear power plants (NPPs), a spot-type smoke detector activation can be used to initiate fire mitigation activities. These could be suppression activities, such as sprinkler system activation or a fire brigade [5]. In applications where estimating the detector activation time is critical, reliable prediction times must be accurately reflective of the intended fire scenario.

However, predicting spot-type smoke detector activation times is not straightforward. There are a variety of factors that can determine when and if a smoke detector will activate, one of which is transport lag [6]. The transport lag time can be defined as the time it takes for the smoke plume to reach the ceiling (plume transport lag) and reach the bounding enclosure (ceiling jet transport lag) [6]. Transport considerations include the time and distance it takes for the aerosol particles to reach the detector from the source. The path from the source to the detector also influences the transport lag time.

Characteristics of the room, such as ceiling height, configuration, and intervening barriers (beams) can all influence the transport lag time [6].

Once smoke reaches the detector, there are other factors that influence the detector activation time. Smoke must first pass through the detector's exterior housing, through a series of baffles, and into the sensing chamber of the detector [7]. Therefore, there is a lag time associated with the smoke moving through detector housing and the entry of smoke into the sensing chamber. In addition, entry resistance of the housing can vary due to different velocity profiles relative to the entry point of the chamber and the orientation of the detector itself [6]. Combined with variable fire scenarios that include different fuel mixtures and fire growth rates, a general model for predicting activation times becomes complex.

Chapter 2: Literature Review

NFPA 72, the *National Fire Alarm and Signaling Code*, prescribes spacing for spot-type smoke detectors [8]. In the absence of performance-based design criteria, the current code requires that the maximum spacing for smoke detectors is a nominal 30 ft and the distance from the detector to the wall cannot exceed half of that nominal distance. Additionally, the code requires that every point on the ceiling must be within 0.7 times the nominal spacing [8]. Furthermore, NFPA 72 mentions that the ceiling height and ceiling size are contributing factors to the response of smoke detectors, but no mention of spacing adjustments are included for these factors. Only sloped, beamed, peaked, shed, and/or a combination are accounted in spacing adjustments for smoke detectors [8].

From a design standpoint, smoke detector activation times are difficult to predict due to a wide variety of variables. Supported by the Fire Protection Research Foundation (FPRF), an in-depth literature review was compiled to evaluate the effects of smoke detector activation caused by several independent room characteristics. The report, *Smoke Detector Spacing for High Ceiling Spaces*, provides an extensive literature review of relevant fire test research pertaining to room characteristics [9]. The key environmental variables identified in the report were temperature, air velocity, ceiling height, room shape, and ceiling obstructions. A total of 17 reports, pertaining to the modeling of smoke detectors in various room geometries were summarized and outlined in the literature review. Of those 17 reports, common conclusions stated were that smoke detector sensitivities were critical for small fires in high ceiling rooms [10], [11]; variations in experimental results for the same fire test, which cannot be accounted for in models [12], [13]; uncertainties within the computational fluid dynamics (CFD) model, Fire Dynamics

Simulator (FDS) [14]; and poor detection accuracy for prediction models [15]. As demonstrated by the various research studies outlined in the literature review, all of which had different experimental conditions, predicting and modeling smoke detector activation heavily relies on a large number of variables. As a result, a single general model may not be able to fully capture the physical phenomenon of interest.

2.1: NUREG 1824 and 1825S

In a separate effort to explore the validation of smoke detector activation models, NRC compiled NUREG 1824 and NUREG 1824s, a report verifying and validating selected fire models within NPPs [4], [5]. Validation is a process that determines how well the model represents the phenomenon of interest. Validation tests for various smoke detector activation models were performed in NUREG 1824s. The experimental data from the Home Smoke Alarm test, performed by the National Institute of Science and Technology (NIST), was used to evaluate smoke detector activation model predictions [16]. The models evaluated in NUREG 1824s were modeled using first-order equations, a zone model, and a CFD model [5]. The experimental compartments consisted of two structures: a one-story and a two-story house. The generic one-story structure was designed to represent an apartment, condominium, ranch home, or a manufactured home. In addition, the two-story house represents a generic two-story single-family house.

The experiments involved a total of seven different detector types that include variations of photoelectric, ionization, carbon monoxide, and aspirated detectors, but the lag time parameters and alarm thresholds were not provided. Therefore, from a modeling standpoint, it is impossible to accurately characterize the entry resistance and lag time of the detector. However, a common method used to represent smoke detectors is to

characterize them as heat detectors or sprinklers, with a low activation temperature of 10 °C above ambient and a response time index (RTI) of 5 $(m \cdot s)^{1/2}$ [5]. By using fixed values of RTI and temperature, this approach defines the activation threshold of all seven detector types to be the same.

The temperature and velocity were predicted using the Alpert jet correlation, explained in section 4.1: Empirical Correlations, and shown in Figure 2-1. Only the smoke detectors located in the fire room were considered since the Alpert jet correlations do not account for multi-compartment structures. The Consolidated Fire And Smoke Transport (CFAST) was used as one of the two selected zone models for comparison to the experimental, as shown in Figure 2-1. Additionally, FDS was used as the selected CFD model, as shown in Figure 2-2. Note that all models applied the same temperature rise method, with a low activation temperature of 10 °C above ambient and a response time index (RTI) of 5 $(m \cdot s)^{1/2}$ [5]. The smoke detector activation time and temperature rise correlation indicate a weak relationship due to the large scattering of data points represented in all three models. The dashed red lines represent the 95% confidence bounds of the model. The solid red line represents the average model bias factor, which characterizes how far the model underpredicts or overpredicts the experimental quantity. Large sparsity between the 95% confidence interval bounds and the model bias factor indicate poor predictions of the activation time. Since the 95% confidence interval bounds falls under such a large range, the variability within the data cannot be attributed to a correlation between temperature rise and smoke detector activation times [5].

5
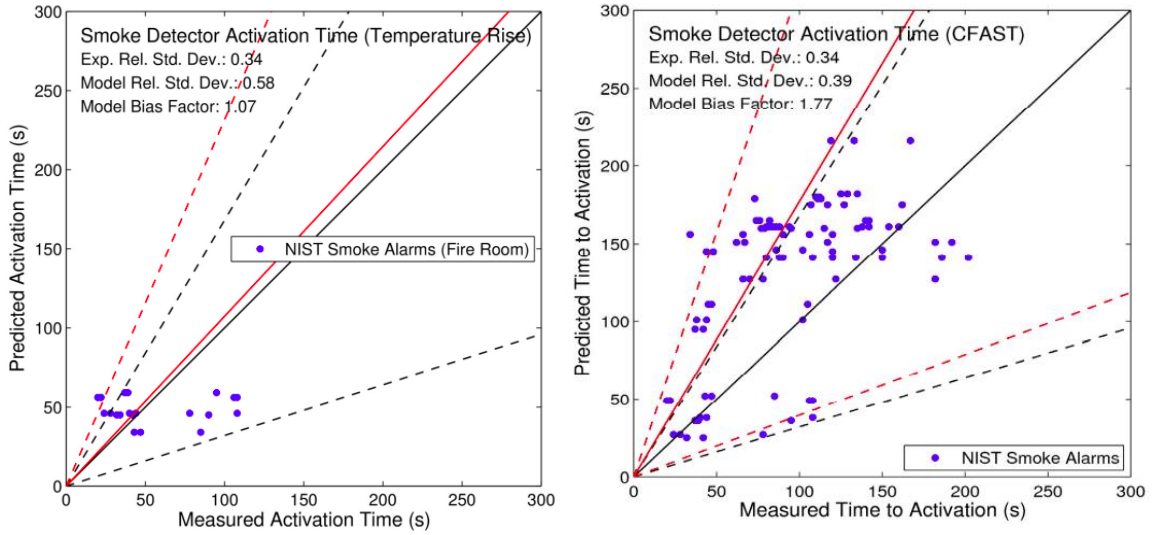
Figure 2-1: Predicted smoke detector activation time using the Alpert jet correlations (left) and CFAST (right) [5].
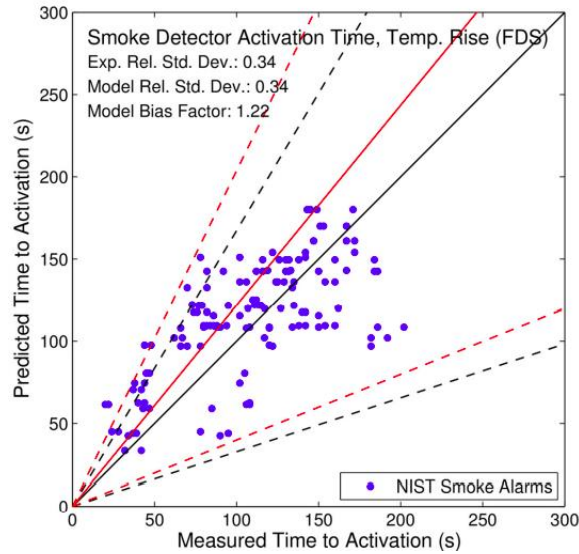
Figure 2-2: Predicted smoke detector activation time using FDS [5].

2.2: CFAST Validation Study

Since NUREG 1824, newer validation experiments have been explored. In 2020, NIST and NRC compared the activation time of detectors from experimental fire tests to

the predicted activation time of detectors using a zone model [17]. The zone model that was used in the validation study CFAST [18]. The experimental room dimensions were 11 m by 7.3 m with 3.7 m high ceilings. Natural ventilation was provided by a single opening 2.44 m high by 1.83 m wide centered along the short wall. A variation of this compartment included two 0.3 m wide and 0.3 m deep ceiling beams [17]. A total of six different fire scenarios were tested. These six scenarios ranged from different fuel mixture ratios of propane and propene; different ramp times to the peak heat release rate (HRR); varying initial HRR values at ignition; and several hold times of the HRR at steady state [17].

Detector	Sensitivity setting	ANSI/UL 268 sensitivity %/m (%/ft) obscuration	Flaming sensitivity %/m Obscuration
Photo 1	SP1, Pre-alarm	3.21 (0.99)	10.9
Photo 1	SP2, Alarm	5.34 (1.66)	17.8
Photo 2	SP3, Pre-alarm	4.84 (1.50)	16.2
Photo 2	SP4, Alarm	7.51 (2.35)	24.6
Laser 1	SP1, Pre-alarm	1.63 (0.50)	5.59
Laser 1	SP2, Alarm	3.24 (1.00)	10.9
Laser 2	SP3, Pre-Alarm	3.24 (1.00)	10.9
Laser 2	SP4, Alarm	6.41 (2.00)	20.7

Figure 2-3: Alarm and pre-alarm sensitivities [17].

Two types of activation models for smoke detectors were studied- a temperature rise activation method and a fixed smoke concentration method. For the temperature rise method, a single RTI of 5 $(m \cdot s)^{1/2}$ was given and three temperature rises of 5 °C, 10 °C, and 15 °C above ambient was proposed to cover a range of detector sensitives [17]. For a fixed smoke concentration method, two forward light scattering photoelectric-type detectors were used, one with an infrared light emitting diode (photoelectric) and the other with a laser light emitting diode (laser). At each location, a set of four photoelectric and four lasers were placed on a 0.3 m wide by 0.91 m long by 6 mm thick mounting boards. On each board, one of the photoelectric and laser detectors were set to a lower pre-alarm

setting and one of the photoelectric and laser detectors were set to a higher pre-alarm setting. Therefore, a total of four different set point (SP) values, were used for the activation obscuration of the detector, as shown in Figure 2-3 [17]. The flaming sensitivity was taken as an empirical 3.5 times the related ANSI/UL 268 smoke box smoldering cotton wick at alarm obscuration values [19], [17].

The smoke detector model activation time, in CFAST, versus the actual photoelectric detector activation times show good correlations, with the slopes of each SP being close to a value of 1, as shown in Figure 2-4 [17]. The same is true for the SP values of the laser detector, as shown in Figure 2-4 [17]. In this validation study, error bars represent ± one standard deviation of the repeated experimental results [17].
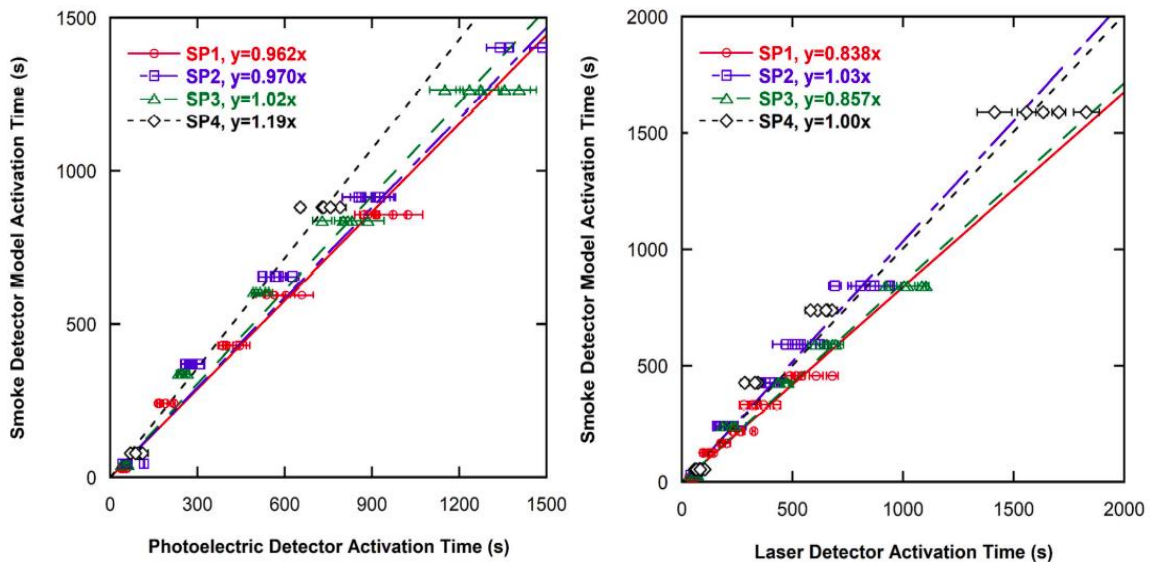
Figure 2-4: CFAST modeled versus experimental time, with photoelectric (left) and laser (right) detectors [17].

Similarly, as discussed in the NUREG 1824 and NUREG 1824s studies, using a temperature rise method showed that temperature rise is not a strong predictor of smoke

8

detector activation times [5]. In the CFAST validation study, temperature rise was shown to not be as well effective of a predictor as the smoke concentration method. An example of this is shown by the large disparity of slope values for a ΔT of 10 °C compared to the actual photoelectric detector activation times shown in Figure 2-5. Other activation temperature rise values were also compared with the actual photoelectric and laser detector activation times, in which none proved to be as accurate as the smoke concentration method. For CFAST to give good predictions, three requirements needed to be met: the soot yield was accurately defined; the activation obscuration was properly adjusted for flaming soot; and the specific extinction coefficient was accurately described.
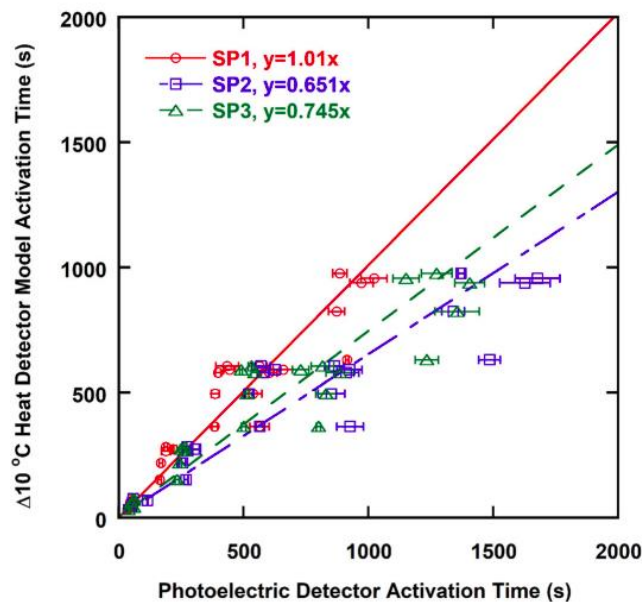
Figure 2-5: Temperature rise model versus photoelectric activation time for smooth ceilings [17].

2.3: FDS Validation Study

In 2021, NRC and NIST performed a validation study for the Fire Dynamics Simulator (FDS) model [20]. The same experimental fire scenarios, room configurations,

and detector configurations were used as those mentioned in section 2.2: CFAST Validation Study. However, in FDS, only a fixed threshold smoke concentration method was used to model photoelectric and laser detectors. Overall, the FDS model demonstrated accurate predictions of the detector activation times for both photoelectric and laser detectors, shown in Figure 2-6. The overall linear regression slopes, for both smooth and beamed ceilings fell between values of 0.88 to 1.13 [21].
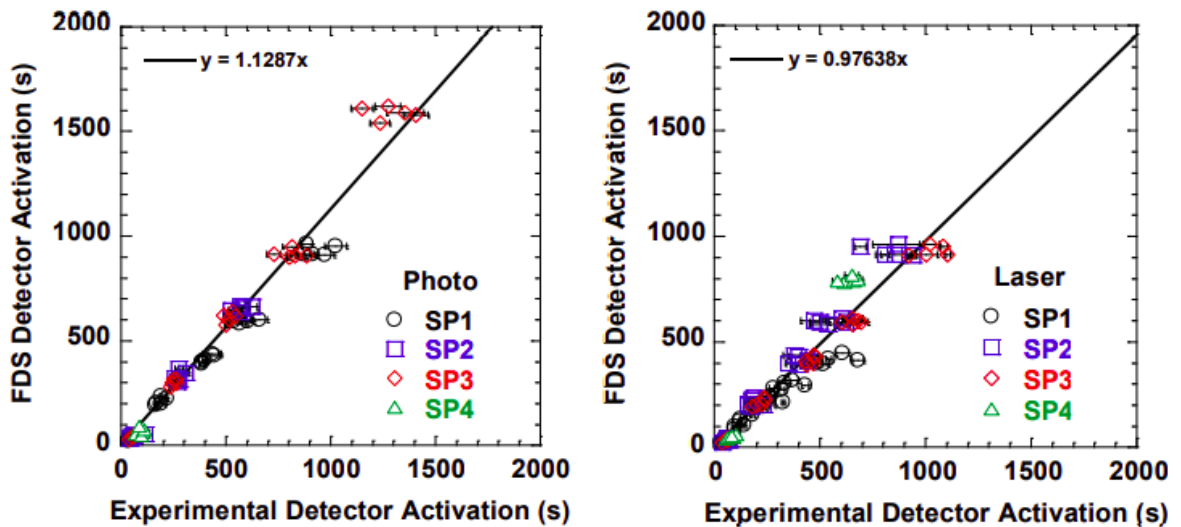
Figure 2-6: FDS modeled detection time versus experimental, with photoelectric (left) and laser (right) detectors [21].

2.4: Conclusion of Literature Review

In a letter to the editor, DiNenno and Beyler emphasize that the method of temperature rise method outlined in NFPA 92B "have significant uncertainties and potentially large errors associated with their development and use (in the context of non-idealized fire sources, normal ventilation, ambient conditions, etc.)" [22]. These uncertainties are later emphasized in NUREG 1824 and 1824s [4], [5]. In newer validation studies, CFAST and FDS have shown accurate predictions of detector times using a smoke

concentration method, where the concentration of the smoke at the layer or grid cell are compared to a set point of the detector [17], [21]. This method has been shown to produce accurate results when compared to the controlled experiments. These fire experiments were controlled using a known fuel, burner, and under well ventilated conditions. However, in order to produce accurate results, variables such as an accurate soot yield, fire HRR curve, and specific extinction coefficient must be known, and in many design cases these variables are assumed, thus introducing possible error into the results. Furthermore, the true mechanism of photoelectric detectors, a light scattering mechanism, has not been modeled, and thus these surrogate measures (temperature rise and smoke concentration) are used in lieu of the true actuation mechanism.

Chapter 3: Gaps in Literature and Motivation

The 2020 and 2021 validation studies for CFAST and FDS demonstrated accurate prediction times when compared to the experimental detection times [17], [21]. These experiments and model evaluations were performed under non-biased conditions, where the predicted activation times for FDS and CFAST were similar to each other. Therefore, under similar conditions, it can be deduced that both CFAST and FDS would have similar and accurate predictions. In biased conditions, the FDS and CFAST models would disagree due to either model not being able to fully capture the physical phenomena in the room. Given that CFAST is a zone model and FDS is a CFD model, it would be interesting to consider the assumptions of each model and how the prediction times would deviate from each other. The FPRF report suggests further research is needed to explore the effects of ceiling height and room size on smoke detector activation times [9]. Smooth and beamed ceilings were considered in the validation studies, but only one room size and room geometry was used [21]. Therefore, the effect of room size and geometry on the predicted activation times for both the zone and CFD model is still needed.

Furthermore, the goal and scope of this research project is to identify under what room conditions a zone model or CFD model may differ from each other in smoke detector response. Due to the high number of key variables that could influence the predicted activation times, the scope of this research is limited to the room configuration. Room configuration is defined here as the area of the room, width/length ratios, and ceiling height. Differences that occur in different configurations between a zone and CFD model are explored such that these biases can be taken account when modeling similar situations. The differences in predicted activation times between FDS and CFAST can be used to identify

biased room configurations that would require further investigation of the actual ongoing physical phenomenon.

Secondly, a correlative model that relates the CFAST and FDS detection times, based on input conditions, will also be determined. This is beneficial for two reasons. First, FDS simulations take longer than simulations in CFAST. In addition, there are an infinite number of combinations of room sizes, width/length ratios, and ceiling height. Therefore, an accurate statistical model that relates CFAST and FDS could be used to predict the actual FDS detector activation times. Coupled with the intent to explore the biases in room configuration between each model, understanding which configurations are biased towards either FDS/CFAST can be applied to determine when and how this statistical model is used. Determination of whether CFAST or FDS portray any of the actual physical phenomena of the fire scenario can only be done by comparing the two models to an experimental data set.

Chapter 4: Background

4.1: Empirical Correlations

Empirical correlations of predicted smoke detector activation times are found in chapter 11 (*Estimating Smoke Detector* Response) of NUREG 1805: the *Quantitative Fire Hazard Analysis Methods for the U.S. Nuclear Regulatory Commission Fire Protection Inspection Program* [23]. Additionally, NFPA 72 describes empirical correlations for fire design cases; in which the temperature of the detector is determined at some critical time rather than determining the time of detector activation. There are a variety of broad assumptions and limitations associated with the empirical correlations presented in NUREG 1805, including a steady state fire, no forced ventilation, non-obstructed overhead area above the fire, and detectors located at or near the ceiling of the compartment [23]. The simplicity provided by these assumptions and limitations allow these correlations to be streamlined into a Microsoft Excel spreadsheet, which can be found in the FDT^s library of NUREG 1805 [23].

4.1.1: NFPA 72 Temperature Rise Method

NFPA 72 describes a method for calculating the temperature of the detector based on a t^2 (time squared) fire [8]. The method is iterative in that the time for detection is inherently assumed based on the design fire scenario, the critical time of activation, and an assumed radial distance between the design fire and detector. If the temperature of the detector is greater than the assumed activation temperature of the detector, then a larger radial distance between the fire and the detector is assumed [8]. If the temperature of the detector is less

than the assumed activation temperature of the detector, then a smaller radial distance between the fire and the detector is assumed [8].

From those calculations, the problem is iteratively solved with varying radial distances until the temperature of the detector is equal to the activation temperature of the detector. Once the temperature of the detector matches to the prescribed activation temperature of the detector, the spacing of the detectors can be calculated. The equations are not shown here because they do not necessarily determine the activation time of the detector, which is the main purpose for these discussed methods. However, the equations can be found in Annex B of NFPA 72 and a worksheet can be used to aid in the calculation process [8].

4.1.2: NFPA 72 Mass Optical Density Method

The second method, described in Annex B of NFPA 72, for calculating the smoke detector response time is the optical density method [8]. This method assumes that the smoke in the room is well mixed, evenly distributed, confined to the room, can reach the ceiling, and can enter the detector [8]. After these assumptions are made, the model conservatively assumes that the smoke layer can be modeled as a cylinder having a depth similar to that of the ceiling jet and centered around the fire. A limitation of this method is that the selected smoke layer thickness heavily influences the results of this calculation [8]. Thus, the designer must take care in selecting the layer thickness assumed in the calculation. Furthermore, this method does not account for smoke entry delay and assumes uniform smoke concentration throughout the entire prescribed smoke layer volume [8]. The predicted detector activation time is shown as

$$t = \left(\frac{3D_A \, \pi r^2 \, h \, \Delta H_c}{\alpha D_m} \right)^{1/3} + t_e \qquad \text{[8] (4-1)}$$

where r (m) is the radial distance between the detector and the fire; α (kW m^{-2}) is the fire intensity coefficient; h (m) is the assumed layer thickness; D_m (m^2/g) is the mass optical density; and D_A (m^{-1}) is the optical density level at which the detector activates; and t_e is the time delay due to smoke entry. The time delay due to smoke entry must be selected by the designer since the method described above does not account for ceiling jet velocity or smoke detector design. Furthermore, certain properties of the fuel must be known, such as the mass optical density.

4.1.3: Method of Alpert

The first method described in NUREG 1805 is the correlation developed by Alpert [24]. A temperature rise method, in which smoke detectors are modeled as heat detectors, can be used in combination with the Alpert correlation to achieve predicted detector activation times [23]. A general smoke temperature rise between 5 °C and 10 °C is typically associated with smoke detector activation [25], [23]. For a temperature rise method, smoke detectors are typically regarded as low-response time index (RTI) devices, such as an RTI of 5 (m·s)$^{1/2}$ [23], [26]. The correlation, developed by Alpert and later presented by Budnick et al, for smoke temperature rise and predicted detector activation time is shown as

$$t_{activation} = \frac{RTI}{\sqrt{U_{jet}}} \ln \left(\frac{T_{jet} - T_a}{T_{jet} - T_{activation}} \right) \qquad \text{[24], [27] (4-2)}$$

where $t_{activation}$ (sec) is the detector activation time, T_a (°C) is the ambient temperature, $T_{activation}$ (°C) is the detector activation temperature, and RTI (m·sec)$^{1/2}$ is the response time index. The velocity, U_{jet} (m·s^{-1}), and temperature, T_{jet} (°C), of the ceiling jet depend

16

on three values: the radial distance, r (m), from the detector to the plume centerline, the difference in height, H (m), between the top of the fuel package and the ceiling, and the heat release rate of the fire, $\dot{Q}$ (kW). The ceiling jet correlation is given as

$$T_{jet} - T_a = \frac{16.9 \, \dot{Q}^{\frac{2}{3}}}{H^{\frac{5}{3}}} \; for \; \frac{r}{H} \leq 0.18 \qquad \text{[23], [27] (4-3)}$$

$$T_{jet} - T_a = \frac{5.38 \, \dot{Q}^{\frac{2}{3}}}{H} \; for \; \frac{r}{H} > 0.18 \qquad \text{[23], [27] (4-4)}$$

The velocity correlation is given as

$$U_{jet} = 0.96 \left(\frac{\dot{Q}}{H}\right)^{1/3} \; for \; \frac{r}{H} \leq 0.15 \qquad \text{[23], [27] (4-5)}$$

$$U_{jet} = \frac{0.195 \, \dot{Q}^{\frac{1}{3}} H^{\frac{1}{2}}}{r^{\frac{5}{6}}} for \; \frac{r}{H} > 0.15 \qquad \text{[23], [27] (4-6)}$$

4.1.4: Method of Mowrer

In 1990, Mowrer developed a method that describes the predicted smoke detector activation time based on the concepts of transport lag [28]. This method, as described in NUREG 1805, is labeled as the "Method of Mowrer" [23]. The activation time of the detector, $t_{activation}$ (sec), is modeled as the transport lag time of the plume, t_{plume} (sec), plus the transport lag time of the ceiling jet, t_{cj} (sec). The predicted activation time is shown as

$$t_{activation} = t_{plume} + t_{cj} \qquad \text{[23] (4-7)}$$

A significant limitation of this method is that the activation time of the detector is modeled as the transport lag and ceiling jet time. Therefore, the activation time is modeled as the

time it takes for a smoke particle to travel from the burner to the detector. This is not physically accurate for photoelectric detectors since they operate on a light scattering or light obscuration, which requires some amount of concentration of smoke to be present within the detector for activation to occur. The plume and ceiling jet lag times correlations were experimentally determined and are shown respectively as

$$t_{plume} = 0.67 \frac{H^{\frac{1}{3}}}{\dot{Q}^{\frac{1}{3}}}; \; t_{cj} = \frac{r^{\frac{1}{3}}}{1.2 \, \dot{Q}^{\frac{1}{3}} H^{\frac{1}{2}}} \qquad \text{[28], [23] (4-8)}$$

where H (m) is the height from the top of the fuel package to the ceiling, r (m) is the radial distance from the detector to the centerline of the plume, and $\dot{Q}$ (kW) is the heat release rate of the fire.

4.1.5: Method of Milke

Lastly, in 1990, Milke presented a correlation to describe the smoke temperature rise versus predicted detector activation time [29]. The "Method of Milke", as described in NUREG 1805, is presented in combination with the stratification calculations from annex H.2d of NFPA 92B [30]. In high ceilings, as the smoke ascends and entrains cool air, buoyancy effects are reduced over time. This results in the smoke failing to ascend to the height of the smoke detectors, since the upward movement of smoke is dependent on it being buoyant relative to the surrounding air. This effect is known as stratification [8]. The calculation for determining the max ceiling clearance that a plume can rise to, H_{max} (ft), is presented as [30]

$$H_{max} = \frac{74 \, \dot{Q}_c^{\frac{2}{5}}}{\Delta T_1} \qquad \text{[30] (4-9)}$$

where $\dot{Q}_c$ (Btu/sec) is the convective heat release rate portion of the fire and ΔT_1 (°F) is the difference in ambient gas temperature between the fuel location and the ceiling level. The convective portion of the heat release rate is estimated to be 70% of the heat release rate of the fire, $\dot{Q}$. Therefore, the convective portion is given as $\dot{Q}_c = 0.7 \, \dot{Q}$ [29], [23]. The difference in ambient gas temperature between the fuel location and the ceiling level is given as

$$\Delta T_1 = \frac{1300 \, \dot{Q}_c^{\frac{2}{3}}}{H^{\frac{5}{3}}} \qquad \text{[29] (4-10)}$$

where H (ft) is the height from the top of the fuel package to the ceiling. Stratification occurs if H_{max} is less than H. Logically, this indicates that the max height at which the plume travels is less than the overall ceiling height, resulting in the smoke not reaching the height at which the detectors are located [23].

If stratification does not occur, meaning that H_{max} is greater than H, then the following equations can be used to solve for the predicted activation time of the detector, shown below as

$$Y = \frac{\Delta T_c \, H^{\frac{5}{3}}}{\dot{Q}^{\frac{2}{3}}}$$

<div align="right">[29], [23] (4-11)</div>

$$X = 4.6 \times 10^{-4} Y^2 + 2.7 \times 10^{-15} Y^6$$

<div align="right">[29], [23] (4-12)</div>

<div align="right">[29], [23] (4-13)</div>

$$t_{activation} = \frac{X \, H^{\frac{4}{3}}}{\dot{Q}^{\frac{1}{3}}}$$

where $t_{activation}$ (sec) is the activation time of the detector, ΔT_c (°C) is the actuation temperature rise, $\dot{Q}$ (kW) is the HRR of the fire, and H (m) is the height of the ceiling above the fuel.

4.2: CFAST Model

The Consolidated Fire and Smoke Transport (CFAST) model was developed and is maintained by NIST. CFAST is a two-zone model capable of predicting the time-evolving environment of multi-compartment structures under prescribed fire conditions [18]. CFAST can provide a plethora of outputs, some of which include the average temperatures of the gas layers, the height of the gas layers, the species concentration, the vent flows, the surface temperature of the compartment, the optical density of the upper and lower layers, and the device activation times [5], [18].

Zone models calculate the time-evolving environment by dividing the compartment into one or two zones. Energy balance and mass conservation equations are solved based on the control volume of each zone, which is dictated by the zonal boundaries of each zone and/or compartment [31]. A zone model needs to be defined by a variety of properties such as the compartment geometry, a prescribed fire scenario, and thermal properties. The geometry of the compartment is needed to define the space and surrounding. The

prescribed fire scenario dictates the combustion products, HRR, and the oxygen concentration. Thermal properties are used to estimate the heat loss to the surrounding compartment [31].

There are two ways to model smoke detectors in CFAST [26]. The first is through a temperature rise method, where the activation of the detector occurs at a specified temperature change and RTI. This is done by modeling the smoke detector as a very sensitive heat detector with an activation temperature of 5 °C and a response time index (RTI) of 5 $(m \cdot sec)^{1/2}$ [25], [26]. The second, and more accurate, method is through a fixed smoke threshold concentration method [5], [17]. A detector located in the smoke layer has a percent obscuration activation associated with it. This value is then compared with the percent obscuration of the layer to determine if the detector activates. Activation of the detector occurs once the percent obscuration of the smoke layer reaches the set percent obscuration threshold of the detector. However, CFAST does not contain an algorithm to determine the transport lag of smoke from the source to the detector nor the lag time associated with smoke penetration into the detector's sensing chamber [26].

Soot production is specified, in CFAST, by the user in terms of mass of soot (kg) produced per unit mass of fuel consumed (kg). Percent obscuration per distance (% m^{-1}) can be obtained from the optical density per unit distance (m^{-1}) [26]. The optical density per unit distance, D_u, can be obtained as a function of the mass of soot per unit volume (kg per m^3), m_s''', using the equation

$$D_u = \frac{K_m m_s'''}{\ln 10} \qquad \textbf{[26] (4-14)}$$

The constant K_m represents the specific extinction coefficient, which has a default value of 8700 (m^2 kg^{-1}) [32]. The definitions of optical density per unit distance (m^{-1}) and percent obscuration per unit distance (% m^{-1}) is shown respectively as

$$D_u = -\log_{10}\left(\frac{I}{I_0}\right); \ O_u = 100\left[1 - \left(\frac{I}{I_0}\right)^{1/I}\right] \qquad \textbf{[6], [26] (4-15)}$$

Therefore, percent obscuration per unit distance can be obtained as a function of optical density per unit distance, shown as

$$O_u = 100\frac{10^{D_u} - 1}{10^{D_u}} \qquad \textbf{[26] (4-16)}$$

which is used to determine smoke detector activation [26].

4.3: FDS Model

The Fire Dynamics Simulator (FDS) contains a computational fluid dynamics (CFD) model, which was developed and is maintained by NIST. FDS numerically solves a form of Navier-Stokes equations for low-speed thermally-driven flow [20]. Features of FDS includes the implementation of hydrodynamic models, combustion models, radiation transport, rectilinear geometry, multiple meshes, parallel processing, and boundary conditions.

Unlike zone models, a CFD model divides control volume into many three-dimensional cells. The environment of the control volume is numerically calculated by solving the conservation equations within each cell [33]. As a result of the large number of cells, a CFD model is generally more refined and has a clearer "resolution" of the three-dimensional space than a zone model. Within each cell, the temperature, density, pressure,

velocity, and chemical composition is determined at a discrete time step [4]. In addition, Lagrangian particles are used to simulate smoke movement and sprinkler discharge.

Despite FDS being a CFD model, only detailed descriptions of the bulk transport of the smoke can be modeled [7]. At its best, FDS can only accurately provide the velocity and smoke concentration of the external ceiling jet flow past the detector. Therefore, activation models in FDS only account for the entry resistance of the smoke relative to the geometry of the detector [7]. Heskestad proposed a model that accounts for the entry resistance of the detector. He proposed that the mass fraction of the smoke in the sensing chamber lags behind the mass fraction of the external free stream outside the detector by a time period of $\delta t = L/u$, where u is the free stream velocity (m/s) and L is the characteristic length (m) of the detector geometry [6]. The characteristic length is a property of the smoke detector and is independent of the smoke and ceiling-jet properties. The change in mass fraction (kg s^{-1}) of smoke in the sensing chamber can be solved as

$$\frac{dY_c}{dt} = \frac{Y_e(t) - Y_c(t)}{L/u} \qquad \text{[7] (4-17)}$$

Furthermore, a more detailed entry model has been proposed by Cleary et al [34]. This model involves two filling times rather than the single lag time required for entry into the sensing chamber. One lag time is associated with the smoke having to pass through the detector housing, and the other lag time is associated with entry into the sensing chamber. The characteristic filling time associated with the entire volume of the external detector housing is described as $\delta t_e = \alpha_e u^{\beta_e}$. The characteristic filling time of the sensing chamber is described as $\delta t_c = \alpha_c u^{\beta_c}$. Each characteristic filling time is a function of the free stream velocity, u [34]. The parameters α and β are empirical constants related to the geometry of

the detector. Suggested values for these parameters are found in the FDS user guide [20].

As a result, the change in mass fraction of smoke in the sensing chamber can be solved as

$$\frac{dY_c}{dt} = \frac{Y_e(t - \delta t_e) - Y_c(t)}{\delta t_c} \qquad \textbf{[7] (4-18)}$$

Finally, the obscuration per unit length can be converted from of the mass fraction, $Y_c(t)$, using the following equation:

$$Obscuration = (1 - e^{-K_m \rho Y_c l}) \times 100\% \qquad \textbf{[7] (4-19)}$$

where K_m is the specific extinction coefficient (m^2 kg^{-1}), ρ is the density of the external gases in the ceiling jet (kg m^{-3}), and l is the unit of length of which the light is attenuated. The specific extinction coefficient has a default value of 8700 (m^2/kg). The unit of length, l, depends on whether the spot detector is listed in percent obscuration per foot or per meter. A value of 0.3048 is typically used for percent obscuration per foot and 1 m is used for percent obscuration per meter [7].

4.4: Multivariable Linear Regression Model

A linear regression model can be used to represent the relationship between independent and dependent variables. Most notably, for one independent variable, x, and one dependent variable, y, the form of a linear relationship is

$$y = \beta_1 x + \beta_0 \qquad \textbf{(4-20)}$$

where β_0 is the intercept and β_1 is the slope. While in most engineering and scientific phenomena the relationship between variables is not perfectly linear, linear regression is useful to express a simple relationship between independent and dependent variables. The

model can then be used to predict the value of the dependent variable, given any value of the independent variable [35].

The least squares method is often used estimate the regression coefficients, β_0 and β_1. Suppose that $b_0 = \beta_0$ and $b_1 = \beta_1$, then the fitted regression line is often given as

$$\hat{y} = b_1 x + b_0 \qquad \text{(4-21)}$$

The error of the fitted model, often called the residual, is the difference between the predicted values from the fitted regression line and the actual data points. For example, given a set of data where $\{(x_i, y_i); i = 1, 2, \dots, n\}$ and $\hat{y}_i = b_i x_i + b_0$, the ith residual, e_i, is given as

$$e_i = y_i - \hat{y}_i \qquad \text{[35] (4-22)}$$

The values of b_0 and b_1 that best estimate the true coefficients β_0 and β_1 minimize the sum of the squared residuals, thus minimizing the error between the fitted regression line and the data. The residual sum of squares, *SSE*, is given as

$$SSE = \sum_{i=1}^{n} e_i = \sum_{i=1}^{n} (y_i - \hat{y}_i)^2 \qquad \text{[35] (4-23)}$$

By minimizing the *SSE*, the least squares method produces estimated b_0 and b_1 parameters of a line that minimizes the residual or vertical deviations from the points to the fitted line, as shown in Figure 4-1 [35].
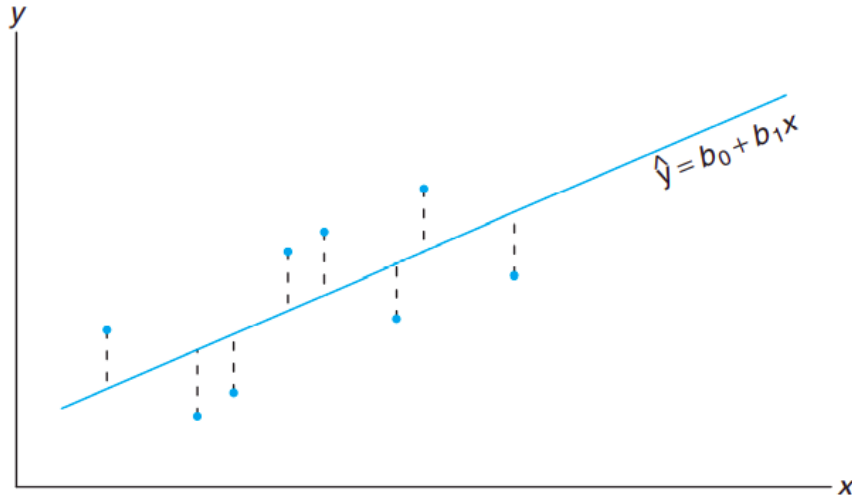
Figure 4-1: Residuals as vertical deviations from the fitted line [35].

Linear regression can also be used when the relationship of interest depends on more than one independent variable. This type of regression is called a multiple linear regression model. Given a set of k independent variables, $1, 2, \dots, k$ and n observations of $y_1, y_2, \dots y_n$ and $x_{1n}, x_{2n}, \dots x_{kn}$, a multiple linear equation can be expressed as

$$\hat{y}_n = b_0 + b_1 x_{1n} + b_2 x_{2n} + \cdots b_k x_{kn} \qquad \text{[35] (4-24)}$$

In matrix form, the equation can be expressed as

$$Y = AX \qquad \text{(4-25)}$$

where,

$$Y = [\hat{y}_1 \quad \hat{y}_2 \quad \cdots \quad \hat{y}_n] \tag{4-26}$$

$$A = [b_0 \quad b_1 \quad b_2 \quad \cdots \quad b_k] \tag{4-27}$$

$$X = \begin{bmatrix} 1 & 1 & \cdots & 1 \\ x_{11} & x_{12} & \cdots & x_{1n} \\ x_{21} & x_{22} & \cdots & x_{2n} \\ \vdots & \vdots & \ddots & \vdots \\ x_{k1} & x_{k2} & \cdots & x_{kn} \end{bmatrix} \tag{4-28}$$

Similar to estimating the regression coefficients for a linear model, the regression coefficients can be estimated by minimizing the sum of the squares of the residual, shown below as [35]

$$SSE = \sum_{i=1}^{n} (y_i - \hat{y}_i)^2 \tag{[35] (4-29)}$$

An analysis of the regression model is important for determining the quality of the model, as in how well it represents the relationship between the independent and dependent variables. One criterion used to determine the adequacy of the model is the coefficient of determination, or R^2 value. The R^2 quantity, which falls between zero and one, is a measure of the proportion of variation that is explained by the regression model. For example, an R^2 of 0.90 means that 90% of the data can be explained by the fitted model [35]. Figure 4-2 illustrates an example of a model that fits well, with an $R^2 \approx 1$, and a poorly fitted model, with an $R^2 \approx 0$.
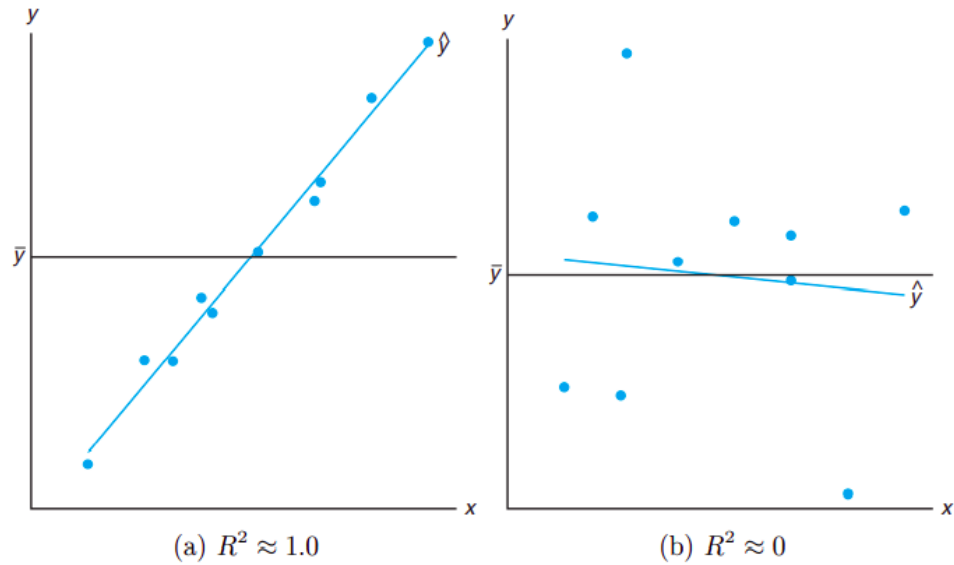
Figure 4-2: Plots with a good fit versus a bad fit [35].

When comparing competing multiple variable regression models for the same data set, the R^2 criterion is a dangerous measure. Adding additional independent variables, such as an additional regressor, can artificially inflate R^2. Therefore, R^2 can be made artificially high by overfitting unnecessary regressors into the model, where in fact the more simple model, with fewer regressors, may be superior for predicting the dependent values [35].

However, there are several indicative values that can further denote the best type of model. The analysis of the quality of the estimated regression line is handled by the analysis-of-variance approach (ANOVA). The *f*-statistic, often given in an ANOVA output, can be used in the *f*-test. This test assumes that the variability in the response data is due to chance random fluctuations from the independent variable. In the case of a linear regression model, the null hypothesis and alternative hypothesis assume the following, shown respectively as [35]

$$H_0: b_0 = 0 \; versus \; H_1: b_0 \neq 0,$$

28

The assumed null hypothesis, H_0, is rejected if $f > f_\alpha(df_{regression}, df_{error})$, where α is the level of significance, which is typically 0.05. If the null hypothesis is rejected, then the conclusion is that a significant amount of variation in the response values can be attributed to the proposed regression model. This same test can be applied for a multiple regression model, in which the null hypothesis and alternative hypothesis is shown as

$$H_0: b_1 = b_2 = \ldots = b_k = 0 \ versus \ H_1: b_1 \neq b_2 \neq \ldots \neq b_k \neq 0$$

where rejection of H_0 means that the regression differs from a constant. Therefore, at least one regressor variable is important [35].

Individual *t*-tests can also be performed on each individual variable. The *t*-statistic tests the importance of each individual regressor coefficient. For example, the following null hypothesis and alternative hypothesis can be proposed:

$$H_0: b_k = 0 \ versus \ H_1: b_k \neq 0,$$

The null hypothesis, H_0, is not rejected if $-t_{crit} < t < t_{crit}$, where t_{crit} is typically the value from the *t*-distribution, with a level of significance divided by 2 ($\alpha/2$) and *n-k-1* degree of freedoms. If H_0 is not rejected, as in $b_k = 0$, then the conclusion drawn is that the variable is not significant; the regressor value times the regressor coefficient of zero would yield no changes in the predictor values [35].

If the P-value, or probability of t, is smaller than the level of significance, then the drawn conclusion is that the null hypothesis is rejected. For example, a P-value of 0.03 indicates that assuming the null hypothesis, H_0, is true, then the probability of $b_k = 0$ is 3%. This would mean that the null hypothesis, $b_k = 0$, is most likely not true and that the variable is a significant predictor to the outcome. Typically, a level of significance of 0.05

or 5% is the threshold for the P-value, which indicates that a probability more than 5% does not support the rejection of the null hypothesis. The t-statistic and P-value can be useful in choosing the most optimal model, where only the most important variables are chosen. As stated earlier, the inclusion of too many regressors may artificially raise the R^2 value, and thus the t-test is another way to ensure that every variable is "contributing" significant predictions for the most optimal model [35].

Chapter 5: Methodology

There are three main processes that involve developing a statistical model that can predict the FDS activation times based on the CFAST times. The first process is to gather enough data on when the smoke detectors will activate in CFAST and FDS for a range of variable room geometries. Secondly, a set of the most influential independent variables are identified, such that a quality statistical model can be used to correlate FDS detection times with CFAST detection times. Lastly, the statistical model is assessed by using the models to predict the activation times of FDS and is compared to the actual FDS detection times for room geometries consisting of random predictor values.

5.1: Defining the Default Room and Model Inputs

The default compartment design is based on the room used in the CFAST and FDS validation study [17], [21]. The default room size is 24 ft wide by 36 ft long by 12 ft tall. The aspect ratio of the room is defined as the width divided by the length. Thus, the default room size has an aspect ratio of 0.667. The room is naturally ventilated, with an 8 ft tall and 6 ft wide opening centered along one of the shortest walls, farthest from the burner. The square burner is 0.65 ft wide by 1 ft tall and is located 6 ft from the shortest and longest wall. The plan and elevation view of the default compartment is shown in Figure 5-1.
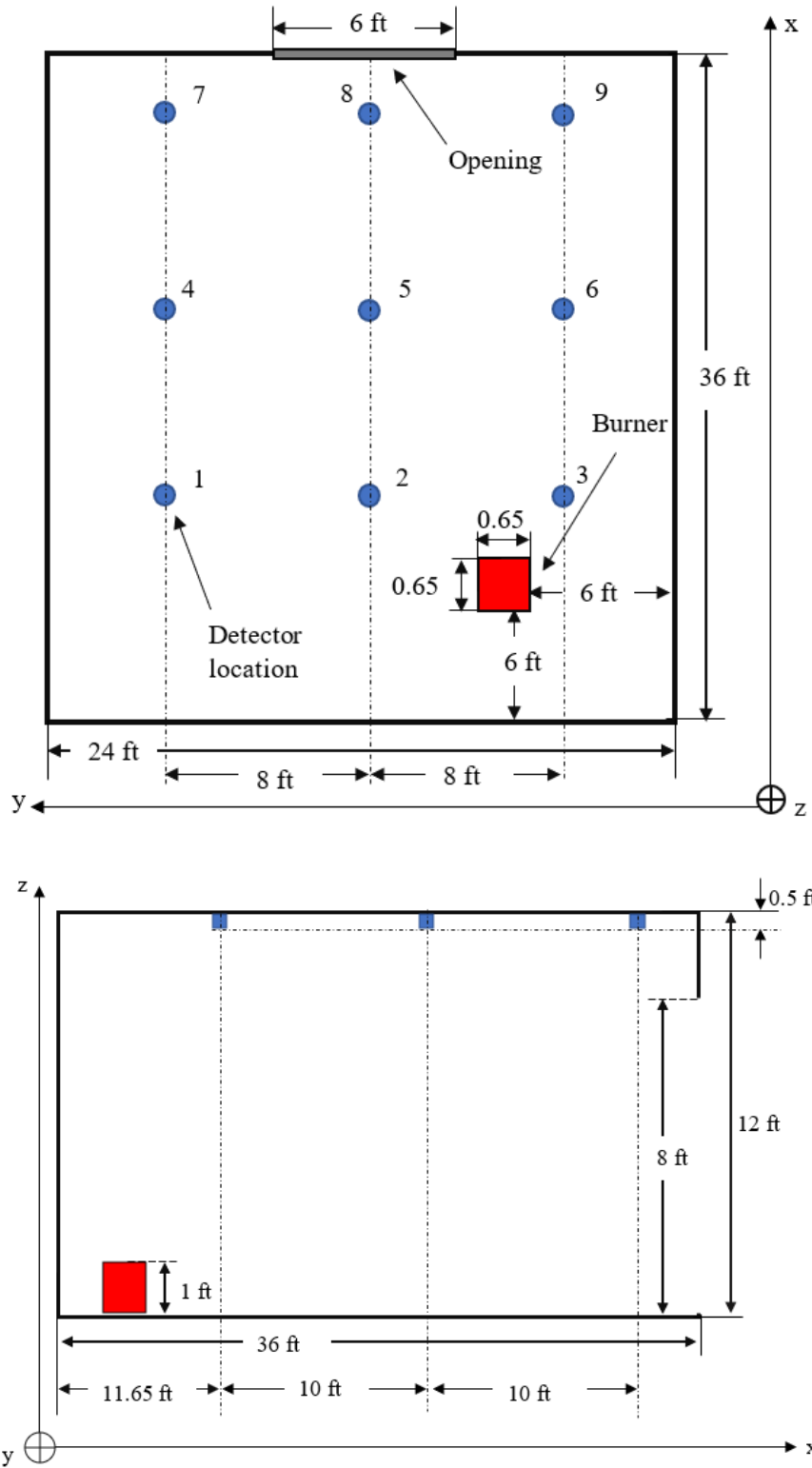
Figure 5-1: Plan (top) and elevation (bottom) views of the default compartment.

The walls and ceiling were modeled as 0.5 in. thick gypsum. The floor, not mentioned in the validation studies, was modeled as a 3 in. concrete slab. The thermal properties, obtained from NBSIR 88-3752 - ATF NIST Multi-Floor Validation, for concrete and gypsum are listed in Table 5-1 [36]. The thickness and thermal properties of the walls, ceiling, and floor have negligible impact on the flow solver in FDS (i.e., negligible impact on the plume and ceiling jet flow from the fire) [20]. Similarly, the thickness and thermal properties of the compartment surfaces in CFAST have no impact on the plume and ceiling jet flow calculations [26]. A default ambient temperature of 293 K and pressure of 101,325 Pa was used for both CFAST and FDS.

Table 5-1: Material Properties [36].

	Concrete	Gypsum
Density (kg/m^3)	2280	930
Heat Capacity (kJ/kg $\cdot$K)	1.04	1.09
Thermal Conductivity (W/m $\cdot$K)	1.8	0.17

A total of nine detector locations were located 0.5 ft below the ceiling and spaced 10 ft by 8 ft between the burner and the opening of the room, as shown in Figure 5-1. Each location contained a total of three photoelectric detectors with varying activation obscurations of 1.64, 3.27, and 6.56% per ft and are identified as low, medium, and high activation obscuration levels respectively. In FDS, the Cleary model was used to account for smoke delay [34], [7]. The assumption that smoke entry delay is negligible for large local velocities (>0.2 m/s) is made in the FDS validation study [34], [7]. However, a smoke entry model was implemented in these simulations to capture the full effect of room geometry on predicted smoke activation times. The recommended α and β parameters, found in the FDS user guide, for the Cleary model are listed in

Table 5-2 [20].

Table 5-2: Smoke Entry Delay Parameters.

Detector Model	α_e	α_c	β_e	β_c
Cleary Photoelectric P1	1.8	1.0	-1.0	-0.8

Additionally, a set of velocity, temperature, and optical density devices are placed at the same location as the detectors, a height of 11.5 ft. Layer measuring devices were also installed at the same locations of the detectors, ranging from 0 to 12 ft. In FDS, the layer height is calculated as a temperature difference between the average upper layer and the lowest mesh cell for that x and y location [20].

Assumptions for each model are as follows. Version 7.6 of CFAST was used. In CFAST, the ability to model the burner above the floor area is non-existent, and thus the flame was set on the floor of the compartment. Pyrosim was used as the main complier for FDS 6.7.5. In FDS, the mesh resolution was set to a fixed set of 0.4 ft cubic grid cells. The computational domain extends 10 ft beyond the opening of the room to allow for simulation of the flow leaving the room. A depiction of the default compartment, modeled in CFAST is shown in Figure 5-2. The same compartment, modeled in FDS, is shown in Figure 5-3.
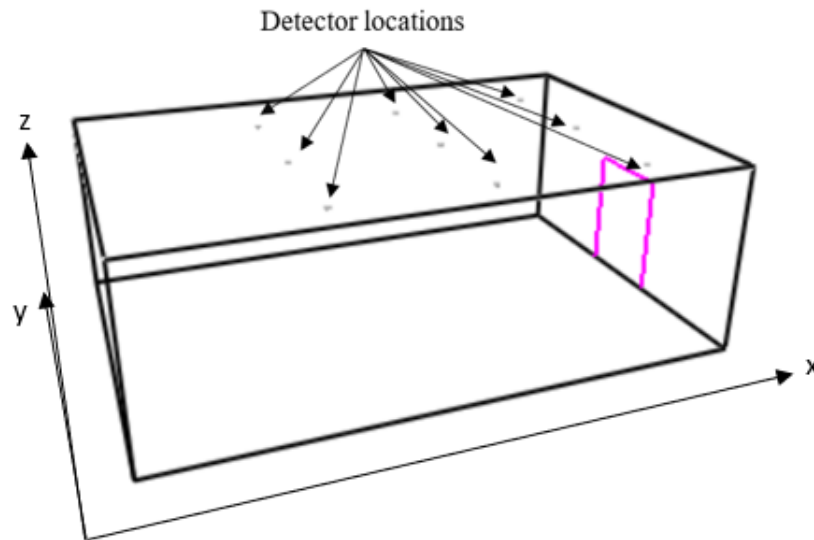
Figure 5-2: Default compartment modeled in CFAST.
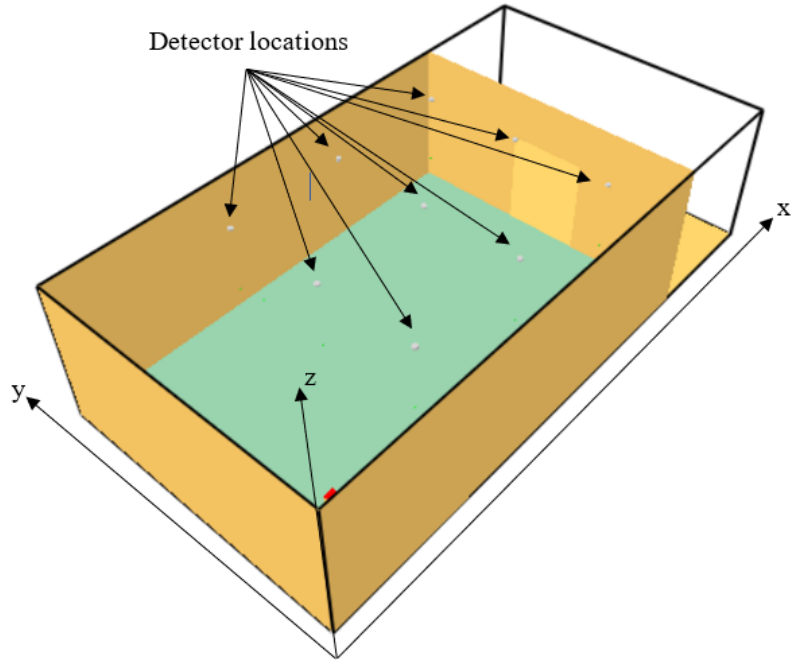
Figure 5-3: Default compartment modeled in FDS.

5.2: Fuel Mixture and Fire Scenario

A single prescribed fire scenario was used for the varying room geometries. A propane mole fraction of 0.5 and propene mole fraction of 0.5 was used as the fuel mixture for the burner. The stoichiometric calculations for the fuel mixture, C_3H_7, is shown as

$$0.5 \ C_3H_8 + 0.5 \ C_3 \ H_6 \rightarrow \ C_3H_7 \qquad \textbf{(5-1)}$$
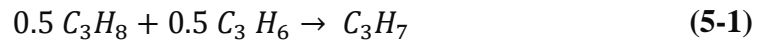
A soot yield of 0.0333 g$_{soot}$/g$_{fuel}$ and specific extinction coefficient of 7900 (m^2/kg). were experimentally determined from NIST [21]. However, a default value of 8700 (m^2/kg) was used in both CFAST and FDS due to the inaccessible option to change the specific extinction coefficient in CFAST. This difference in value has no impact on the comparison between CFAST and FDS since both models are using the same specific extinction coefficient value. A radiative fraction was set to 0.35, an average between 0.30 and 0.40.

The average fuel mass fraction of the mixture at which carbon particles began to form, f_s, was calculated as 0.173 [37]. This parameter is calculated as

$$f_s = \frac{12n + m}{12n + m + [n/2(137.3)]}$$ [37] (5-2)

where n is the number of carbons and m is the number of hydrogens in 1 mol of hydrocarbon fuel. The radiative fraction and f_s have an inverse relationship in which a larger radiative fraction is associated with a smaller fuel mass fraction. A comparison of fuel mass fraction and radiative fraction for different fuels is shown in

Table 5-3 [37], [38]. Since the fuel mass fraction of the mixture falls between propane and other fuels with carbons larger than five, the radiative fraction of the mixture is taken as the average between the two.

Table 5-3: Relationship between fuel mass fraction and radiative fraction [37], [38].

Fuel	Fuel Mass Fraction, f_s	Radiative Fraction, x_r
Hydrogen	1.0	0.2
Methane (C_1)	0.189	0.2
Ethylene (C_2)	0.170	0.25
Propane (C_3)	0.176	0.3
Butane (C_4)	0.175	0.3
C_5 and higher	-	0.4

At ignition, the fire is held steady at 3 kW for 90 seconds and then linearly ramps up to 30 kW for 810 seconds. The fire is then held steady at 30 kW for an additional 60 seconds. After 60 seconds, at a steady 30 kW, the fire rapidly decreases to 0 kW until the end of the simulation. The total simulation time was set for to run for 1200 seconds. A simple combustion model, which assumes that there is no nitrogen in air, was used for the FDS and CFAST models [20]. Propane has an estimate combustion of about 46.4 (kJ/g). Thus, the fuel had an estimated heat of combustion of 46.3 (kJ/g) [39]. The fire, modeled in both FDS and CFAST, outputs the HRR curve shown in Figure 5-4. Since both models

follow the same fire curve, it can be assumed that the fire scenario accurately represents the same fire scenario for both models. This fire scenario and fuel mixture were chosen so that the soot production could be accurately prescribed. Since this is the same fire scenario described in the FDS and CFAST validation study, the prescribed soot production can be related back an experimentally determined value of 0.033 g of soot per g of fuel burned [21].
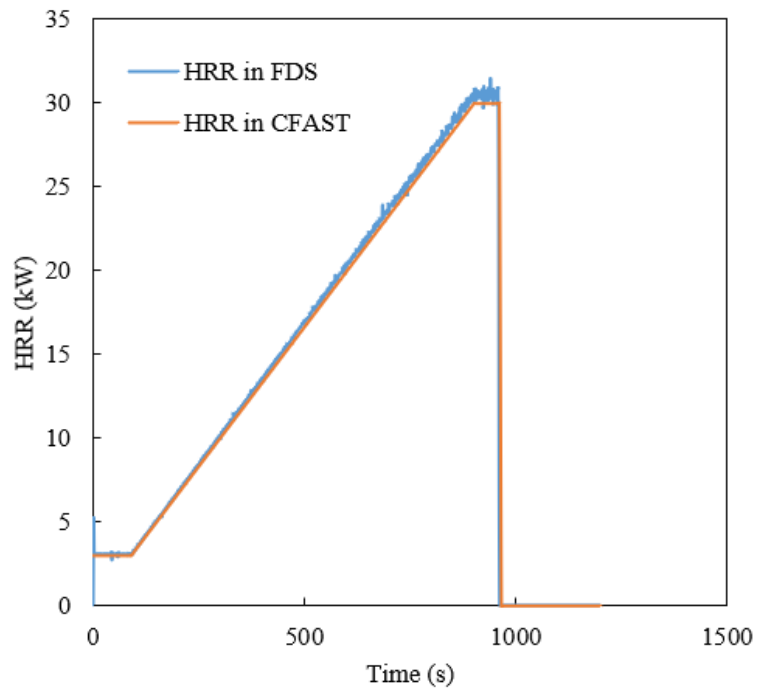
Figure 5-4: HRR curve of the fire in FDS and CFAST.

5.3: Model Validation in FDS

The initial default compartment was compared with an FDS file from the *Validation Study for Smoke Detector Response in FDS*, received from Cleary et al. [21]. The room size and fire scenario were modeled the same in both FDS and CFAST. There are two main changes

that were made from the original FDS file: the mesh size and the combustion model. A mesh size, with a grid resolution of about 0.328 ft, was used in the original input file.

5.3.1: Grid Cell Size

The mesh extended about 15 ft beyond the opening of the compartment. Because this research project included a variety of scenarios, the grid resolution was reduced. Thus, an increase in cell size to 0.4 ft instead of the original 0.328 ft was made. This had negligible impact on when the detectors activated. Figure 5-5 shows a comparison of the same room dimensions and fire scenario between the two different mesh sizes and how slightly decreasing the grid resolution does not change the overall activation of the detectors. The slope of the linear regression with an intercept of zero is shown as 0.915, thus indicating that increasing to a slightly larger grid cells have minimal effect on the quality of the model.
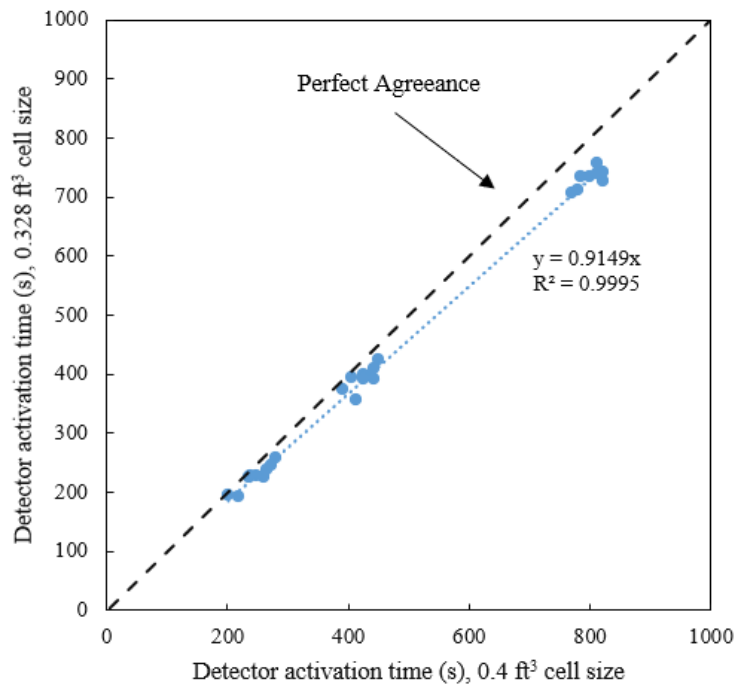
Figure 5-5: Comparison of detector activation time with different cell sizes in FDS.

Additionally, the finer grid cell, 0.328 ft, was compared to the larger grid cell size of 0.4 ft. Since smoke detector activation and the smoke properties are areas of interest, the characteristic length can be defined as the smoke layer depth. Using the 0.328 ft grid resolution, the layer height is shown to be around 1.35 m, which is around 4.9 ft. Typically, the grid cell size is recommended to be less than the characteristic length divided by 10, which in this case holds true for the selected grid cell size of 0.4 ft. As a note, the burner is 0.65 ft and using that as the characteristic length would require a much smaller grid cell size. However, a smaller grid cell may not be necessarily as the 0328 ft resolution has shown that it provides enough accuracy to achieve results similar to that of the experimental data from the FDS and CFAST validation studies [21], [17].

5.3.2: Combustion Model

In FDS, there are two types of ways to model combustion, a simple or complex chemical reaction [20]. In a simple chemical reaction, only the chemical formula of the fuel is specified. The reaction of the fuel is assumed to be in the form of

$$C_x H_y O_z N_v + \nu_{O2}\, O_2 \rightarrow \nu_{CO2}\, CO_2 + \nu_{H2O}\, H_2O + \nu_{CO}\, CO + \nu_s\, Soot + \nu_{N2}\, N_2 \qquad \textbf{[20] (5-3)}$$
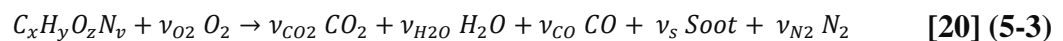
The chemical formula of the fuel along with the yields of CO and soot, and the volume fraction of hydrogen in the soot only need to be specified in a simple reaction. FDS will then use that information to automatically calculate the remaining coefficients of the chemical reaction using the following equations shown below as

$$v_{O2} = v_{CO2} + \frac{v_{CO}}{2} + \frac{v_{H2O}}{2} - \frac{z}{2} \qquad\qquad \text{[20] (5-4)}$$

$$v_{CO2} = x - v_{CO} - (1 - X_H)\, v_s \qquad\qquad \text{[20] (5-5)}$$

$$v_{H2O} = \frac{y}{2} - \frac{X_H}{2}\, v_s \qquad\qquad \text{[20] (5-6)}$$

$$v_{CO} = \frac{W_F}{W_{CO}}\, y_{CO} \qquad\qquad \text{[20] (5-7)}$$

$$v_s = \frac{W_F}{W_{CO}}\, y_s \qquad\qquad \text{[20] (5-8)}$$

$$v_{N2} = \frac{v}{2} \qquad\qquad \text{[20] (5-9)}$$

$$W_s = X_H\, W_H + (1 - X_H) W_c \qquad\qquad \text{[20] (5-10)}$$

The energy release rate of the reaction can be determined by "taking the sum of the net change in mass for each species in a given time step multiplied by the respective species' enthalpy of formation (kJ/kg)" [20]. The enthalpy of formation can manually be specified for non-predefined species. For a given reaction, if the only unknown enthalpy value is that of the fuel, the missing value can be determined from the heat of combustion of the fuel. However, if neither the enthalpies nor heat of combustion of the fuel is known, heat of combustion of the fuel can be estimated by

$$\Delta h \approx \frac{v_{O2}\, W_{O2}}{v_F\, W_F}\, EPUMO2 \qquad\qquad \text{[20] (5-11)}$$

where EPUMO2 (kJ/kg) is the energy per unit mass of oxygen consumed [20]. The default value is 13,100 (kJ/kg) [20]. As shown in Figure 5-6, specifying the heat release rate of the fuel directly or allowing FDS to estimate has negligible effect on the HRR of the fire and the prediction of smoke detectors within FDS. A heat of combustion of 46 (kJ/g), which is close to that of propane, was used for the FDS simulation with a specified heat of

combustion. An EPUMO2 value of 13,100 (kJ/kg) was used for the simulation in which FDS estimated the heat of combustion. Both ways of defining the heat of combustion are valid, as shown by Figure 5-6. A linear trendline was fitted to the data, with a y-intercept of zero, and a slope of 0.968. This indicates that making a reasonable estimate of the heat of combustion or allowing FDS to estimate it both have little difference in the outcome of the model.
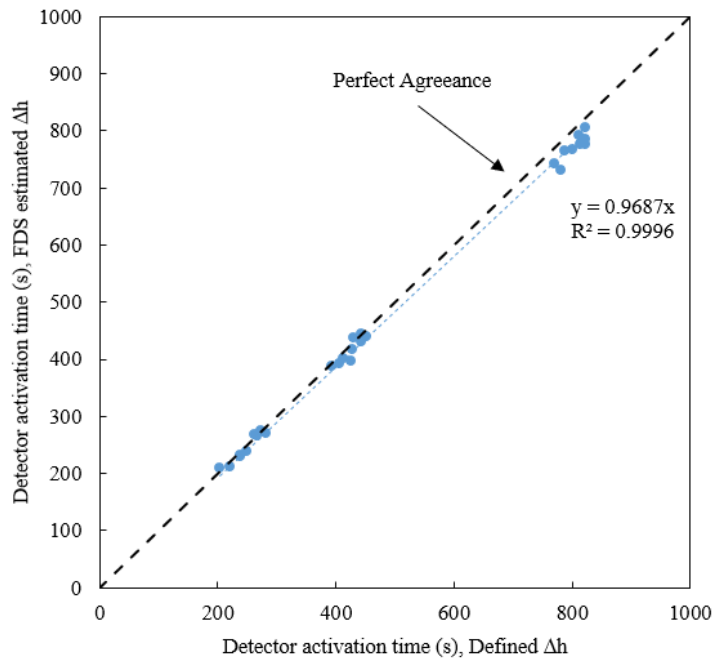
Figure 5-6: Comparison of defined Δh versus FDS predicted Δh.

Additionally, a complex combustion model entails explicitly specifying the component mixture and stoichiometry of the reaction [20]. The FDS file, as provided by Cleary et al. uses this complex combustion model [21]. In this case, the fuel mixture of propane and propylene are identified as two separate fuels instead of the C_3H_7 mixture that was determined earlier. The component "fuelmix" was specified as 0.5 propane and 0.5 propylene by volume. The component "air" is specified as 3.76 nitrogen and 1.0 oxygen

by volume. The component "products" is defined as 2.88 carbon dioxide, 17.42 nitrogen, and 4.39 water vapor by volume. The soot yield is included separately as 0.9 carbon and 0.1 hydrogen. Each (primitive) component, i.e., propane, propylene, nitrogen, etc., are defined as a "lumped component", meaning that each species will not be explicitly tracked, hence the required stoichiometric input. The components for the complex combustion reaction is shown below as,

$$fuel + air \rightarrow products + soot$$
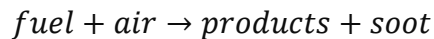
where fuel, air, and soot contain the lumped primitive components.

A comparison between using a simple combustion model, with the fuel as C_3H_7 and a specified heat of combustion of 46 (kJ/g), is compared to the complex combustion model as mentioned earlier. As shown by Figure 5-7, the detector activation times do not differ much from each other. A linear regression, with a y-intercept of zero, and a slope of 0.923 indicates that the compared detector times are near 1:1, indicating negligible variation of detector response times based on which combustion model is defined.
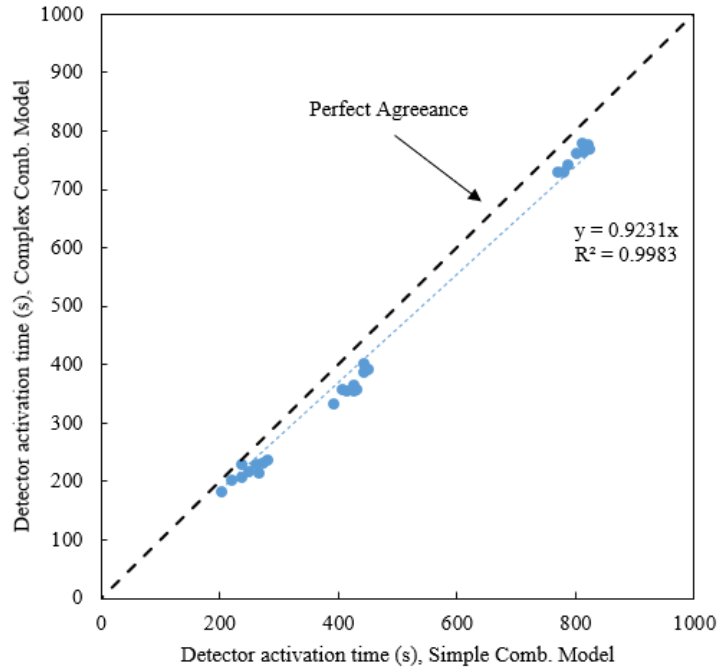
Figure 5-7: Comparison of using a complex versus simple combustion model in FDS.

5.3.3: Verification of Soot Production

Lastly, a comparison of the soot yield for a 24x36 ft no-vent compartment, between FDS and CFAST, was used to ensure that each model was correctly set up. Because there is no doorway, the soot in the room should be roughly the same for both CFAST and FDS. As shown in Figure 5-8, the soot yield for both CFAST and FDS are nearly identical. This means that the fire scenario and soot output for FDS and CFAST are modeled identically. Thus, the factors that influence the discrepancies between FDS and CFAST can be attributed to the mathematical calculations of the models itself and not the way each model was set up.
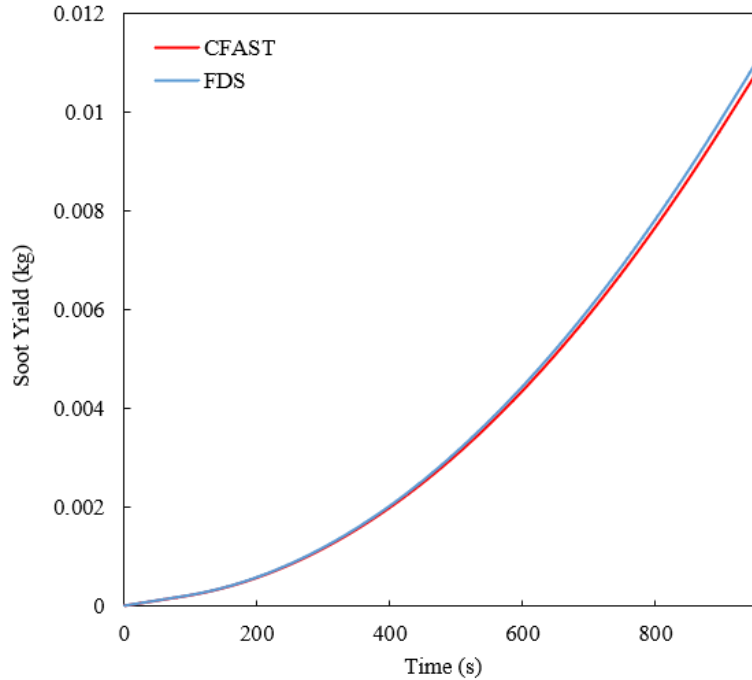
Figure 5-8: Soot concentration of CFAST and FDS for a 24x36 ft compartment with no doorway.

5.4: Establishing Other Various Room Geometries

In addition to the default compartment room, described in section 5.1: Defining the Default Room and Model Inputs, tests were also conducted in three different additional room geometry variations under the same fire conditions. These room geometries were chosen somewhat arbitrarily. However, using realistic aspect ratios of each room was considered and could be represented as a long hallway fire versus an open room fire. The additional room geometries are 8x36, 16x36, and 36x36 ft, with the same 12 ft tall ceiling and 6x8 ft doorway centered along the shortest wall. The 36 ft side of the wall remained constant so that the distance from the burner to the doorway relatively stayed the same.

The location of the detectors with respect to the burner also remained constant between each varying room size.

The ceiling height of the room was varied to also explore the effects of ceiling height on each model. The original 24x36 ft dimensions were used with the 6x8 ft wide doorway, except the ceiling height of the compartment was varied. A total of four ceiling heights were examined, including the original 12 ft ceiling and an additional three ceiling heights of 24, 36, and 48 ft. However, the location of the detectors with respect to the burner remained constant. In order to narrow the effects of each variable, a variety of models were created, such that the examined variable could be modified while keeping all other variables the same. The dimensions of each configuration can be shown in Table 5-4.

Table 5-4: Various Room Geometries

Room Variation	Width-x (ft)	Length-y (ft)	Height-z (ft)	Number of detector locations	Total number of detectors
24x36 ft (Default Room)	24	36	12	9	27
36x36 ft	36	36	12	9	27
16x36 ft	16	36	12	6	18
8x36 ft	8	36	12	3	9
24 ft Ceiling	24	36	24	9	27
36 ft Ceiling	24	36	36	9	27
48 ft Ceiling	24	36	48	9	27

5.4.1: Verification of Additional Room Geometries in FDS

To verify that each aspect ratio of the room was modeled correctly, the different room sizes were simulated without a vent. In these simulations, the total amount of soot production in each compartment should be the same. The total soot of the 8x36, 16x36, 24x36, and 36x36 ft compartments are plotted in Figure 5-9. As shown below, the total amount of soot in each compartment is roughly the same, at around 0.0105 kg or 10.5 g.
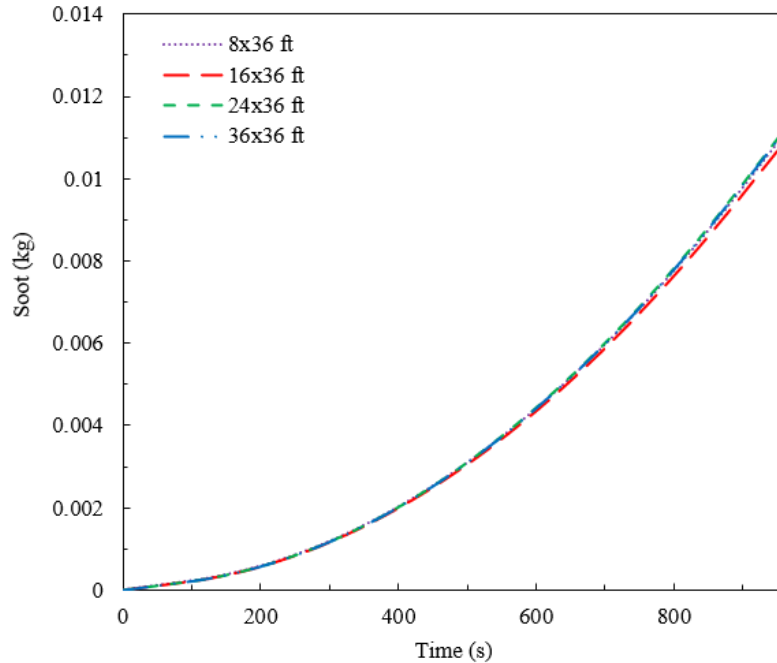
Figure 5-9: Comparison of total soot yield for varying compartment sizes with no doorways.

The total amount of soot can be verified through hand calculations by taking the mass loss rate (MLR) curve, shown in Figure 5-10, and integrating to get the total amount of mass loss in the compartment. Additionally, because the soot yield is defined as 0.033 kg of soot per kg of fuel burned, the total amount of soot can be determined by multiplying the two values. The total mass loss of fuel is estimated to be about 0.3213 kg. Multiplied by the soot yield of 0.033 kg of soot per kg of fuel burned, the total amount of soot yield is around 0.0106 kg of soot or around 10.6 g of soot. The hand calculations verify the same amount of soot that is presented in the FDS model shown in Figure 5-9.
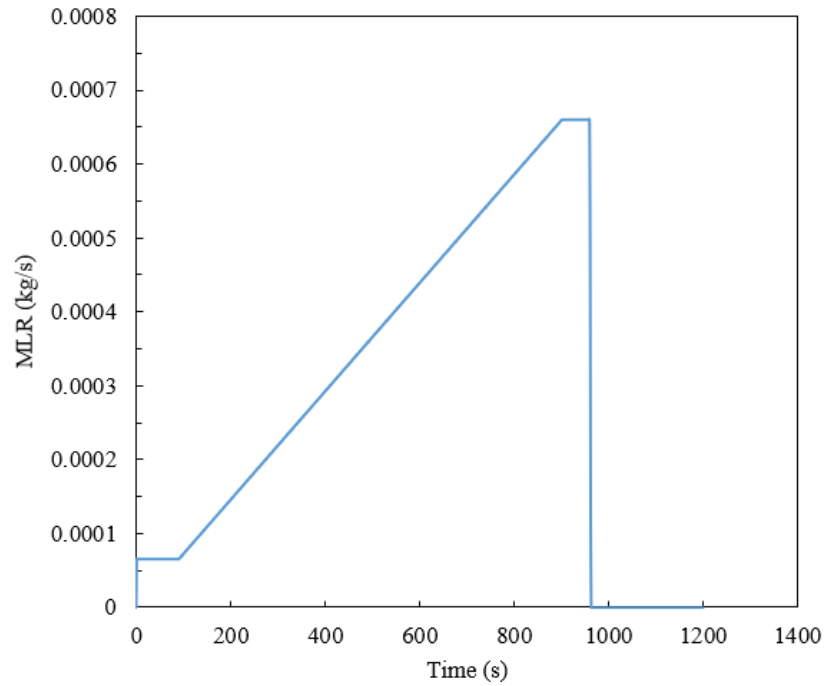
Figure 5-10: Mass loss rate of the fuel

5.5: Applying a Linear Regression Model for CFAST and FDS

A correlative linear regression model relating various input properties of the detector and the room can be determined from the set of training data. The training data includes a total of five tests, each of different room geometries and ceiling height, as shown in Table 5-5. Not all the data sets were used in to train the model. There were tests that included altering the soot yield and adding beam obstructions, but these sets of data were excluded from the training data set to isolate the effect of the room size and ratio on predicted smoke detector activation times.

Table 5-5: Room geometries performed in both CFAST and FDS.

Room Variation	Width-x (ft)	Length-y (ft)	Height-z (ft)	Number of detector locations	Total number of detectors	Total number of activated detectors
Test 1 (default room)	24	36	12	9	27	27
Test 2	36	36	12	9	27	27
Test 3	16	36	12	6	18	18
Test 4	8	36	12	3	9	9
Test 5	24	36	36	9	27	18
Total sample size				36	108	99

Input parameters were considered based on the parameters used in empirical models. A total of eight regressors were initially identified:

- the CFAST ceiling jet velocity at the time of detector activation

- the CFAST ceiling jet temperature at the time of detector activation

- the activation obscuration of the detector, as prescribed by the user in CFAST

- the actual CFAST activation time of the detectors

- radial distance from the detector to the center of the fire plume

- the height of the room

- area of the room

- aspect ratio of the room

Each regressor was selected with the predicted intent of the variable adequacy affecting the predicted activation time of a detector. For example, the activation obscuration affects the sensitivity of the detector. The velocity influences the entry lag for the detector. A weak correlation between the temperature of the ceiling jet and the time the detector activates was also shown. The distance from the detector to the center of the fire plume affects the lag time it takes for the ceiling jet to reach the detector. Detectors near the opening may affect the detector's ability to receive sufficient soot for activation. The

ceiling height impacts the plume lag time, which is the time it takes fpator the smoke to travel from the burner to the ceiling. The area and aspect ratio of the room affects the smoke layer height and mass balance of the room.

Although CFAST can predict the detector activation times, it does not however contain an algorithm for the transport lag from the fuel source to the detector, nor the lag time associated with smoke penetrating into the sensing chamber. Because CFAST operates as a zone model but does not account for the physical phenomenon mentioned previously, the CFAST detection time is used as an initial starting point on when the detector will activate in that compartment. Additionally, by introducing these other external variables and applying an appropriate multivariable linear regression model, it could predict the appropriate amount of variability and apply a "correction factor" between CFAST and FDS.

Each repressor variable was input into Microsoft Excel. A total of 99 data points were used, with each detector acting as a data point. Each detector contains information about the velocity and temperature at alarm; the distance from the burner to the detector; the height of the detector; the size of the compartment it is in; the aspect ratio of the room; and the activation time of the detector in CFAST. The dependent or predictor variable was the actual FDS time.

The goal is to optimize an appropriate statistical model by starting with a single variable and introducing the number of independent variables. There are three areas of interest that determine how well the model can predict: the R^2 coefficient, the f statistic of the model; and the p-value of each regression coefficient. The R^2 coefficient indicates how well the model fits to the data. The f statistic can be used in the f test, which determines if

the variability in the data is due to chance or if there is an actual underlying model that can fit the data. Lastly, the t-test and P-value determines if the regression coefficient for that variable is zero or not. Thus, meaning if the variable is significant to the model. Each statistical measure is further explained in section 4.4: Multivariable Linear Regression Model.

The CFAST activation time was used as an initial parameter for the statistical model because it considers conservation balances between two zones. The dependent variable as the FDS activation time. Introducing other variables, as mentioned earlier, allows for consideration of transport and entry lag, which is not inherently considered in CFAST. However, before introducing these other variables, a correlation matrix was performed using Excel to determine dependencies between these assumed independent variables. A value less than -0.8 or greater than 0.8 was used as a threshold to determine whether the assumed variables were dependent on each other. Table 5-5 shows the correlation matrix values determined in Excel. As highlighted in yellow, the activation obscuration of the detector and the temperature at the detector location are dependent on each other. Similarly, the room area and the aspect ratio of the room are dependent on each other. Therefore, only one of the independent variables that are dependent on the other should be included in the model, otherwise there is risk of overfitting the model and usage of insignificant variables.

Table 5-6: Correlation matrix of assumed independent variables.

	Aspect Ratio	Distance	Room Area	CFAST Det. Time	Activation Obs.	Ceiling Height	Temp	Velocity
Aspect Ratio	1							
Distance	0.092	1						
Room Area	0.999	0.091	1					
CFAST Det. Time	0.261	0.046	0.258	1				
Activation Obs.	0.004	-0.009	0.005	0.668	1			
Ceiling Height	-0.014	0.032	-0.019	0.459	-0.269	1		
Temp	0.025	-0.310	0.027	0.501	0.914	-0.410	1	
Velocity	0.004	-0.731	0.001	0.443	0.122	0.480	0.255	1

Multivariable linear regression models were developed using the regression function in Excel. Each model was optimized such that the P-value was less than 0.05, which assumes a 95% confidence that each variable is significant. Additionally, performing an *f*-test with a significance of 0.05, *k* number of $df_{regression}$, and *n-k-1* number of df_{error} ensures whether to conclude if the model is significant or not. A rejection of the null hypothesis, H_0, is concluded by

$$f > f_\alpha(df_{regression}, df_{error})$$

(5-12)

where α is the level of significance. In addition, the R^2 coefficient threshold is 0.7, meaning that 70% or more of the data can be attributed to the model.

A total of two optimized models were determined from Excel. Each model includes the variable of the CFAST detection time and a combination of other independent variables. The statistically significant models, along with the input parameters and statistical measures are shown in Table 5-7 and Table 5-8. For *n* number of data points and *k* number of input variables the first linear regression model is shown as

$$\hat{y}_n = \hat{b}_0 + \hat{b}_1 x_{1n} + \hat{b}_2 x_{2n} + \hat{b}_3 x_{3n}$$

(5-13)

where $\hat{b}_0, \hat{b}_1, \hat{b}_2,$ *and* $\hat{b}_3$ are the intercept, temperature, velocity, and CFAST detection time regression coefficients, respectively, as shown in Table 5-7. The input parameters for

the temperature, velocity, and CFAST detection time for each data point are respectively

shown as $x_{1n}, x_{2n}, and\ x_{3n}$.

Table 5-7: Regression coefficients and statistics for model 1.

	R Square	$df_{regression}$	df_{error}	F-value	$F_{0.05}$ (3, 95)
Regression Statistics	0.949	3	95	592	0.117
	Intercept	Temperature (°C)	Velocity (m/s)	CFAST Detection Time (s)	
Regression Coefficients	-313.78	15.727	-113.77	0.8744	
P-value	6.76E-11	4.62E-15	1.35E-05	5.58E-51	

Similarly, the second proposed regression model is shown as

$$\hat{y}_n = \hat{b}_0 + \hat{b}_1 x_{1n} + \hat{b}_2 x_{2n} + \hat{b}_3 x_{3n} + \hat{b}_4 x_{4n} \qquad \textbf{(5-14)}$$

where $\hat{b}_0, \hat{b}_1, \hat{b}_2,\ and\ \hat{b}_3$ are the intercept, temperature, velocity, CFAST detection time,

and ceiling height regression coefficients, respectively, as shown in Table 5-8.

Table 5-8: Regression coefficients and statistics for model 2.

	R Square	$df_{regression}$	df_{error}	F-value	$F_{0.05}$ (4, 94)
Regression Statistics	0.951	4	94	461.36	0.176
	Intercept	Temperature (°C)	Velocity (m/s)	CFAST Detection Time (s)	Ceiling Height (ft)
Regression Coefficients	-509.59	23.392	-162.83	0.7722	3.7992
P-value	2.75E-06	7.33E-08	0.0381	2.97E-24	5.29E-06

In addition to the two proposed optimized linear models, another model was

developed with the dependent variable being an absolute error between the CFAST and

FDS actuation times of the detector. The absolute error is calculated as

53

$$Error_{abs} = |t_{CFAST} - t_{FDS}|$$ (5-15)

A model with the dependent variable as the error is different in that now the model is explicitly fitted to match the variation between CFAST and FDS activation times based on the independent variables, as opposed to just fitting to the activation time. This may lead to a better fit model that can account for conditions in CFAST and FDS where actuation times vastly differ from each other.

Table 5-9: Regression coefficients and statistics for model 3.

	R Square	$df_{regression}$	df_{error}	F-value	$F_{0.05}$ (5, 93)	
Regression Statistics	0.713	5	93	46.2	0.227	
	Intercept	**Room Area (ft²)**	**Activation Obs. (%/m)**	**Ceiling Height (ft)**	**CFAST Detection Time(s)**	**Distance between fire plume and detector (ft)**
Regression Coefficients	186.53	-0.069	28.03	-8.883	0.701	-1.540
P-value	6.1E-05	0.012	1.25E-11	5.95E-05	1.6E-09	0.013

Similarly, the variation or error between CFAST and FDS can be predicted with the linear regression model shown as

$$\hat{y}_n = \hat{b}_0 + \hat{b}_1 x_{1n} + \hat{b}_2 x_{2n} + \hat{b}_3 x_{3n} + \hat{b}_4 x_{4n} + \hat{b}_5 x_{5n}$$ (5-16)

where $\hat{b}_0, \hat{b}_1, \hat{b}_2, \hat{b}_3, \hat{b}_4,$ and $\hat{b}_3$ are the intercept, room area, activation obscuration, ceiling height, CFAST detection time, and distance regression coefficients, respectively, as shown in Table 5-9.

Chapter 6: Results and Discussion

6.1: Aspect Ratio Compartment Variations

6.1.1: Analysis of Detector Response

The activation times are represented as bar charts, where each bin corresponds to the location of the detector spacing. Each detector location was further subcategorized into separate bar charts for their respective obscuration activation levels. An obscuration activation level of 1.64, 3.27, and 6.56% per ft are identified as low, medium, and high activation obscuration levels respectively.

6.1.1.1: 8x36 ft Compartment Detector Responses

In the smallest compartment, the 8x36 ft configuration, only three detector locations were present within the compartment. The Smokeview model of the compartment with the soot density is shown in Figure 6-1 at 400 seconds. Only locations 3, 6, and 9 were present in the 8x36 ft compartment. A visual representation of the model is presented so as a visual verification that the model was setup as intended.
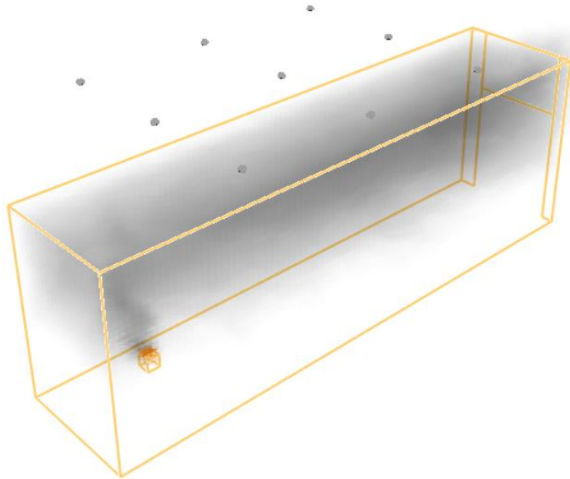
Figure 6-1: Smokeview model of 8x36 ft compartment at 400 seconds.

The activation times for detectors with a low activation obscuration are shown in Figure 6-2. FDS predicts the activation times slightly earlier than CFAST by about 4 seconds for detector locations 3 and 6. For location 9, FDS slightly lags behind CFAST by about 14 seconds. For the medium activation obscuration, CFAST was consistently activating earlier than FDS for all three detector locations, as shown in Figure 6-2. The difference in detection times was more signficant for location 9 by about 21 seconds. For detector locations 3 and 6, the difference in activation times had a difference of about 4 and 8 seconds, respectively. For all the high activation obscuration detector locations, FDS activated significantly later than CFAST by about 450 seconds. On the contrary, detector locations 3, 6, and 9 which displayed minimum differences in Figure 6-2, had significant differences for the high activation obscuration detectors.
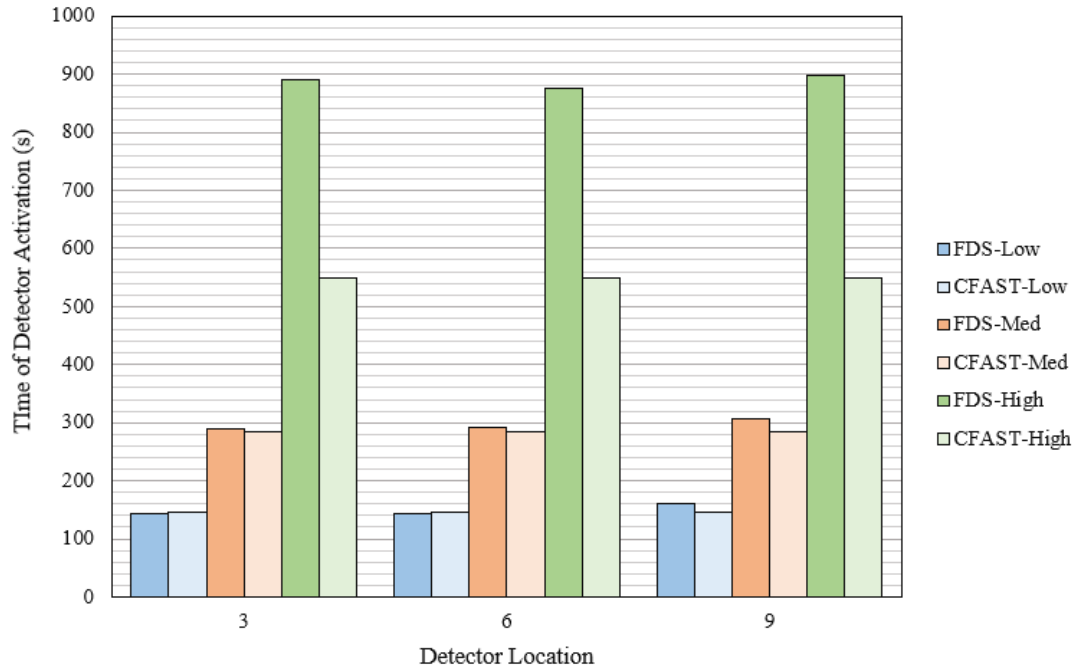
Figure 6-2: Detector response times for 8x36 ft configuration.

The detection times for CFAST is plotted on the x-axis and the averaged FDS detection times are plotted on the y-axis, as shown in Figure 6-3. The error bars represent two times the standard deviation of the FDS detector times. A linear trendline, with an intercept of zero and a slope of 1.47, was applied to the data. The first two data points, detection obscuration levels of low and medium, have nearly perfect agreement and fall into a slope of 1. However, for the high obscuration activation detectors, the difference between FDS and CFAST is significantly larger. This is also shown in Figure 6-2. The large difference between FDS and CFAST, for the high obscuration activation detector, may misrepresent the overall slope of the trendline and influence it to be larger than what it may actually be for the lower and medium activation detectors.
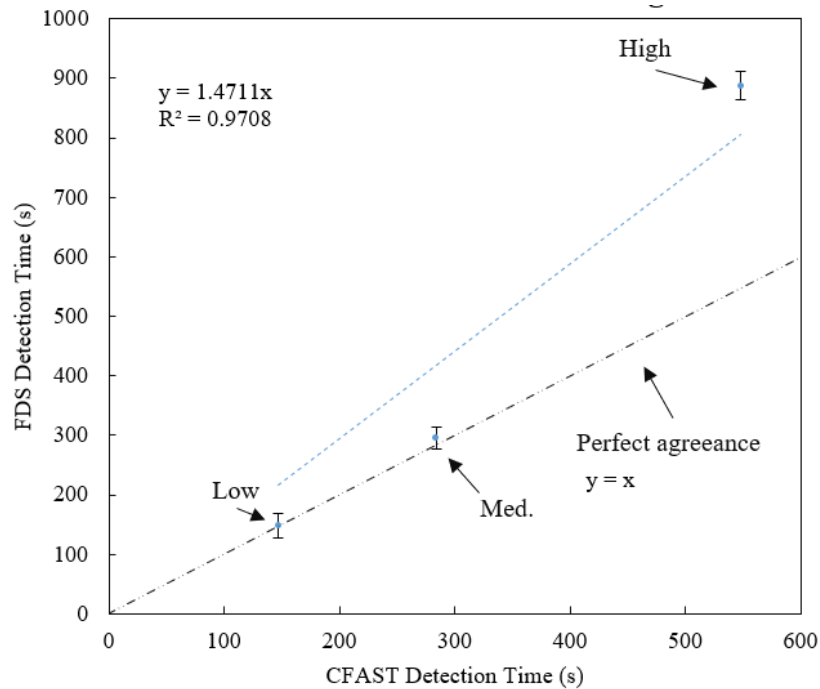
Figure 6-3: CFAST versus FDS detector response times for 8x36 ft configuration.

6.1.1.2: 16x36 ft Compartment Detector Responses

The low activation obscuration detectors in the 16x36 ft configuration show good agreement for all detector locations, as shown in Figure 6-5. The Smokeview model for the 16x36 ft compartment is shown in Figure 6-4. As shown, locations 2, 3, 5, 6, 8, and 9 are only present within the compartment. The snapshot of the soot density within the compartment was taken at 400 seconds.
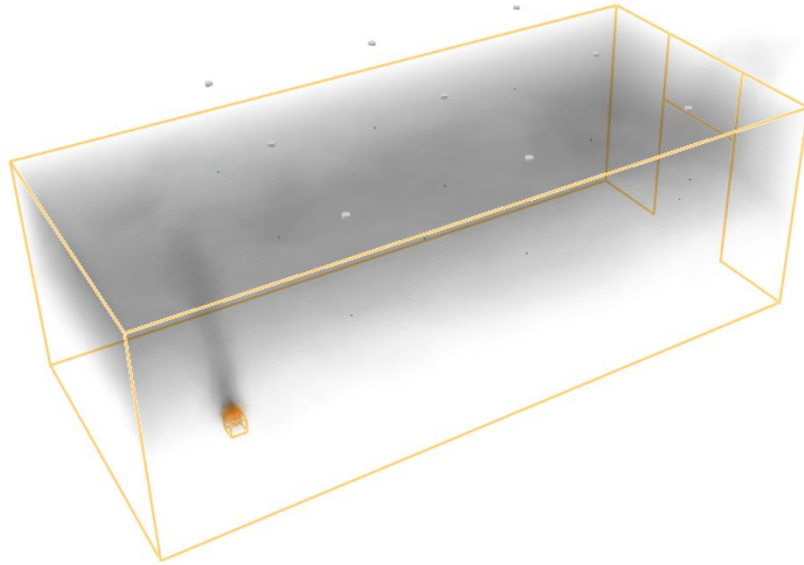
Figure 6-4: Smokeview model of 16x36 ft compartment at 400 seconds.

Detector location 8 had the largest difference between CFAST and FDS, which was about 35 seconds. The other detector locations show agreement amongst CFAST and FDS, with a time difference no greater than 15 seconds. For the medium activation detectors, a greater difference amongst FDS and CFAST is present, as shown in Figure 6-5. For all detector locations, except for location 8, FDS predicts detector activation before CFAST by a difference ranging from 10 to 28 seconds. Similar to the 8x36 ft configuration, the high activation obscuration detectors activate much later in FDS than CFAST for all detector locations, as shown in Figure 6-5. The difference in activation time, for high obscuration detectors, ranges from 35 to 106 seconds.
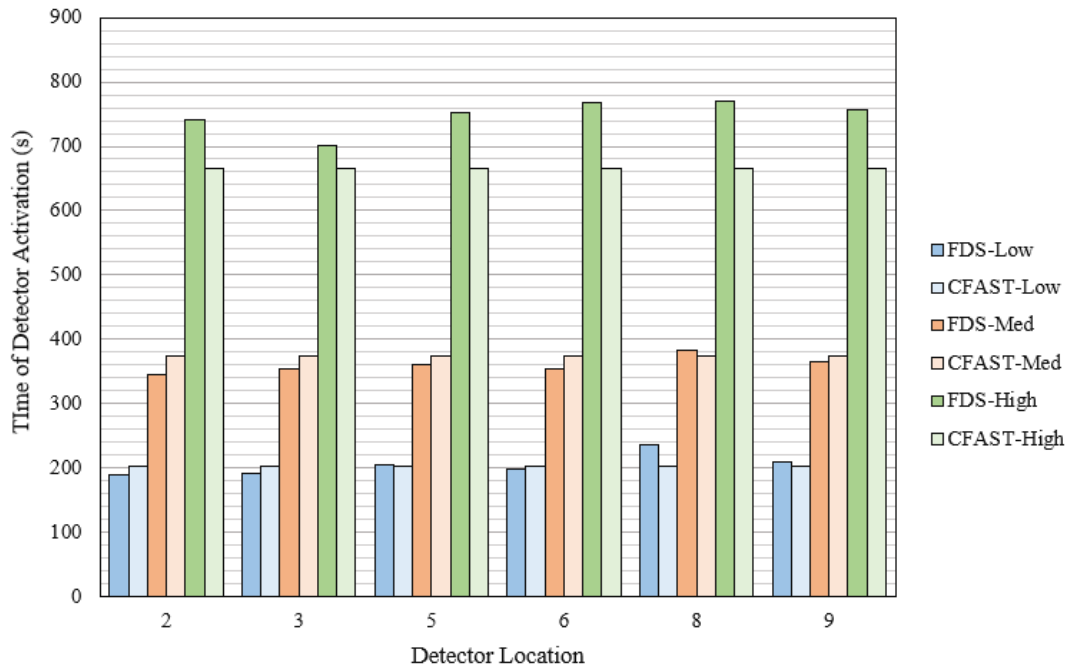
Figure 6-5: Detector response times for 16x36 ft configuration.

The CFAST activation times are plotted on the x-axis and the averaged FDS activation times, per obscuration activation level, is plotted along the y-axis as shown in Figure 6-6. The error bars represent two times the standard deviation of the FDS activation times. Similar to the 8x36 ft configuration, the low and medium detectors fall along the slop y = x, which shows near perfect agreement between CFAST and FDS. The high activation obscuration detectors fall slightly over the line of perfect agreeance, creating trendline with a slope of 1.08. However, the disagreement between CFAST and FDS is not as large in the 16x36 ft configuration as the 8x36 ft configuration because the slope is closer to 1.
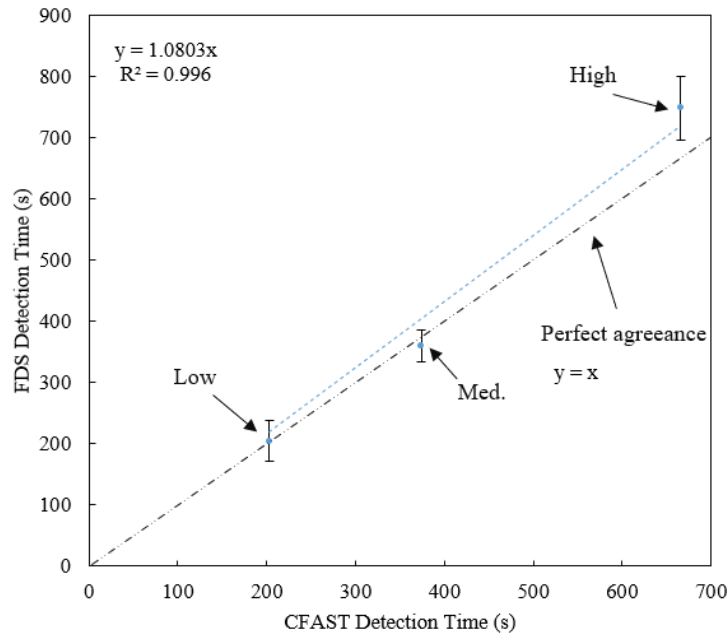
Figure 6-6: CFAST versus FDS detector response times for 16x36 ft configuration.

6.1.1.3: 24x36 ft Compartment Detector Responses

In the 24x36 ft compartment, FDS and CFAST have reasonably good agreement for detectors with low activation obscuration. The Smokeview model is shown in Figure 6-7. In this configuration, all nine detector locations are present within the compartment. The smoke view model is presented as a visual confirmation that the 24x36 ft configuration model was setup and runs correctly, such as ensuring the doorway and the detectors are all placed within the compartment.

Figure 6-7: Smokeview model of 24x36 ft compartment at 400 seconds.

In Figure 6-8, for low obscuration detectors, locations 3 and 6, are the only locations where FDS predicts activation before CFAST. This is because these locations are near the burner and are activated due to the ceiling jet, which would reach the detector before the optical density of the upper layer attains activation levels in CFAST. Fo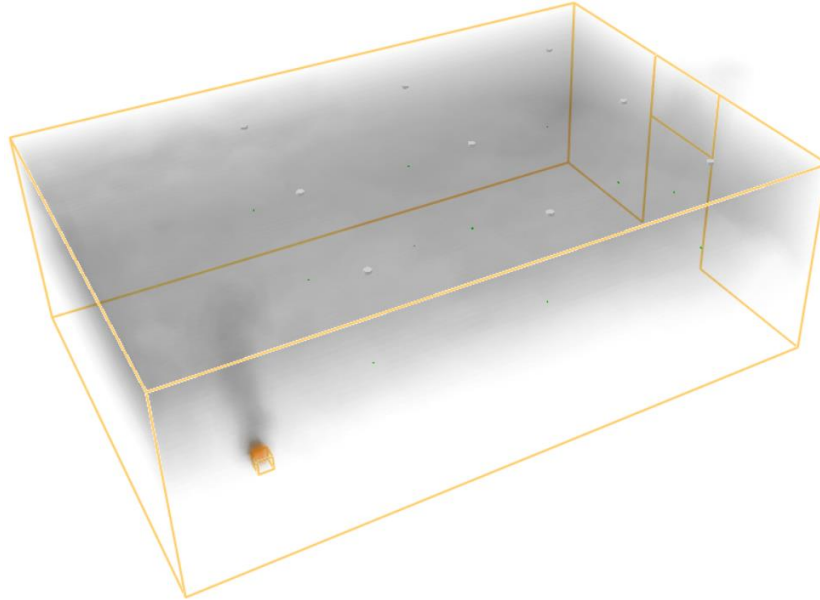r the medium activation detectors, as shown in Figure 6-8, FDS predicts activation before CFAST for the majority of detector locations. FDS activation for detector locations 1, 3, 6, and 9 activate significantly quicker than CFAST. These locations are close to the detector and are along the junction between the walls. Due to the burner being located in the corner, the ceiling jet flows along that junction and initially pools around the area and corner before spreading along other areas of the ceiling. This may be why those locations activate quicker in FDS than CFAST.

The high activation detectors, as shown in Figure 6-8, follow similar trends of the 8x36 ft and 16x36 ft configurations, where the majority of FDS predicted detectors activate

after CFAST predicts activation. Although, not as significant as the 8x36 ft and 16x36 ft configurations, the high obscuration detectors for FDS activate after CFAST. However, similar to the medium obscuration detectors, locations 3, 6, and 9 shows the closest agreement to CFAST for the high obscuration detectors. This further suggests that the ceiling jet and smoke accumulating at the wall/ceiling junctions, modeled in FDS, are responsible for earlier localized activation times.

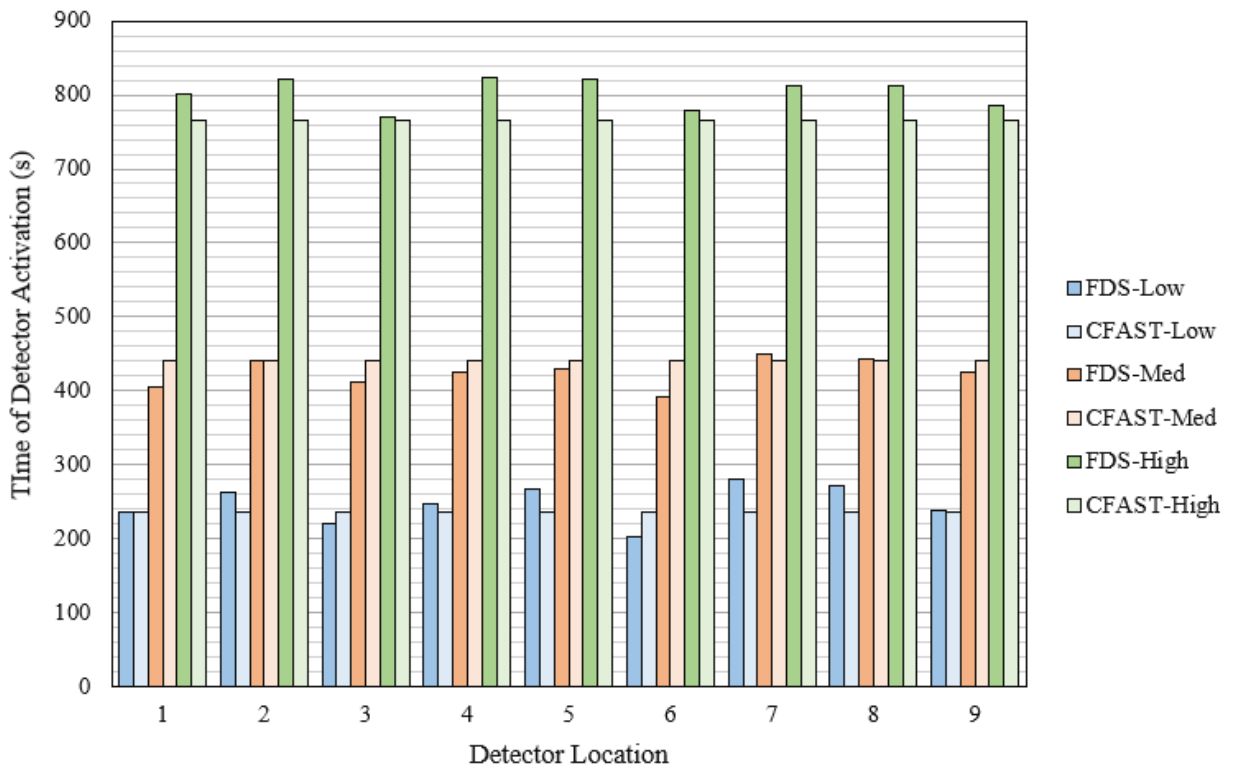**Figure 6-8: Detector response times for 24x36 ft configuration.**

A linear trendline, with a slope of 1.0285, was determined for the 24x36 ft compartment shown in Figure 6-9. CFAST and FDS show almost perfect agreement since the slope is close to 1. For FDS, the low activation detectors have an average time of 247 seconds and two times the standard deviation of 51 seconds; the medium activation

detectors have an average time of 425 seconds and two times the standard deviation of 39 seconds; finally, the high activation detectors have an average time of 803 seconds and two times the standard deviation of 40 seconds. Both the low and medium detectors fall close to the perfect agreement line, with the high activation detector falling slightly above it. This trend, although not as significant in this configuration, is also seen in the 16x36 ft and 8x36 ft compartments.

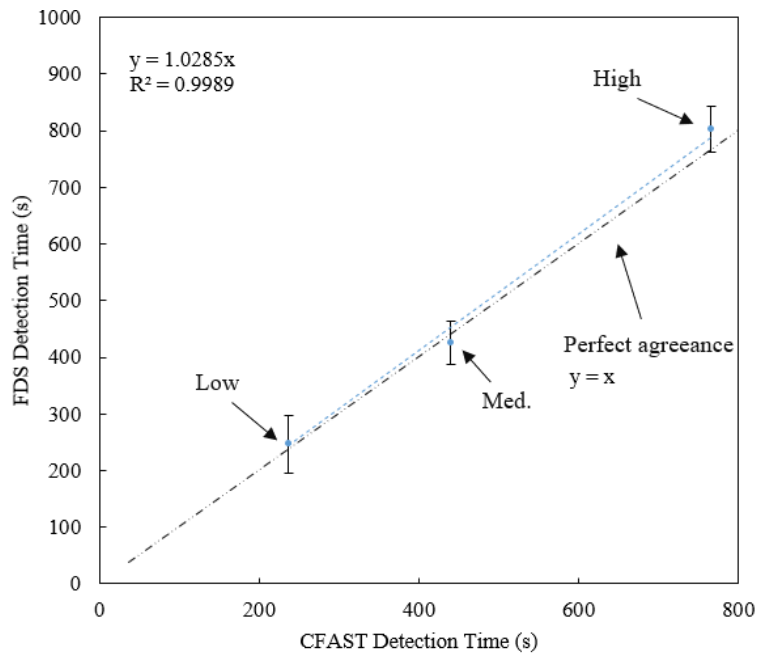**Figure 6-9: CFAST versus FDS detector response times for 24x36 ft configuration.**

6.1.1.4: 36x36 ft Compartment Detector Responses

The Smokeview model for the 36x36 ft configuration is shown in Figure 6-10. In this configuration, all nine detector locations are present within the compartment. The soot density and HRR of the fire is shown in Smokeview as a visual confirmation that the model was setup correctly.
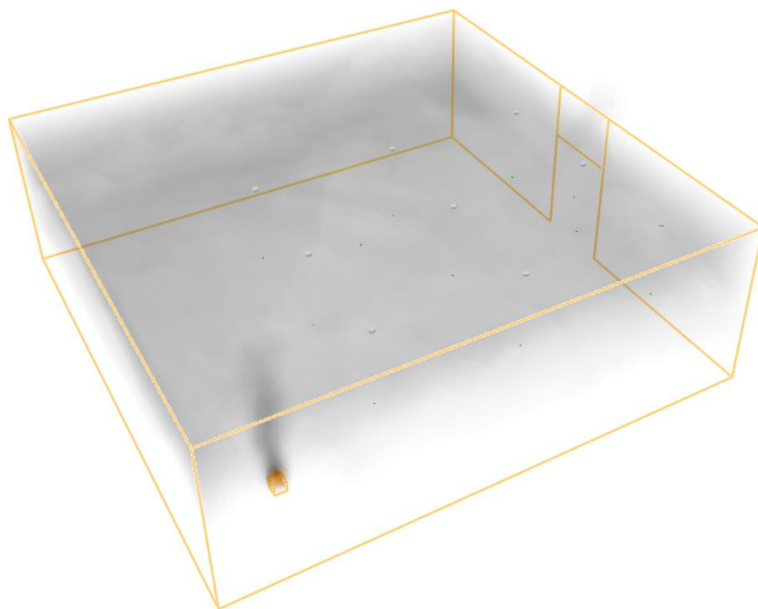
Figure 6-10: Smokeview model of 36x36 ft compartment at 400 seconds.

For the 36x36 ft configuration, the low activation obscuration detectors activate quicker in CFAST than FDS, except for detectors 3 and 6 shown in Figure 6-11. Overall, for the low activation detectors, FDS and CFAST predicted closely to each other with only a difference in activation times ranging from about 5 to 60 seconds. For the medium activation detectors, as shown in Figure 6-11, agreement is also good between CFAST and FDS. The difference between activation times ranges from around 6 to 75 seconds.

The high activation detectors, as shown in Figure 6-11, have a difference in acivation times ranging from about 10 to 50 seconds. Similar to the 24x36 ft configuration, high obscuration detectors in FDS activates before CFAST in locations 3, 6, and 9. This may be due to the larger compartment and a delay of diffussion from smoke into other areas of the compartment. Since locations 3, 6, and 9 are all located along the wall near the burner, smoke would initally collect along the junction of the wall and ceiling before

diffussing across the rest of the room. Smoke buildup in those spaces must be quicker than the overall upper layer buildup of soot calculated in CFAST, hence FDS activating quicker at those locations.
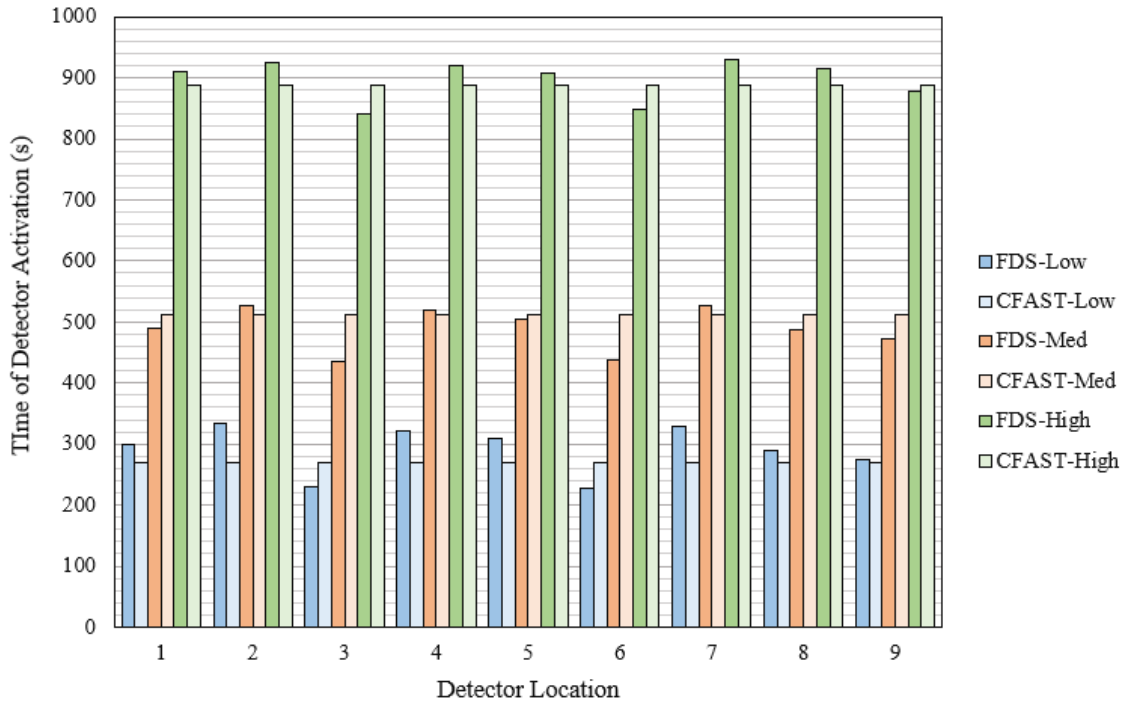
Figure 6-11: Detector response times for 36x36 ft configuration.

A linear trendline was fit to the data, where the averaged location times are plotted along the y-axis and the CFAST times along the x-axis, as shown in Figure 6-12. A slope of 1.161 was determined with an intercept of zero. The averaged detector times for the low, medium, and high obscuration levels are 290, 489, and 897 seconds, respectively. Each obscuration level also has error bars that are two times the standard deviation, which are 79, 70, and 67 seconds, respectively. Surprisingly, both the low and medium activation obscuration detectors fall slightly above the perfect agreement line, which is different than that of the previously discussed configurations above. However, similar to the other

configurations, the high obscuration detector falls above the perfect agreement line. Although not perfect, a slope of 1.16 shows reasonable agreement between CFAST and FDS.
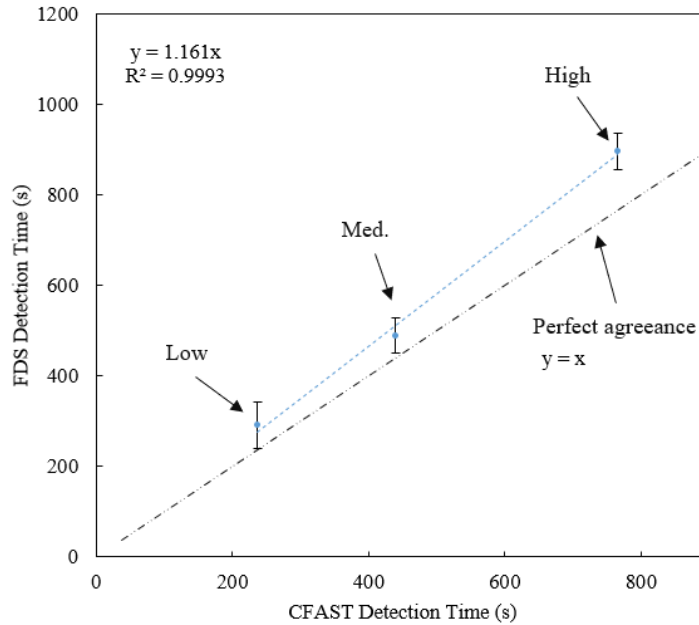
Figure 6-12: CFAST versus FDS detector response times for 36x36 ft configuration.

6.1.1.5: Conclusion of Detector Responses

Overall, CFAST and FDS have good agreement in detection times. The slopes of the linear trendlines ranged from 1.0285 to 1.4711, with the 24x36 ft and 36x36 ft configurations having a slope closest to 1. Therefore, larger compartments, with larger aspect ratios, have been shown to have a slope closer to 1, and thus better agreement overall. The low and medium obscuration detectors have near perfect agreement, falling on/or close to a slope of 1 for the 8x36, 16x36, and 24x36 ft configurations.

The absolute difference, or error, between FDS and CFAST was calculated and is organized per obscuration activation level and per compartment, as shown in Figure 6-13.

The low and medium obscuration had minimal differences in the 8x36 ft, 16x36 ft, and 24x36 ft configurations, ranging from 1 to 50 seconds. The 36x36 ft compartment has low and medium differences ranging from 5 to 80 seconds. This slightly higher range of difference can be attributed to the larger ceiling area of the compartment.
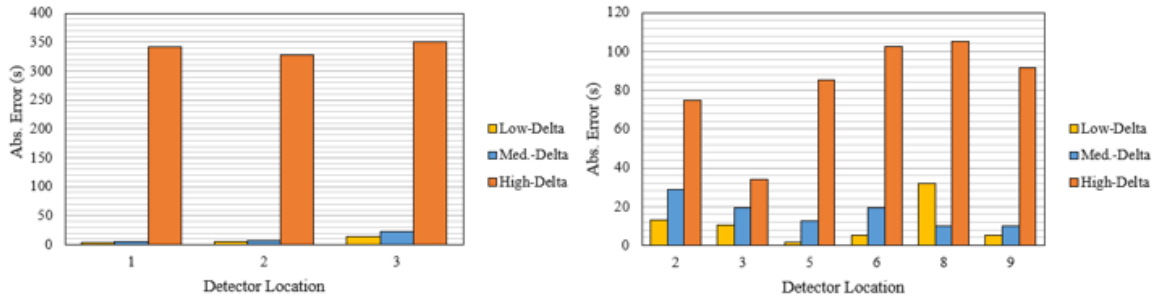
Figure 6-13: Abs. error between CFAST and FDS for 8x36 ft (left) and 16x36 ft (right) compartments.

The high obscuration detectors are typically where the gap in CFAST and FDS detection times vary the most, as shown in Figure 6-13 and Figure 6-14. This can be seen in all four of the tested configurations, where the differences between CFAST and FDS ranged from 11 to 350 seconds, for all compartments. However, agreement between CFAST and FDS appeared to get better for the high obscuration detectors at larger compartments. As shown in Figure 6-14, the maximum difference in the 36x36 ft compartment for high obscuration detectors is about 50 seconds, as compared to the 350 second difference in the 8x36 ft compartment.
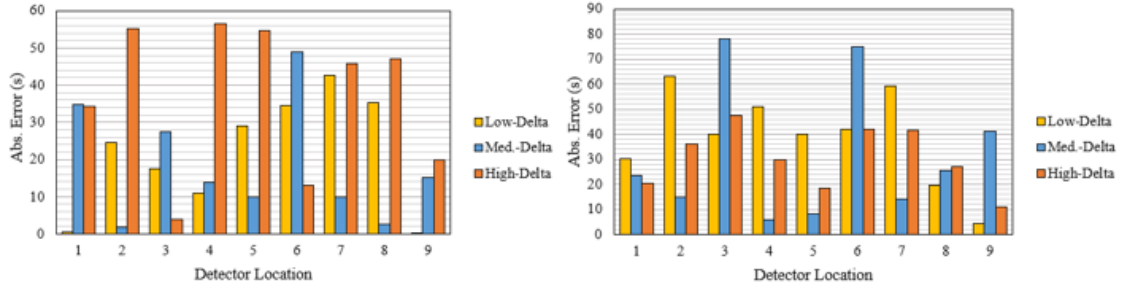
Figure 6-14: Abs. error between CFAST and FDS for 24x36 ft (left) and 36x36 ft (right) compartments.

6.1.2 Analysis of Smoke Properties

The predicted detection times for both CFAT and FDS are discussed below for each room configuration. Additional smoke properties, such as the optical density, soot concentrations, average layer height are also logged as a function of time.

6.1.2.1 8x36 ft Compartment Smoke Properties

The total soot in the compartment, as a function of time, is plotted in Figure 6-15. Both CFAST and FDS curves follow the same shape and start with a total soot of 0 kg. However, FDS begins to diverge from CFAST at around 65 seconds. The total soot in the compartment peaks at 0.0022 kg for CFAST and 0.0015 kg for FDS. The difference in soot between CFAST and FDS, at the peak, is 7E-4 kg, or 0.7 g.
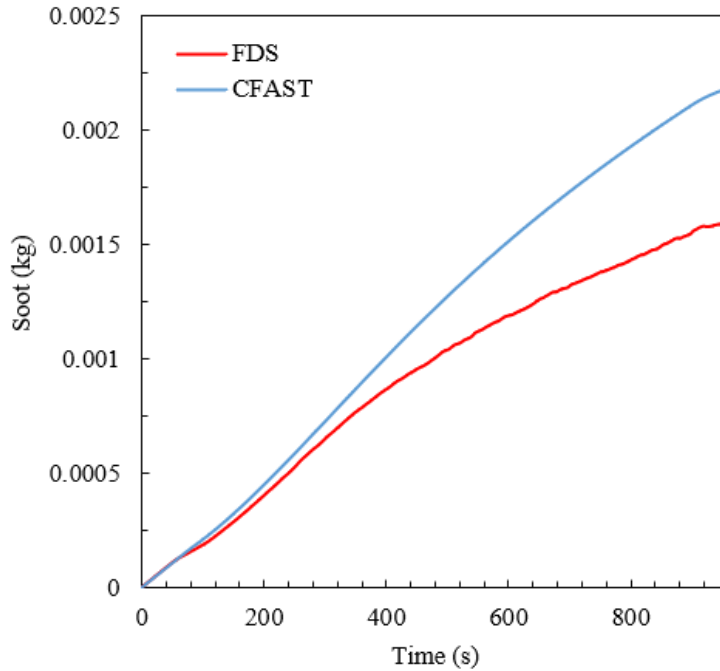
Figure 6-15: Total soot in the 8x36 ft configuration.

The optical density is plotted as a function of time, as shown in Figure 6-16. As in Figure 6-16, the optical density of FDS tends to diverge and peak at a lower value than CFAST. However, this divergence occurs at around 250 seconds. The optical density peaks to 0.1 m^{-1} for FDS. For CFAST, the peak occurs at 960 seconds, with an optical density of 0.16 m^{-1}. Using [26] (4-16), the difference in obscuration levels between CFAST and FDS can be calculated at 960 seconds. For CFAST, the obscuration level is around 30.8% per m or 9.40% per ft. For FDS, the obscuration level is around 20.57% per m or 6.27% per ft, resulting in a difference of 10.23% per m or 3.13% per ft between CFAST and FDS.
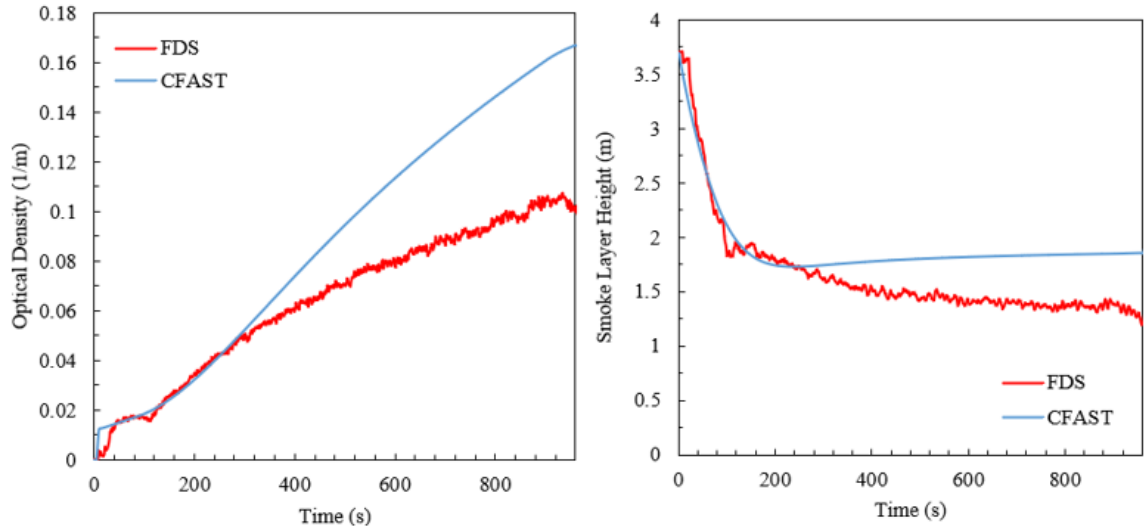
Figure 6-16: Optical density (left) and layer height (right) for 8x36 ft configuration.

On average, the smoke layer height of FDS is lower than that of CFAST, as shown in Figure 6-16. Both models follow a similar decrease in layer height up until 250 seconds, where FDS diverges away from CFAST and decreases towards a lower layer height. FDS settles at a layer height of around 1.5 m and CFAST has a steady layer height of 1.75 m, resulting in a 0.25 m layer height difference. Both models see a sharp increase in layer height at around 960 seconds, which is when the fire starts to decay. This extinction of the fire means that soot is no longer being produced, but soot is still leaving the room, leading to the increase in layer height. FDS has an overall lower layer height than CFAST.

6.1.2.2: 16x36 ft Compartment Smoke Properties

The total soot of the compartment is plotted as a function of time for FDS and CFAST, as shown in Figure 6-17. Both models follow a similar trend, as shown in the 8x36 ft compartment of Figure 6-15. FDS peaks at a soot concentration of 0.0035 kg and CFAST peaks at a soot concentration of 0.0043 kg. The difference between the peak soot

concentration is similar to that of the soot concentration shown in the 8x36 ft compartment. The difference between the peak soot concentration is roughly 8E-4 kg or 0.8 g.
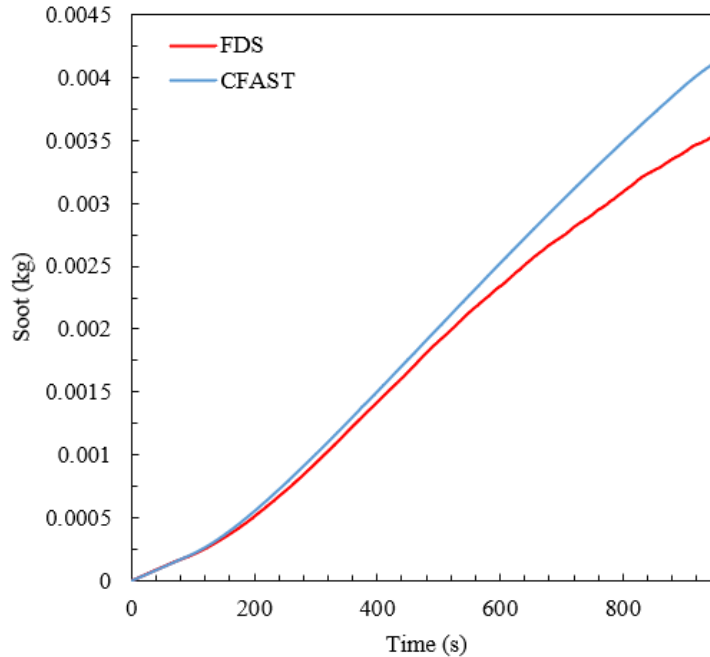
Figure 6-17: Total soot in the 16x36 ft configuration.

The average optical density at the detector locations is plotted as a function of time, as shown in Figure 6-18. Similar to the 8x36 ft compartment, both CFAST and FDS follow a similar trend to each other. However, in the 16x36 compartment, the optical density for both models follow closely up until about 520 seconds, where FDS diverges to a lower optical density. This follows a similar trend as the 8x36 compartment, where FDS diverges towards a lower optical density. However, in this configuration, both models closely follow each other for 520 seconds as compared to the 250 seconds from Figure 6-16. At 960 seconds, the optical density is at 0.15 m^{-1} for CFAST 0.12 m^{-1} for FDS. Using [26] (4-16) the obscuration is 29.21% per m or 9.01% per ft for CFAST and 24.14% per m or 7.45% per ft for FDS. The difference between CFAST and FDS is 5.07% per m or 1.56% per ft.

Despite having a similar difference in soot concentration, the difference in optical density is about half of the optical density difference from the 8x36 ft compartment. This may be due to a larger compartment volume, where a zone model assumption is more applicable because the mixture of flows from the fire plume and the vent are more negligible in larger open rooms. Therefore, devices that are sensitive to flow and location, such as optical density devices or detectors, can be somewhat accurately represented in a zone model under uniformly spatial dependent flow conditions.
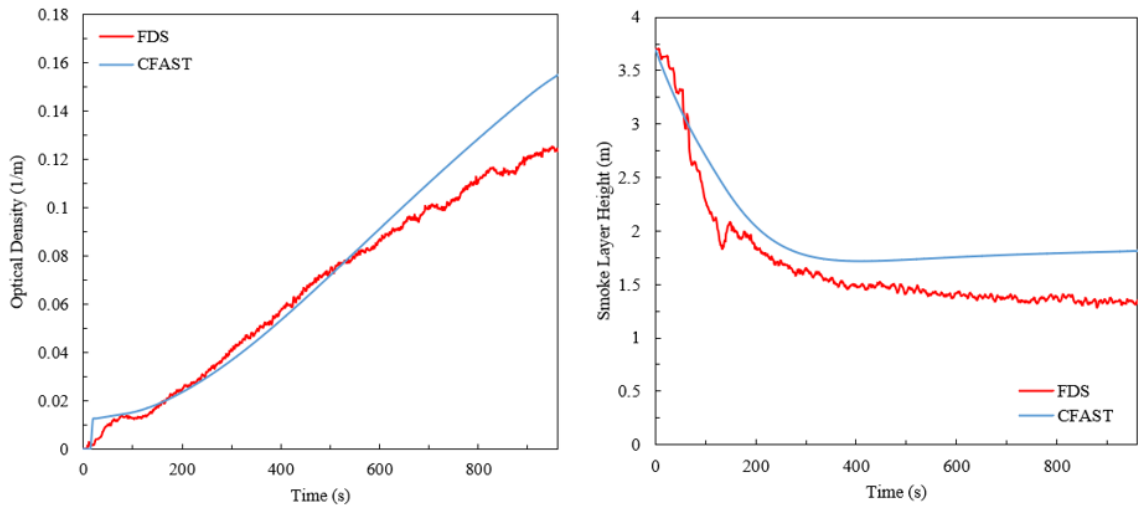
Figure 6-18: Optical density (left) and layer height (right) for 16x36 ft configuration.

The average layer height of the smoke layer is plotted as a function of time, as shown in Figure 6-18. Both CFAST and FDS models follow a similar curve. However, unlike that of the 8x36 ft compartment, the models diverge from each other at around 100 seconds as opposed to the 250 seconds. Consistent to the 8x36 ft configuration, the FDS layer height is lower than that of the CFAST model. Similarly, the difference between the layer heights, once they both plateau, is around 0.25 m. An overall lower smoke layer height may have some contribution in having a lower soot concentration. However, due to

the consistencies in layer height differences, but inconsistencies in the soot and optical density differences, layer height shows it has a negligible effect on the optical density and soot concentration, as evidenced by this configuration.

6.1.2.3: 24x36 ft Compartment Smoke Properties

The total soot in the 24x36 ft compartment is shown in Figure 6-19. Both CFAST and FDS follow similar curves in soot concentration. Similar to the previously discussed compartments, FDS underpredicts the amount of soot, when compared to CFAST. However, the divergence of the two models occurs much later, at a time of around 600 seconds. The peak in soot for both models occur roughly at the same time of fire extinction, at around 960 seconds. At this peak, the largest amount of soot is 0.00575 kg for CFAST and 0.00525 kg for FDS, resulting in a total difference of 5E-4 kg or 0.5 g. This is slightly less than the difference in soot concentration for the 8x36 ft and 16x36 ft compartment, which was 0.7 g and 0.8 g respectively.
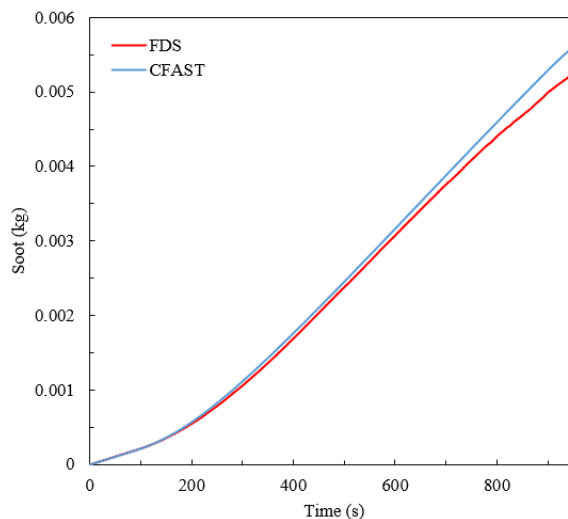
Figure 6-19: Total soot in the 24x36 ft configuration.

74

The optical density for FDS and CFAST, plotted as a function of time, is shown in Figure 6-20. CFAST and FDS follow similar curves. However, FDS begans to diverge at around 700 seconds. Similar to the previous compartments, a break in the curve occurs at the fire extinction time of around 960 seconds. At this time, the optical density is 0.14 m^{-1} for CFAST and around 0.12 m^{-1} for FDS. Using [26] (4-16), the obsucration level for CFAST is 27.56% per m or 8.4% per ft and for FDS is 24.14% per m or 7.36% per ft. This results in an obsucration level difference of 3.42% per m or 1.04% per ft. This difference is less than the difference of the previously discussed configurations above.
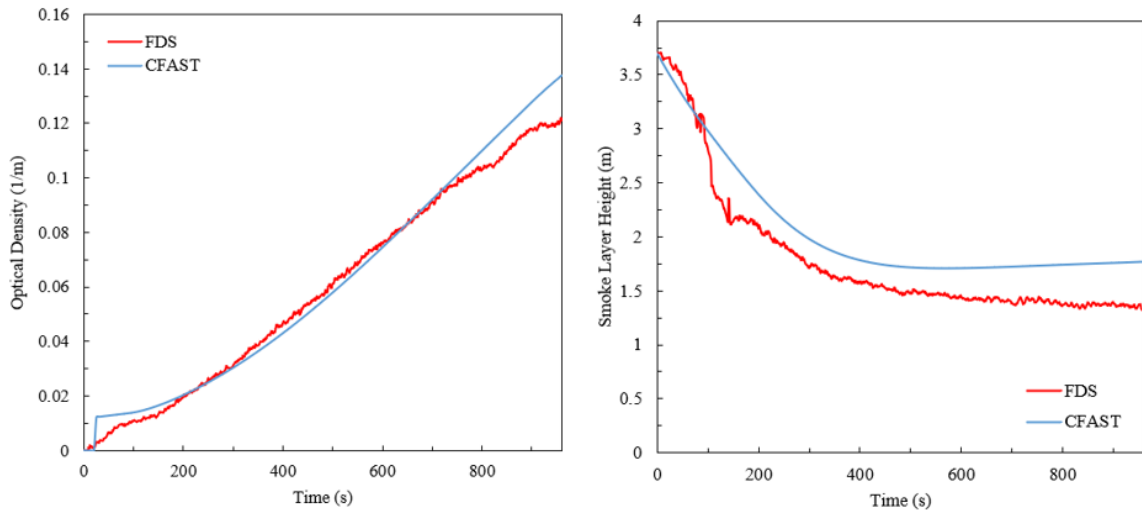
Figure 6-20:Optical density (left) and layer height (right) for 24x36 ft configuration.

The layer height, comparing CFAST and FDS, for the 24x36 ft configuration is plotted as a function of time shown in Figure 6-20. The layer height for FDS and CFAST began to diverge at around 100 seconds, where FDS plateaus at around 1.5 m and CFAST plateaus at around 1.75 m. The smoke layer height, in FDS and CFAST, remains consistently constant when compared to the previously discussed configurations. Thus, it

appears that it has negligible effect on the actual soot and optical density differences between the two models.

6.1.2.4: 36x36 ft Compartment Smoke Properties

The 36x36 ft compartment represents an aspect ratio of 1 and is the largest compartment of the four comparable configurations. The soot concentration is plotted as a function of time, as shown in Figure 6-21. The soot concentration for FDS and CFAST match well with each other. Minimum divergence appears to occur only at the peak of the curve, where the fire becomes extinct at 960 seconds. The 36x36 ft compartment, out of all the other three configurations, has the least amount of difference in soot concentration between the two models. Similarly, a common trend is that the larger the compartment, the lower difference in soot concentration between the models.
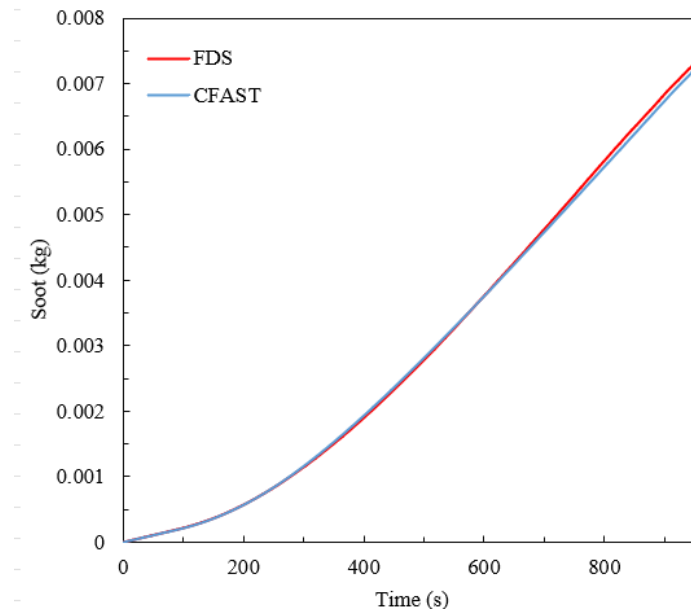
Figure 6-21: Total soot in the 36x36 ft configuration.

Similarly, the optical density curves between the two models match well, as shown in Figure 6-22. The divergence between the two models appears to occur at around the extinction time of 960 seconds. The difference in optical density at this time is negligible, thus the obscuration level difference is also negligible. Similarly, the larger the compartment such as the 36x36 ft configuration, has shown a smaller difference in optical density.
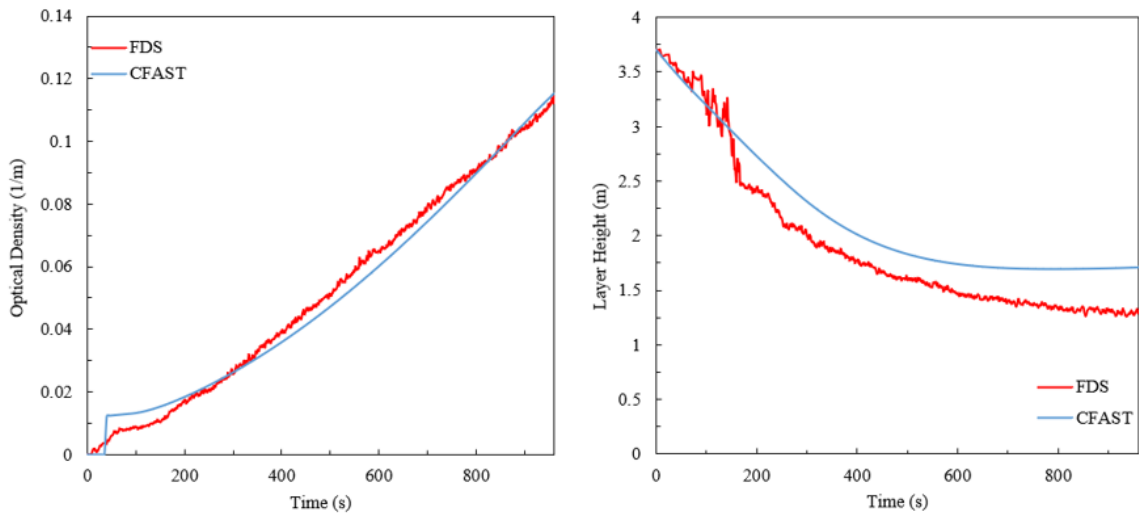
Figure 6-22: Optical density (left) and layer height (right) for 36x36 ft configuration.

The layer height, shown in Figure 6-22, is plotted for FDS and CFAST as a function of time. The difference and values of this smoke property seems to be the most consistent amongst the change in room configurations. The FDS model begins to diverge from the CFAST model at around 150 seconds, where FDS plateaus at a smoke layer height of around 1.25 to 1.5 m and CFAST plateaus at around 1.75 m. This plateau height and time of divergence is similar to that of the previous configurations, with the exception of the 8x36 ft configuration having a slightly longer time until divergence. Overall, the layer height at steady state is expected to be constant because it is mainly a function of the area

of the doorway rather than a function of the room size or aspect ratio. The room size or aspect ratio appears to only affect the time of divergence, as displayed in the 8x36 ft configuration.

6.1.2.5: Smoke Property Error Analysis between Compartment Configurations

This section covers an analysis comparing the error between CFAST and FDS of the smoke properties. Because the timesteps of FDS are largely dependent on the spatial resolution of the CFD model, the timesteps are often mismatched from that of CFAST. CFAST can log output values per a pre-defined timestep; which in this case was five seconds. This makes it difficult to compare the values of these smoke properties as a function of time since CFAST and FDS timesteps are misaligned. However, since FDS has a smaller timestep than CFAST, the smoke properties from FDS were linearly interpolated at the CFAST time such that FDS and CFAST match accordingly. A relative error for smoke properties, i, where $i = 1, 2,$ and 3 for the optical density, soot concentration, and layer height receptively can be calculated as

$$Error_{rel} = \frac{|CFAST_i - FDS_i|}{CFAST_i} \quad \text{(6-1)}$$

The relative error of the soot concentration and optical density in the compartment is calculated and shown in Figure 6-23. The relative error of the soot concentration occurs at a time of 960 seconds at around 0.27 or 27% for the 8x36 ft configuration. As the compartment increases in volumetric size and aspect ratio, the error between FDS and CFAST decreases. At the same time, the relative error between CFAST and FDS for the 16x36 ft compartment is 0.14 or 14%; for the 24x36 ft compartment is 0.067 or 6.7%; and

for the 36x36 ft compartment is 0.014 or 1.4%. The relative error between the four compartments ranges from 5% to 60%.

Similarly, the relative error in optical density captures a similar trend. All compartments have an initial high relative error, from the slight delay in which CFAST reports an optical density of zero and FDS does not. Assuming that FDS and CFAST have similar layer thickness and soot concentration at the beginning, as evidenced by Figure 6-15, Figure 6-17, Figure 6-19, and Figure 6-21, the slight delay difference in CFAST can be attributed to a uniform upper layer. Since CFAST models a uniform upper layer, the total amount of soot in the upper layer per volume of layer thickness means that the overall soot concentration is spread throughout the layer evenly. This can lead to CFAST not reaching a significant soot mass concentration at the beginning. Thus, the optical density of the upper layer starts off at or close to zero.

Since FDS is a CFD model, the soot concentration is thermally driven, where a larger amount of soot accumulates closer to the ceiling. Therefore, for the same total amount of soot in the upper layer, a larger percentage of the soot will end up at near the ceiling. Thus, the optical density sensors in FDS report larger amounts of optical density at the very beginning.

Regardless, the relative error for optical density converges at around 200 seconds, where then each configuration's error diverges. The largest relative error occurs at 960 seconds. The 8x36 ft configuration has a relative error of 0.40 or 40%; the 16x36 ft configuration has an error of 0.196 or 19.6%; the 24x36 ft configuration has an error of 0.118 or 11.8%; and the 36x36 ft configuration has an error of 0.24 or 2.4%. The relative error in optical density has a range of error from 2.4% to 40%. Like the relative error in

total soot, the relative error in optical density follows a similar trend where the larger the compartment, the smaller relative error between CFAST and FDS.
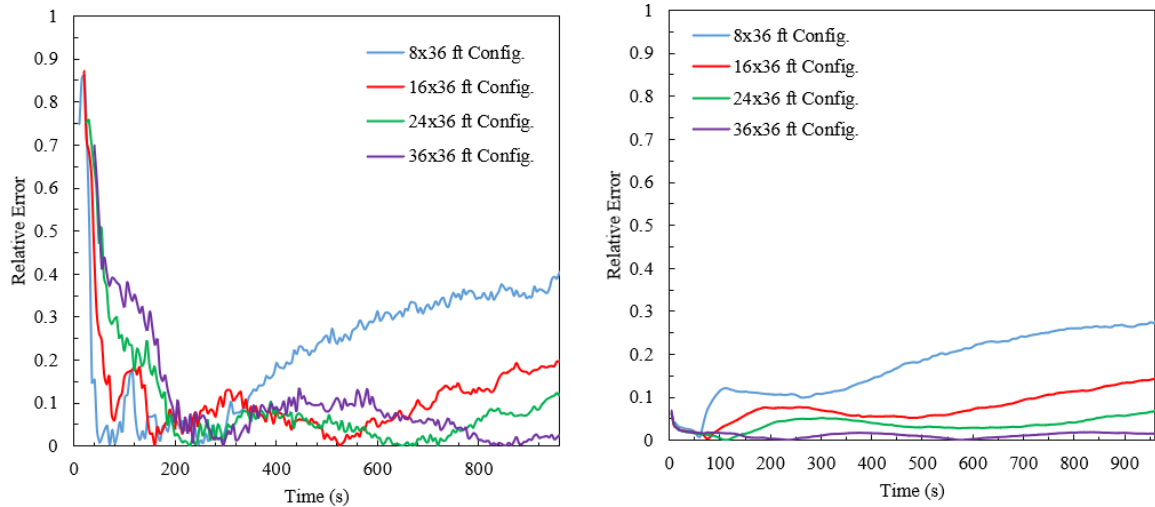
Figure 6-23: Relative error in total soot (left) and optical density (right).

The relative error for the layer height, for all four configurations, is shown in Figure 6-24. The overall relative error match well to each other, which is shown by the consistent smoke layer heights in FDS and CFAST, regardless of the configuration. When compared to the relative error of the other smoke properties, the smoke layer height has the tightest error range. The largest relative error occurs at 0.338 or 33.8% for the 8x36 ft configuration; then the 16x36 ft and 24x36 ft configuration at 0.24 or 24; and the least amount of error in the 36x36 ft configuration at 0.2385 or 23.8%. The error range for the smoke layer height is between 23.8% and 33.8%, which shows that smoke layer height is not heavily impacted by the size and aspect ratio of the room.
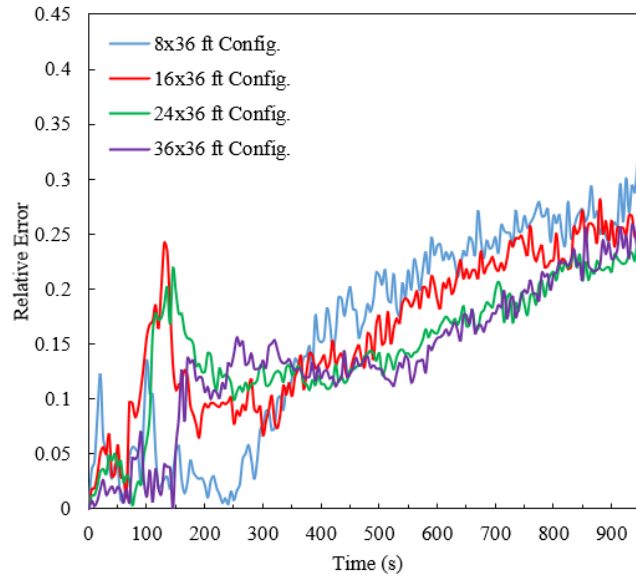
Figure 6-24: Relative error in layer height.

6.1.3: Conclusion of Aspect Ratio

The main biases between FDS and CFAST, based on the four having a different aspect ratio, appear to occur under two conditions: high obscuration activation detectors in smaller comapartments and medium/high obsucration activation detectors for specific locations in larger compartments.

In the smaller compartments, i.e. the 8x36 ft and 18x36 ft compartments, the high obscuration detectors varied the most as opposed to the low and medium obscuration detectors. This can be supported by the the soot concentration and optical density plots, where an inverse relationship to the larger aspect ratio and/or larger volumetric rooms size yields smaller discrepancies between FDS and CFAST. A smaller room, such as the 8x36 ft configuration has an aspect ratio of 0.22, displays a larger error between CFAST and FDS. This is more prevalent at later times in which the optical density and soot

81

concentration differ more than what is shown in a larger room with a larger aspect ratio, such as the 24x36 ft or 36x36 ft configuration.

This larger deviation, typically at later times, means that the high obscuration detectors are affected more because of the deviation occurring at higher optical density and soot concentrations. The reason for this deviation may be partly due to the uniform upper layer that is modeled in CFAST. At later times, the uniform layer does account for gradients and spatial mixtures between layers, which can lead to a higher soot concentration and optical density. On the other hand, FDS does not model a uniform upper and lower layer. Instead, FDS models the spatial flow mixture and gradient of the smoke, which may be more heavilty influenced by the size of the doorway and the smaller volume of the compartment, especially at steady state. Therefore, at later times, CFAST would predict larger concentrations of soot than FDS. This difference could be the explanation as to why there is an overall quicker activation of the high obsucration detectors in CFAST, but not in FDS. The low and medium detectors appear not to be as affected by the doorway and smaller volume. As a matter of fact, the smaller volumetric size of the compartment appears to allow the initial ceiling jet to diffuse across the ceiling and create an upper smoke layer quite quickly in FDS. This would explain the almost, exact agreement between the two models for low and high obscuration detectors in the 8x36 ft and 16x36 ft compartments. However, once higher concentrations of soot are required to activate the higher obscuration detectors, disparity between CFAST and FDS occurs due to the doorway size and/or volumetric size of the compartment.

As shown by the soot concentration and optical density error plots, the larger compartments show less differences between CFAST and FDS, on average. The 24x36 ft

compartment shows the best agreement amongst CFAST and FDS because none of the low, medium, or high ohscuration detectors at any location surpasses a difference of 60 seconds. The 36x36 ft compartment, on average, shows good agreement. However, larger errors typically occured at certain locations, where FDS activates before CFAST, such as the medium obscuration detectors in location 3, 6, and 9, which have the highest differences ranging from 40 to 80 seconds. For both the 24x36 ft and 36x36 ft compartment, larger deviations in activation times mostly occurres under instances where FDS activates before CFAST. In FDS, the ceiling jet tends to move along the junction of the wall and around the perimeter of the room, causing localized activation in FDS at sites 3, 6, and 9. At the same time, in CFAST, the soot concentration is overall lower because of the larger ceiling area, and thus layer volume that is taken into account. Therefore, this causes FDS to activate before CFAST for medium obscuration levels.

Overall, the 24x36 ft configuration displays the least amount of errors between the two models; the 36x36 ft configuration exhibits slight errors in certain locations, but overall shows good agreement; the 8x16 ft and 16x36 ft configurations display good agreement in only the low and medium obscuration detectors. Better agreement displayed in the larger compartments could be a result of the larger volumetric area, which was unaccounted for when changing the aspect ratio of the room. The other hypothesis is that the area of the vent relative to the size of the room may play a larger role than the actual aspect ratio of the room. Thus, for compartments having the same doorway dimensions, smaller compartments may have more deviations in FDS and CFAST than larger compartments. Therefore, an analysis of changing doorway areas, while keeping the volumetric size of the room constant is discussed further in section 6.2: Doorway Area Compartment Variations.

In general, biases between the two models occur in high obscuration detectors for the 8x36 ft and 16x36 ft compartments, but not for the low and medium obscuration detectors. In FDS, the small ceiling area facilitates fast diffusion of the ceiling jet and essentially creates an upper layer of smoke, similar to that of CFAST; hence the good agreement between the two models for low and medium obscuration detectors. However, at higher obscuration detectors, where more soot is required for activation, a fluctuation of soot concentration occurs between the two models either to volumetric compartment size and/or doorway area. The other bias occurs in the 24x36 ft and 36x36 ft compartments. For certain locations, localized detector activation occurs in FDS resulting in FDS activating before CFAST. These detector locations are typically along the junction of the ceiling and room, such as locations 3, 6, and 9. The reason for these location-based differences is because of the larger ceiling area. There is delay in establishing an appropriate amount of soot in the larger upper uniform smoke layer volume for CFAST. When compared to FDS, which has a larger spatial resolution, can model the ceiling jet needing to diffuse across the ceiling area. This means that certain locations will activate before the smoke layer is established, hence why FDS will activate before CFAST in those locations but on average show good agreement.

6.2: Doorway Area Compartment Variations

Additionally, the size of the opening was modified to further investigate whether the differences shown in the smaller compartments are due to the volumetric size of the compartment or the size of the opening. The volumetric size of the compartment stays constant as the 24x36 ft configuration, but the area of the doorway is modified such that the ratio of the doorway area and the volumetric size of the room is representative of the

36x36 ft and 16x36 ft compartment. The ratio between the volume of the compartment and the area of the doorway can be determined as

$$ratio_{door:comp} = \frac{volume\ compartment}{doorway\ area} \qquad \textbf{(6-2)}$$

Therefore, in order to represent the doorway and volumetric ratio of the 16x36 ft compartment, the doorway was modified to a 9x8 ft wide opening, with the original 24x36 ft room dimensions. In the case mentioned above, a larger doorway area relative to the volumetric size of the compartment is established, similar to the 16x36 ft compartment. On the opposite end of the spectrum, in order to represent the doorway and volumetric ratio of the 36x36 ft compartment, the doorway was modified to a 4x8 ft wide opening, with the original 24x36 ft room dimensions. Therefore, under those dimensions, a smaller doorway area relative to the volumetric size of the compartment is established, similar to that of the 36x36 ft compartment.

The soot concentration, and optical density were recorded in both FDS and CFAST. The relative error for each was found, using (6-1), and is shown in Figure 6-25. As shown below, the relative error in the 4x8 ft vent was the lowest for both optical density and soot concentration. The 9x8 ft wide opening had the largest relative error. This shows that relative vent size and volume of the compartment was a contributing factor in the error presented in the 8x36 ft and 16x36 ft compartment. The 4x8 ft wide opening and the 9x8 ft wide opening represent the same volume to doorway area ratio as the 36x36 ft and 16x36 ft configurations, respectively, and both follow the same trend in relative error. The larger doorway area to compartment volume, such as the 16x36 ft configuration, has a larger error than the default 24x36 ft compartment. Similarly, the 9x8 ft wide doorway, which has the

same ratio as the 16x36 ft compartment, also has a larger error relative to the default compartment. The same parallelism can be seen for the 4x8 ft wide doorway and the 36x36 ft compartment.
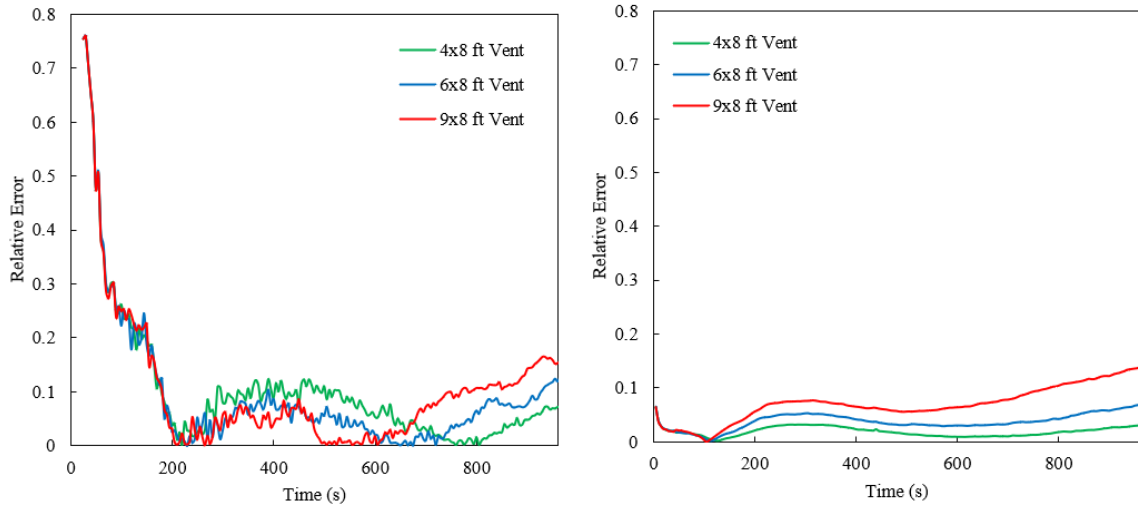

Figure 6-25: Relative error in total soot (left) and optical density (right), with varying vent sizes.

Additionally, the relative error of soot and optical density was also compared by doorway area to the orginal 16x36 ft and 36x36 ft volumetric compartments. Since the 4x8 ft and 9x8 ft wide doorway have the same doorway area to compartment volume ratio as the 36x36 ft and 16x36 ft compartments, respectively, a similar level of error is expected. As shown in Figure 6-26, the 4x8 ft wide doorway configuration is plotted with the 36x36 ft configuration having the default 6x8 ft wide doorway. Similarily, the 9x8 ft wide doorway is plotted with the 16x36 ft configuration with the default doorway, as shown in Figure 6-26 and Figure 6-27. The relative error between the two plots indicate that despite the differences in total volumetric room size, the doorway area to compartment volume ratio partakes in a larger role in determining the FDS and CFAST differences in optical

density and soot yield. For optical density, the relative error differs by about 0.05 or 5% for both the 4x8 ft wide doorway and 9x8 ft wide doorway ratio comparison, as shown in Figure 6-26. The same trends can be seen in Figure 6-27 for the soot concentration, where the error differs by negligible amounts for both the doorway area/volume compartment ratio.
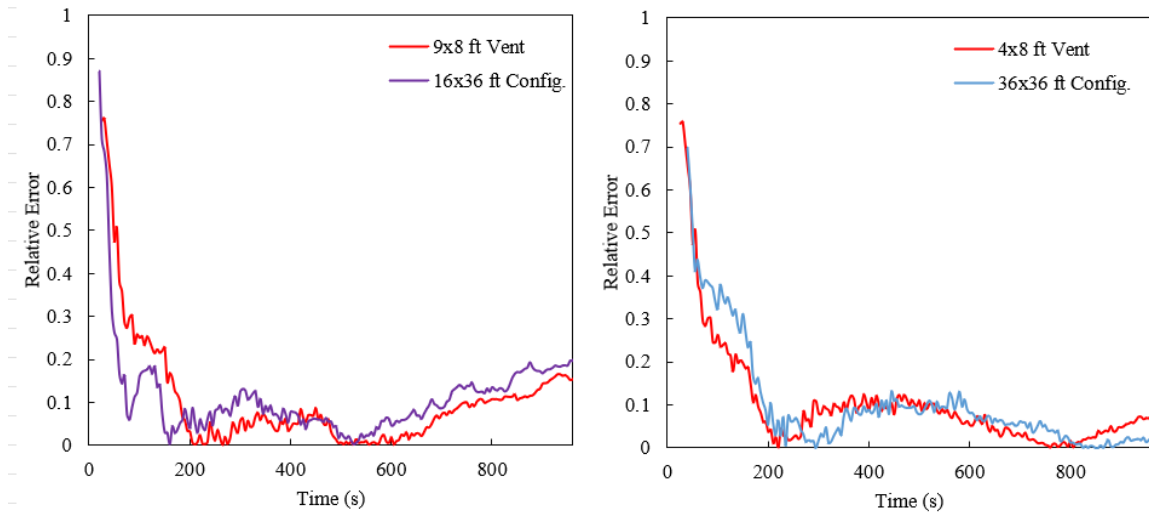

Figure 6-26: Relative error in optical density, comparing vent size to compartment volume ratio.
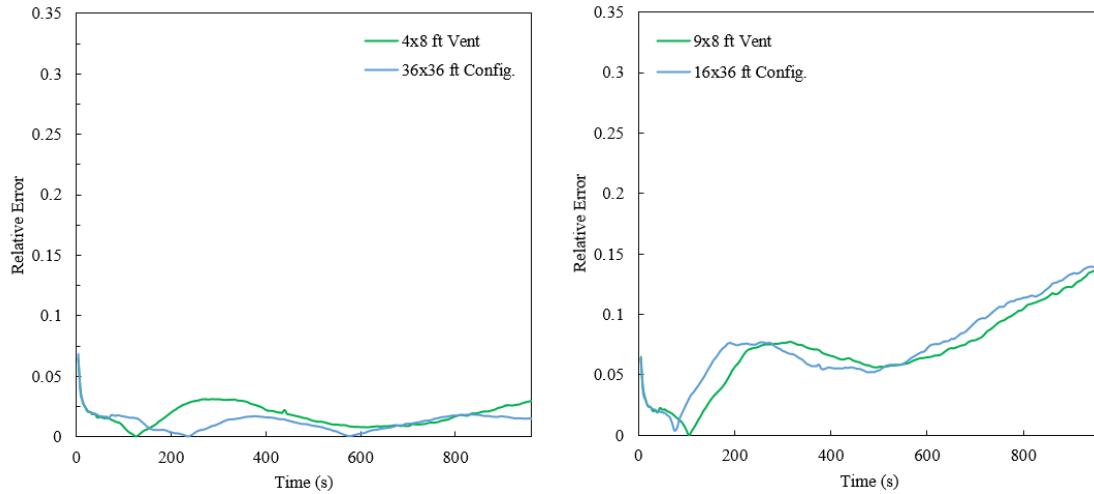
Figure 6-27: Relative error in total soot, comparing vent size to compartment volume ratio.

6.2.1: Comparison of Mass Flows Through Doorway

The net mass flow of the compartments was compared within CFAST and FDS to determine if the doorway was a major factor in the discrepancies shown from the 8x36 ft and 16x36 ft compartments. The net mass flows for the 8x36 ft and 36x36 ft comparisons are shown to be the same, as per Figure 6-28. However, it was shown that more soot had left the 8x36 ft compartment than the 36x36 ft configuration. This can be explained by a larger mass inflow and outflow in FDS, but the net difference is the same. Hence, further verification the fact that both models correctly balance the mass flows in and out of the room.
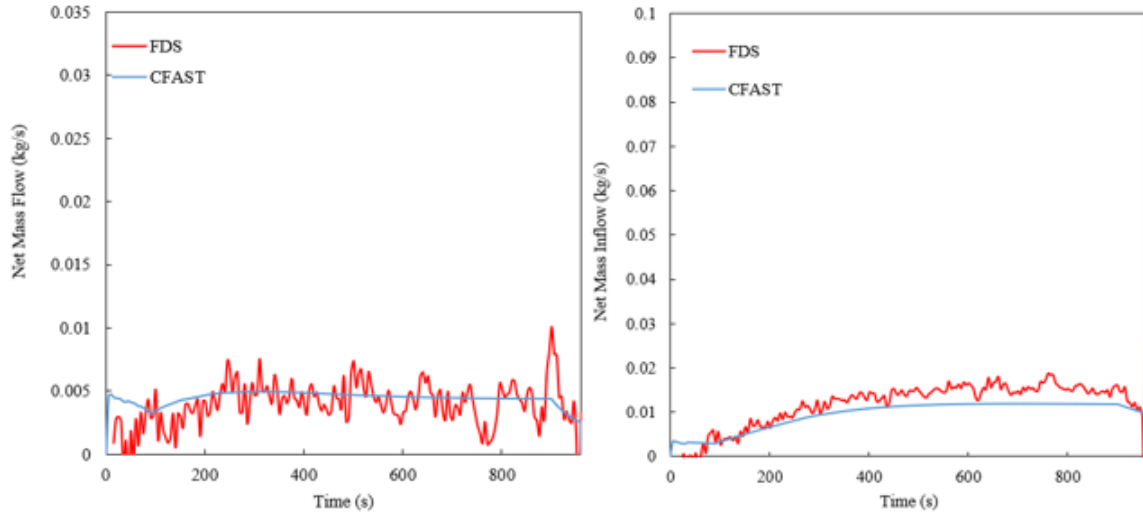
Figure 6-28: Net mass flow of 8x36 ft (left) and 36x36 ft (right) compartments.

However, a larger mass flow in and mass flow out can be hypothesized for FDS since the lower height was consistently lower than that of CFAST. This is shown in Figure 6-29 and Figure 6-30 , where the mass inflow and mass outflows were consistently larger than that of CFAST, regardless of the compartment size. Larger mass outflows and inflows within FDS are reflected by the inherent lower layer heights seen previously. Additionally, the differences between the two models in mass outflow and inflow, at 960 seconds, is about 0.3 kg/s for the 8x36 ft compartment. For the 36x36 ft compartment, the difference is only about 0.12 kg/s. Therefore, in larger doorway configurations, the difference in mass flows is larger within FDS and CFAST.
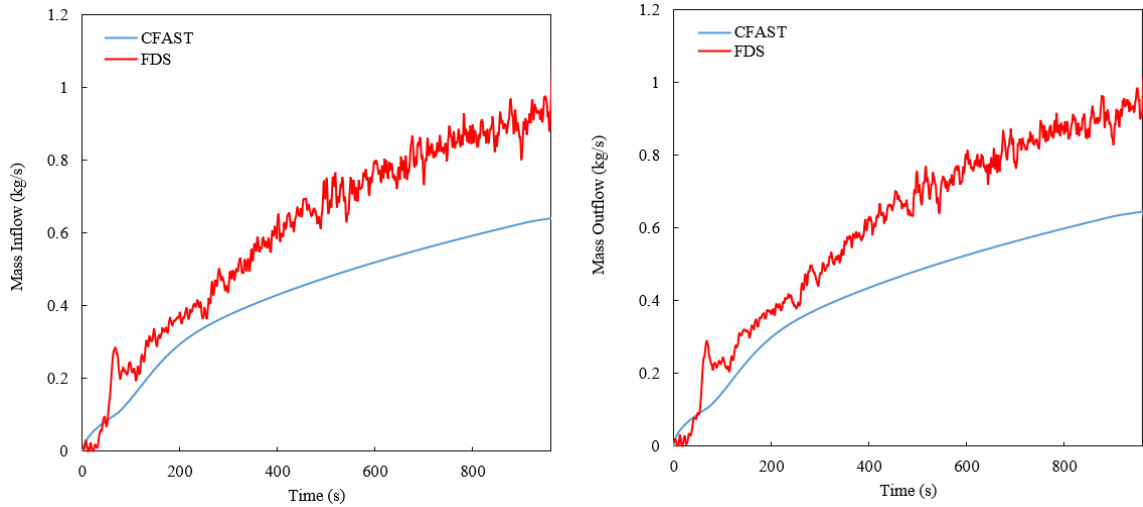
Figure 6-29: Mass inflow (left) and outflow (right) for 8x36 ft compartment.
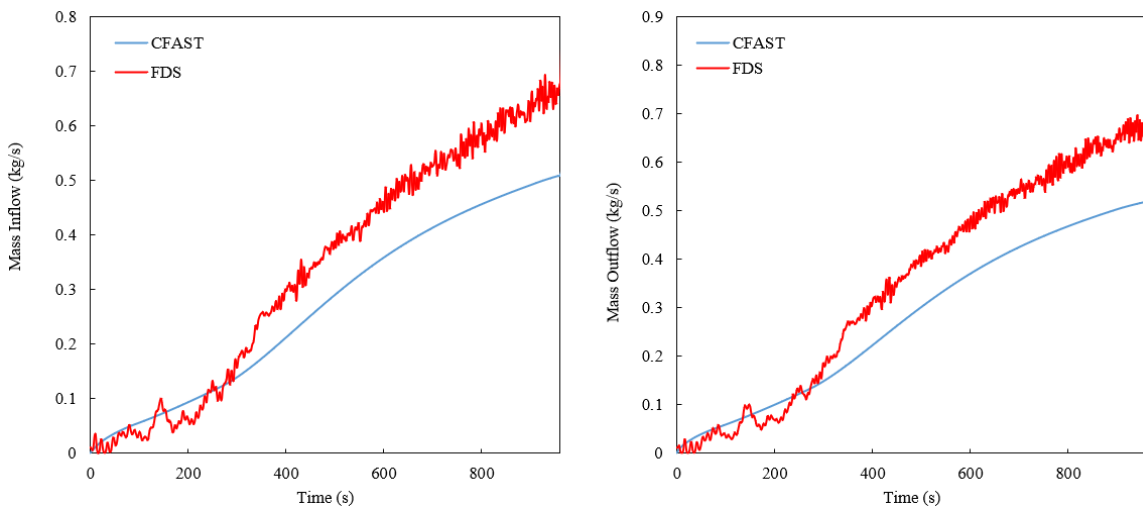
Figure 6-30: Mass inflow (left) and outflow (right) for 36x36 ft compartment.

Furthermore, in larger volume spaces, the smoke layer volume is also larger. Thus, discrepancies that occur in large doorway configurations, are more likely to have a larger impact on the overall soot in the compartment. Discrepancies within the mass flows are smaller and are more negligible in a larger room, which can explain why a larger volume

90

room compared to a smaller doorway would show better agreement within CFAST and FDS. On the other hand, in the 8x36 ft and 16x36 ft compartments, the doorway is larger. Thus, the differences in mass inflows and outflows are larger, which has a greater effect on the total soot within the smaller compartment.

6.2.2: Conclusion of Doorway Area

The error plots match similar to that of the 8x36 ft and 36x36 ft compartments, which means that the ratio between the doorway area and the volume of the compartment is the catalyst for these discrepancies. Either the volume of the compartment or the doorway area was varied, but the ratios between the two were kept constant. Thus, it indicates that the ratios between the two variables influence the discrepancies seen between CFAST and FDS. Additionally, the mass inflows and outflows are affected by the overall vent size and compartment volume. Both models displayed larger mass inflows and outflows for the 8x36 ft compartment than the 36x36 ft compartment. However, FDS consistently overpredicted the mass inflows and outflows when compared to CFAST. CFAST may underpredict the mass inflows and outflows based on its two layer assumption. In contrast, FDS accounts for turbulent flows and mixing within the compartment, which is heavily more influenced by a larger doorway and smaller compartment.

6.3: Ceiling Height Compartment Variations

The ceiling height of the room was another variable that was examined when determining the biases between FDS and CFAST. There was a total of four heights that were examined: the default 12 ft high ceiling, a 24 ft, 36 ft, and 48 ft high ceiling, all of which use the width and length dimensions of the 24x36 ft compartment.

6.3.1: Analysis of Detector Response for Varying Ceiling Heights

A comparison of four ceiling heights were evaluated, as noted above. A total of nine detectors, each having three obscuration activation levels, for a total of 27 detectors per compartment. However, only the low and medium activation obscuration detectors activated, in both FDS and CFAST, for the 24 ft and 36 ft ceiling high compartments. For the 48 ft ceiling high compartment, only the low activation detectors were activated. The FDS and CFAST detection times, per location, is shown in Figure 6-31 and Figure 6-32.

For all the detector locations, at all ceiling heights greater than the default 12 ft, has shown that FDS predicts activation before CFAST. For the low activation detectors, FDS activates at around 350 to 400 seconds for the 24 ft high ceiling and 480 to 550 seconds for the 36 ft high ceiling. For the 48 ft ceiling, the low activation detectors did not activate until around 600 to 650 seconds for FDS. Similarly, for FDS, the medium obscuration detectors for the 24 ft high ceiling activated between 600 and 680 seconds and 790 to 800 seconds for the 36 ft high ceiling. No medium activation obscuration detectors activated in neither FDS nor CFAST for the 48 ft high configuration.

Additionally, CFAST was shown to activate after FDS for all the high ceiling cases, which is interesting because CFAST does not account for smoke transport. Therefore, no smoke transport model means that the smoke layer starts instantaneously at the top of the ceiling, which is why CFAST would be expected to activate first. However, the activation times in FDS happens after 350 seconds, which would be well after the smoke plume has reached the ceiling jet. Therefore, a discussion and analysis into the smoke properties is discussed further in section 6.3.2: Analysis of Smoke Properties for Varying Ceiling Heights, which discusses why FDS activates before CFAST.

92
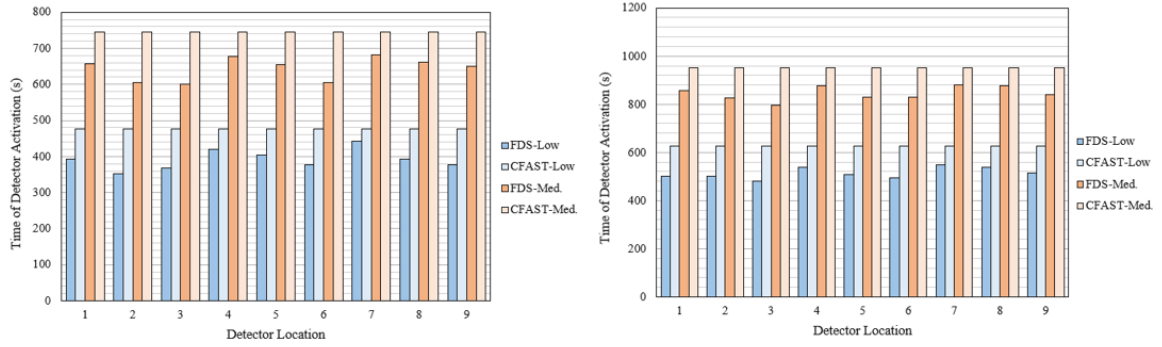
Figure 6-31 Detector times for 24 ft (left) and 36 ft (right) tall compartments.
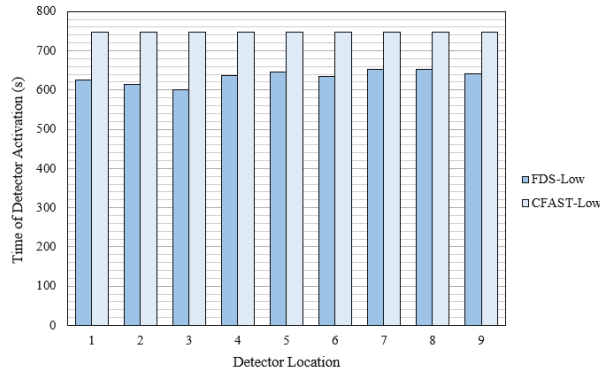
Figure 6-32 Detector times for 48 ft tall compartments.

The absolute error, or difference, between the predicted detection times were calculated and plotted as a per location and obscuration level. The largest error occurs in the 36 ft and 48 ft high ceilings, for the low obscuration detectors, as shown in Figure 6-33. In general, as the ceiling height increases, the difference between CFAST and FDS increases. This can be seen where the 24 ft, 36 ft, and 48 ft ceiling, have a significantly larger difference than the default 12 ft ceiling. However, once the 36 ft and 48 ft ceilings are attained, the discrepancies between the error are negligible. The 36 ft and 48 ft high

ceiling have relatively similar amounts of error despite one configuration having a taller ceiling.

Figure 6-33: Abs. error between CFAST and FDS for low (left) and med. (right) obscuration detectors.

6.3.2: Analysis of Smoke Properties for Varying Ceiling Heights

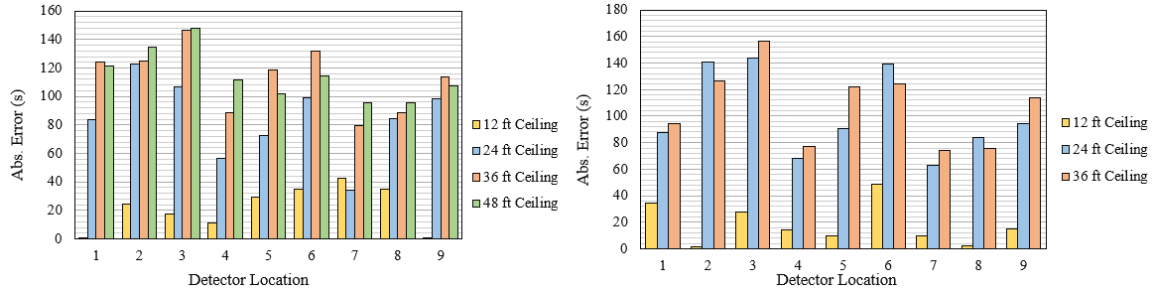The soot yield, layer height, and optical density were plotted in FDS and CFAST. Similarly, the relative error was calculated for each smoke property. The total soot in the compartment for the 12 ft (same as Figure 6-19) and the 24 ft high ceilings are shown in Figure 6-34. Originally, the 12 ft ceiling showed good agreement between FDS and CFAST, but the 24 ft ceiling shows even better agreement. The differences between CFAST and FDS, for the high ceilings, is negligible. A small divergence between FDS and CFAST starts at 600 seconds for the 24 ft high ceiling configuration. The 36 ft and 48 ft ceilings also show very good agreement between CFAST and FDS, as shown in Figure 6-35 and Figure 6-36.

The same trend can also be seen for the optical density. The optical density for the 24 ft ceiling configurations is shown in Figure 6-34. Similar to what is seen in the soot concentration, FDS actually overpredicts the average optical density for the 24 ft ceiling.

For the 36 ft and 48 ft high ceilings, FDS also overpredicts the optical density when compared to CFAST, as shown in Figure 6-35 and Figure 6-36.
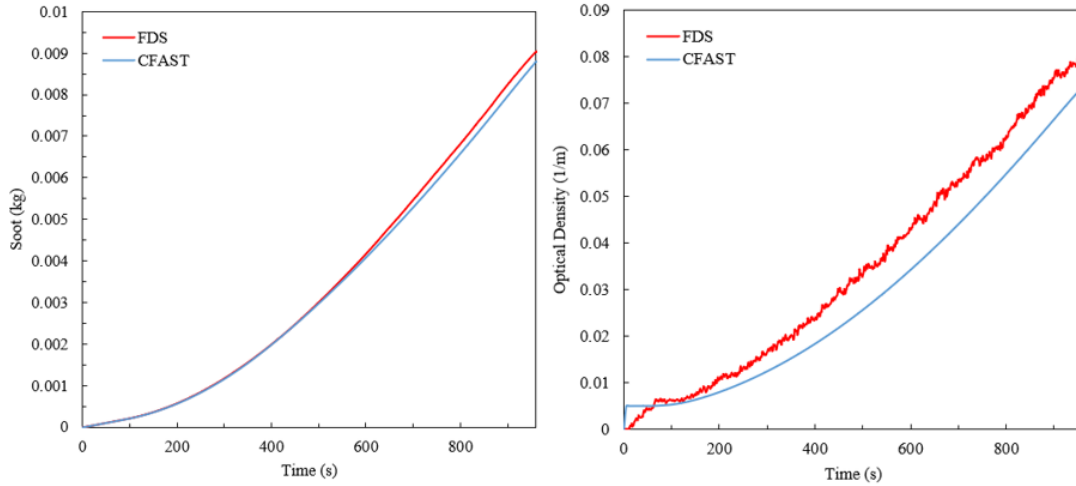

Figure 6-34: Total soot (left) and optical density (right) for 24 ft tall ceiling.
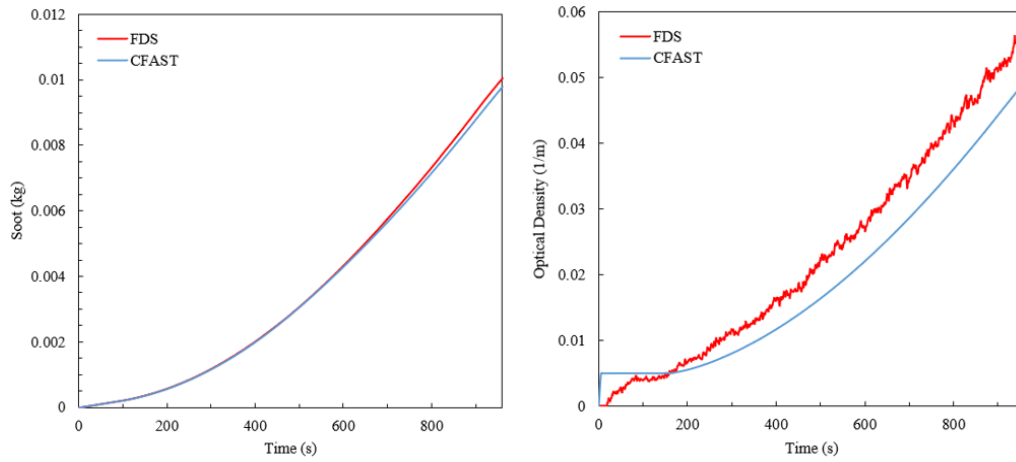

Figure 6-35: Total soot (left) and optical density (right) for 36 ft tall ceiling.
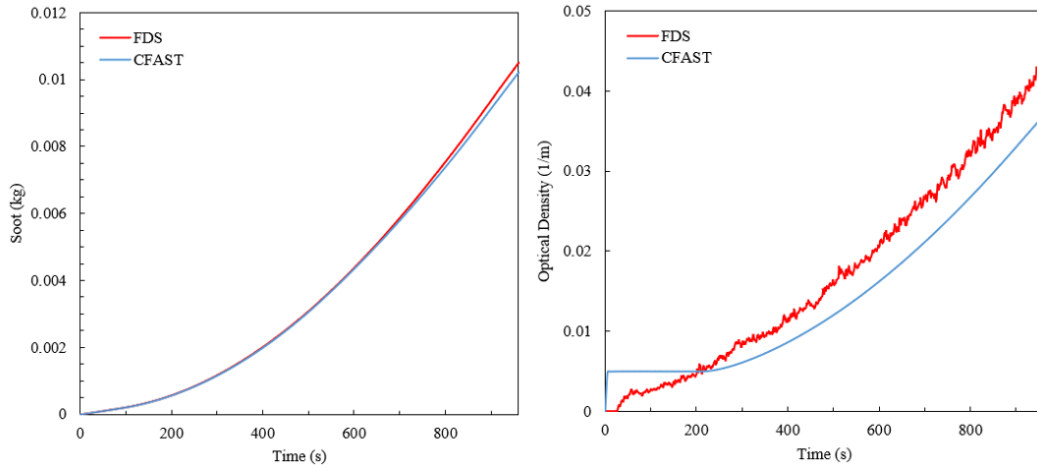
Figure 6-36: Total soot (left) and optical density (right) for 48 ft tall ceiling.

Similar to the to the optical density and soot concentration, the layer height displayed similar trends. The analysis for the configurations with different aspect ratios, as per section 6.1.2 Analysis of Smoke Properties, showed that FDS constiently predicted a lower upper layer height by about 0.25 m. Unlike, the 12 ft layer height, CFAST and FDS layer heights converge towards 1.5 m to 2 m once steady as shown in Figure 6-37 and Figure 6-38. Additionally, the taller ceiling heights showed greater varriance in the beginning of the simulations. The layer heights for FDS and CFAST do not converge until 200 seconds for the 24 ft ceiling; 300 seconds for the 36 ft ceiling; and 400 seconds for the 48 ft ceiling. Thus, about 100 seconds of delay in layer height for FDS per 12 ft of raised ceiling.

The initial delay in smoke layer height is expected in FDS because there is a plume travel and ceiling jet model that would delay the formation of the smoke layer. Additionally, the higher the ceiling, the farther the smoke has to travel before dispersing across the ceiling, hence the reason a longer delay in the smoke layer layer descending is

96

seen for higher ceiling configurations. Since CFAST does not have a smoke transport model, the smoke layer can be seen descending almost instanteously.
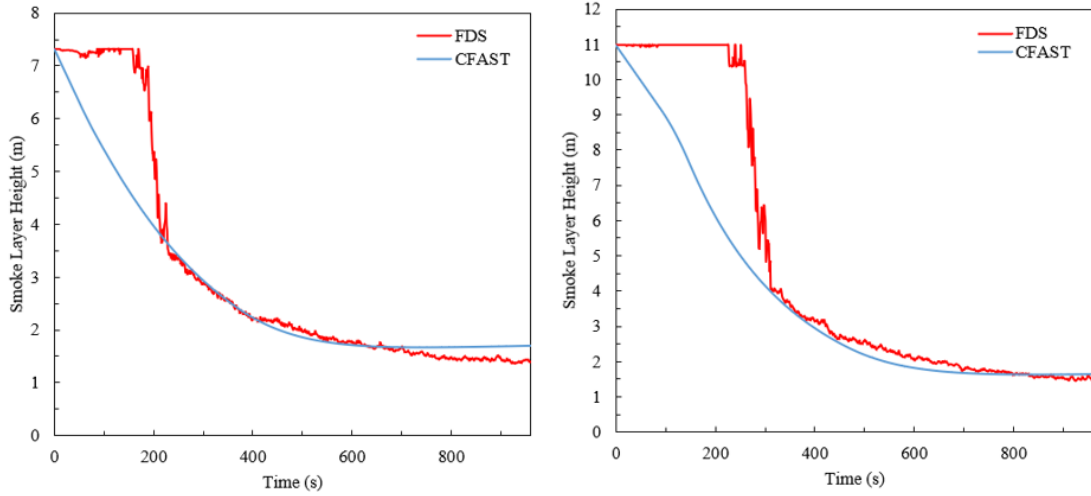

Figure 6-37: Layer height for 24 ft (left) and 36 ft (right) tall ceilings.
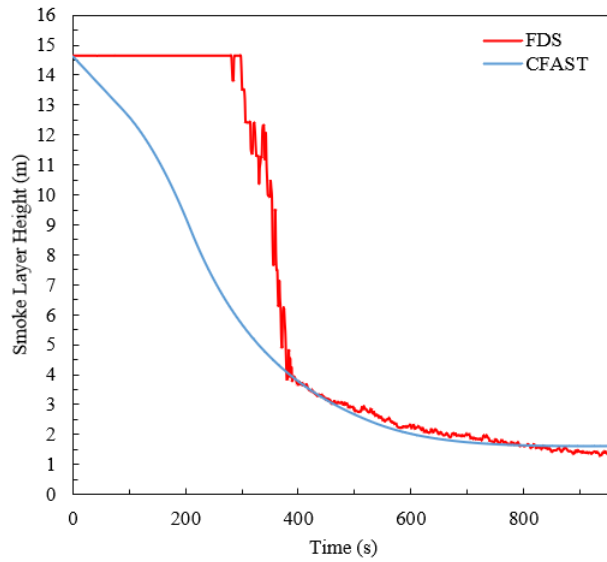
Figure 6-38: Layer height for 48 ft tall ceiling.

6.3.2.1: Smoke Property Error Analysis for Varying Ceiling Heights

The relative error for the soot concentration and optical density was calculated and plotted per ceiling height, as shown in Figure 6-39 and Figure 6-40. The relative error shows that neither the soot concentration nor the optical density have negligible changes per ceiling height. The relative error difference, at time 960 seconds, for the soot concentration ranges from 0.026 or 2.6% to 0.029 or 2.9%. Similarly, the error for the optical density at 960 seconds ranges between 0.013 or 1.3% to 0.015 or 1.5%. The largest error can be seen from the layer height, as shown in Figure 6-39 and Figure 6-40. It appears that the largest differences in layer height, per ceiling configuration, occurs at the initial peak, ranging from 0 to 400 seconds. This initial peak in error comes from the delay in the smoke layer descent for FDS. For the 24 ft high ceiling, the largest relative error occurs at around 180 seconds, with a relative error of about 0.65 or 65%. The 36 ft high ceiling has a largest relative error of about 1.09 or 109% at a time of 255 seconds. Lastly, the 48 ft high ceiling has a relative error of 1.52 or 152% at a time of 295 seconds. As discussed above, the layer height shows a larger relative error at a later time per higher ceiling height.
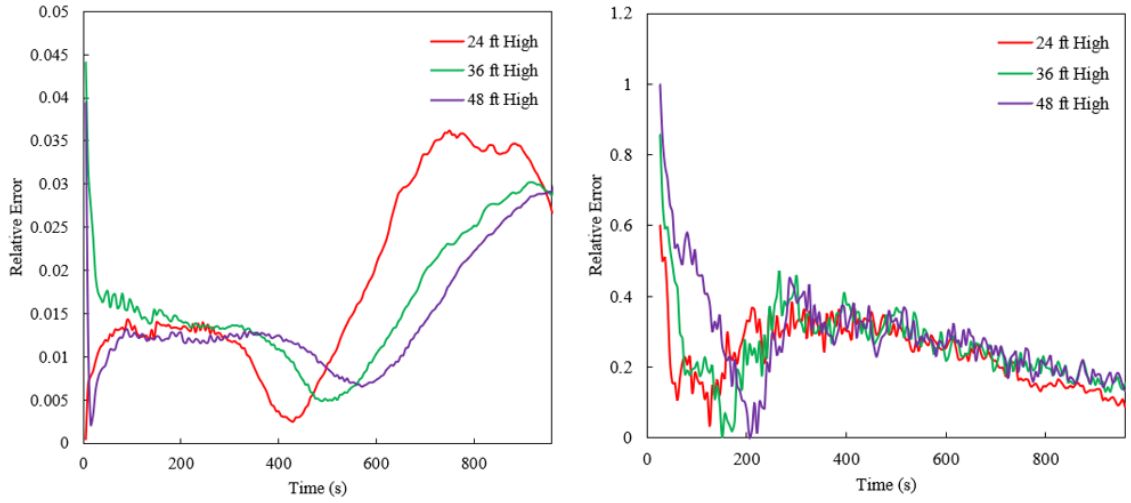
Figure 6-39: Abs. error for total soot (left) and optical density (right) for varying ceiling height configurations.
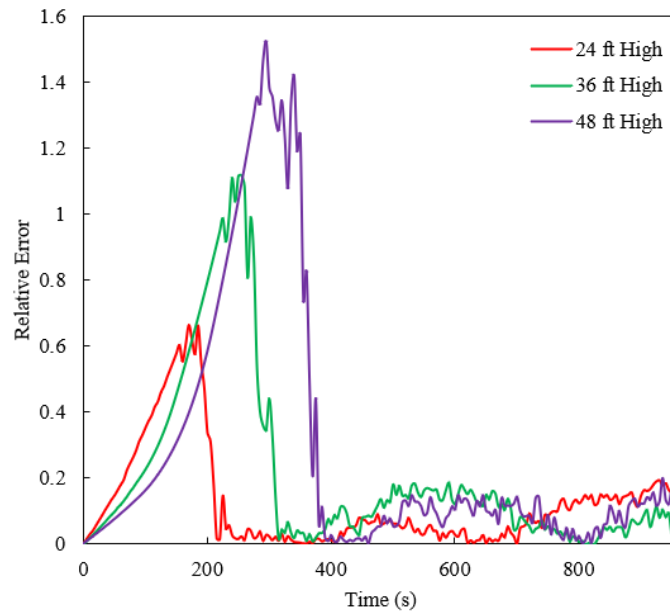
Figure 6-40: Abs. error for layer height for varying ceiling height configurations.

6.3.3: Smoke Layer in Tall Ceiling Spaces

Quicker smoke detector activation in FDS may be attributed to the thermally buoyant smoke layer. Since FDS has a finer resolution than CFAST, the smoke layer can be modeled as a gradient. Therefore, in a thermally driven smoke layer, the hotter soot will accumulate towards the top of the smoke layer and the cooler soot settles towards the bottom of the smoke layer. This causes a gradient in soot concentration, where more soot accumulates towards the top of the compartment. Since CFAST models the upper layer is uniform, the same amount of soot in the upper layer will be uniformly spread, which results in less overall soot.
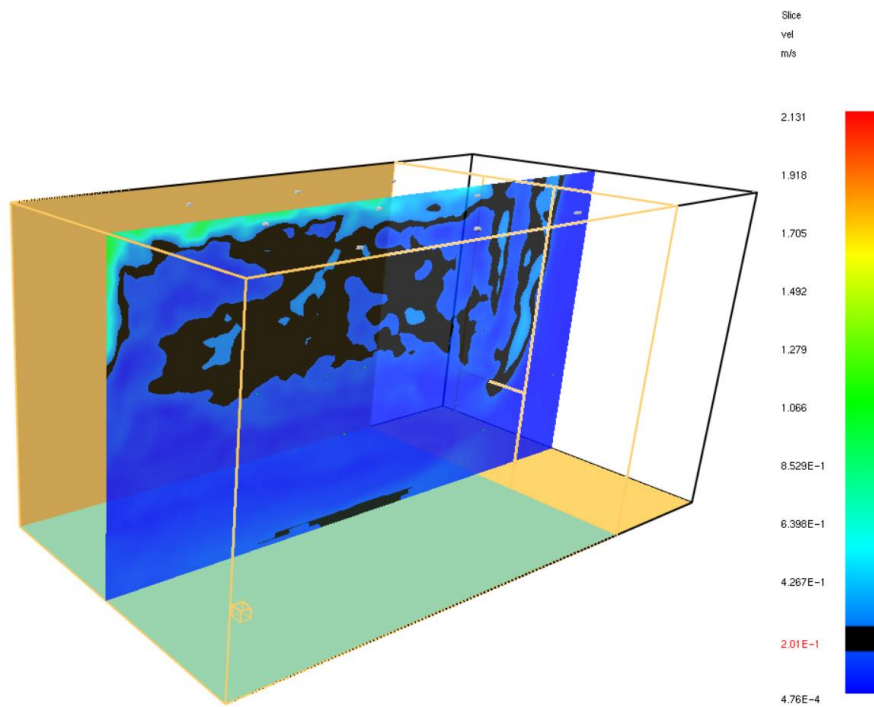
Figure 6-41: Velocity of smoke layer for 24 ft ceiling.

The assumption that the smoke layer has a thermal gradient is only valid if the smoke layer is not well mixed. The smoke layer is not well mixed if the velocity within the

smoke layer is low, such as less than 1 m/s. A velocity slice, taken at half the width of the compartment, is shown in Figure 6-41, Figure 6-42, and Figure 6-43 for the 24 ft, 36 ft, and 48 ft ceilings respectively. The snapshot of the velocity is taken at about 400 seconds, roughly half the time of the linear growth phase of the fire. Thus, if the smoke layer were to be well-mixed, velocities greater than 1 m/s should be present within the smoke layer. However, low velocities within the smoke layer are shown in all the tall ceiling configurations. The black color represents velocity areas of around 0.2 m/s. In the 24 ft, 36 ft, and 48 ft ceiling configurations, aside from the ceiling jet, the majority of the smoke layer has a low velocity. This indicates that the smoke layer, below the ceiling jet, is not well mixed.
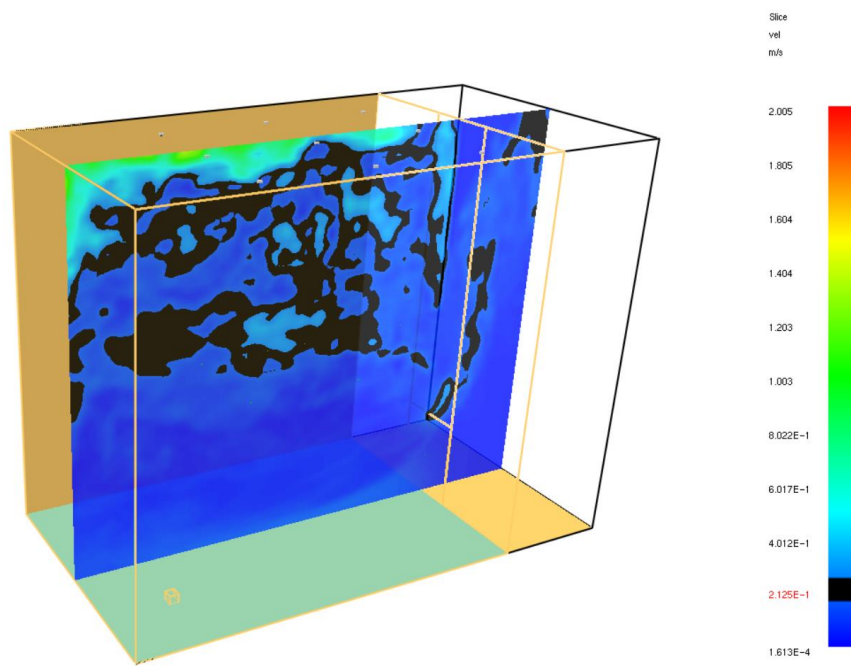
Figure 6-42: Velocity of smoke layer for 36 ft ceiling.
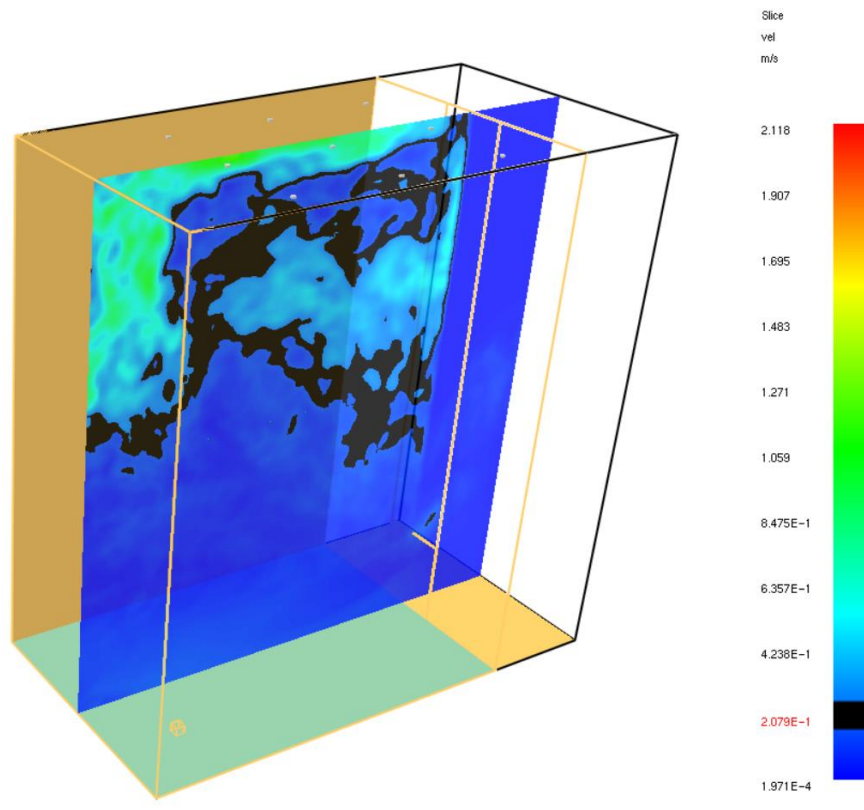
Figure 6-43: Velocity of smoke layer for 48 ft ceiling.

6.3.4: Conclusion on Varying Ceiling Height Configurations

The varying ceiling heights showed that the soot concentration was relatively similar for both CFAST and FDS. This can be expected since it was established that in section 6.2: Doorway Area Compartment Variations, a larger volumetric compartment relative to the doorway area shows less differences between the two models. Within FDS, a smaller doorway area and/or larger volumetric compartment ensures that the turbulent conditions near the doorway do not interfere with the mass flows of the upper and lower layers. Subsequently, when the ceiling height is increased, the volume of the compartment is drastically increased. This further validates that a larger compartment compared to a smaller doorway reduces discrepancies between FDS and CFAST, as shown by the near

identical plots of soot concentration in the compartment. The layer height descent is also shown to be delayed in FDS when compared to CFAST due to the incorporation of a smoke transport model in FDS.

Finally, the optical density plots in FDS are seen to be consistently larger than the plots shown in CFAST. However, as noted above, it was shown that CFAST and FDS predict the same amount of total soot and the higher FDS optical density does not occur until CFAST and FDS have the same upper layer volumetric size. Therefore, under the same amount of soot and smoke layer volume, FDS still predicts a higher optical density. This can be explained by FDS having a larger spatial resolution. Since the smoke layer height is thermally driven, much of the soot accumulates at the top of the smoke layer and less towards the bottom of the layer. In CFAST, the soot concentration is uniformly distributed within the volume of the defined upper layer. Therefore, for the same amount of soot in the upper layer, CFAST will prescribe a lower soot mass per unit volume, which is used to calculate optical density. On the other hand, for the same amount of soot in the upper layer, FDS will model a gradient in which the majority of soot accumulates at the ceiling. This leads to a larger mass concentration of soot near the optical density detectors and thus a higher optical density when compared to CFAST. One thing to note is that the fire scenario is inherently going to be thermally driven. Therefore, they may be some biases in which the chosen fire scenario influences the differences between CFAST and FDS, rather than the ceiling height of the compartment.

6.4: Statistical Model Results

A total of five cases were used to determine three possible linear regression models. These five cases included the four different aspect ratios: the 8x36 ft, 16x36 ft, 24x36 ft, and

36x36 ft room configurations, each having a 12 ft high ceiling and a 6x8 ft wide doorway. The last case was the 24x36 ft configuration with a 36 ft high ceiling and a 6x8 ft wide doorway. From those five cases, three linear regression models were established as shown in Figure 6-44, Figure 6-45, and Figure 6-46. To test the validity of each model, another set of data was randomly generated by using the random number function in Excel. This data included a total of four randomly generated sized rooms, with ten randomly placed detector locations. Three randomly generated obscuration activation levels were generated, thus a total of thirty detectors were located within the room. An additional two rooms including the 24x36 ft configuration width and length, and height of 24 ft and 48 ft, were also used in the test data to validate the models.

6.4.1: Model 1

The first proposed model uses k as the number of parameters, for which $k = 1$, 2, and 3 for the velocity and temperature values at the detector, as well as CFAST detection time, respectively. For n number of detectors, and k number of parameters, the following regression model is stated as

$$y_n = 15.727\, x_{1n} - 113.77\, x_{2n} + 0.8744\, x_{3n} - 313.78 \qquad \textbf{(6-3)}$$

The predicted FDS time from the model, as shown on the y-axis in Figure 6-44, to the actual FDS activation time shows good agreement because the slope of the fitted linear trendline is 1.049 and has an R^2 value of 0.9704. The second (right) graph, as shown in Figure 6-44, plots the predicted absolute error against the actual absolute error. The predicted absolute error can be determined as the absolute difference between CFAST and the predicted FDS time. Similarly, the actual absolute error is the absolute difference

between CFAST and the actual FDS time. The error plot, as shown in Figure 6-44, has a fitted linear trendline with a slope 1.4459 and an R^2 value of 0.4883. The data points are very sparse from each other and do not follow a clear trend. Thus, despite this model's ability to predict the FDS activation times, it predicts the error between CFAST and FDS poorly.
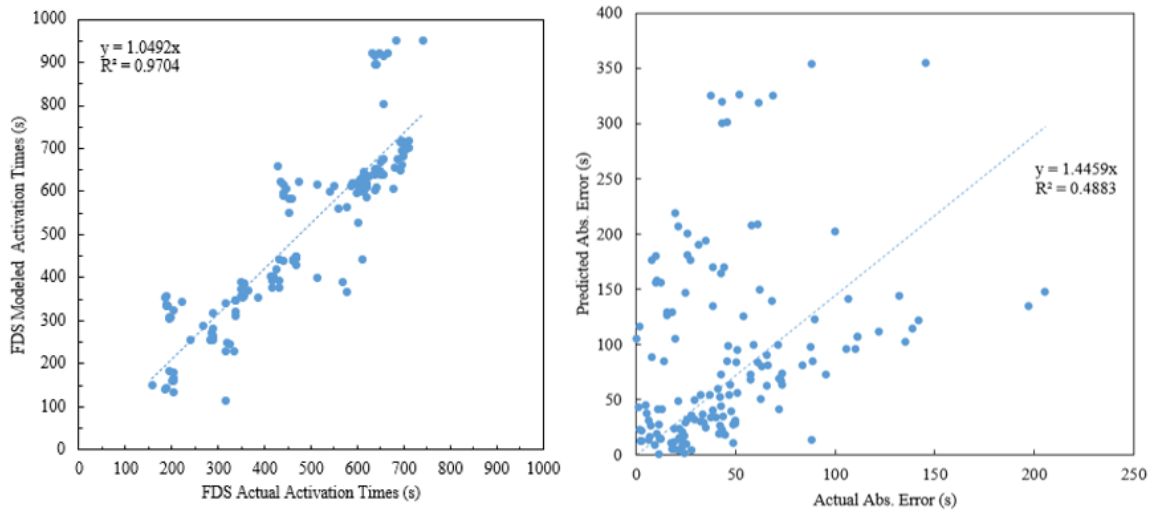
Figure 6-44: Predicted versus actual FDS (left) and abs. error (right) for model 1.

6.4.2: Model 2

The second proposed model has a total of four predictor variables. For k number of variables, and k = 1, 2, 3, and 4; the input parameters are temperature, velocity, CFAST detection time, and ceiling height, respectively. Thus, for n number of detectors, the proposed model takes the form as

$$y_n = 23.392\ x_{1n} - 162.83\ x_{2n} + 0.7722\ x_{3n} + 3.7992\ x_{4n} - 509.59 \quad \textbf{(6-4)}$$

The predicted versus actual FDS time for model 2 is shown in Figure 6-45. A linear trendline was fitted to the data with a slope of 0.96 and an R^2 value of 0.9748. The predicted

error and the actual error, between CFAST and FDS, was also plotted in the right graph of Figure 6-45. A linear trendline was fitted to the error data and has a slope of 0.9495 and an R^2 of 0.7231. Similar to model 1, the predicted FDS and actual FDS activation time plot shows that the model can somewhat predict the FDS times based on the input parameters. However, when backing out the error from the predicted FDS times, the predicted error and actual error shows less agreement. The data points are mostly clustered around the origin and begin less clustered as the error increases.
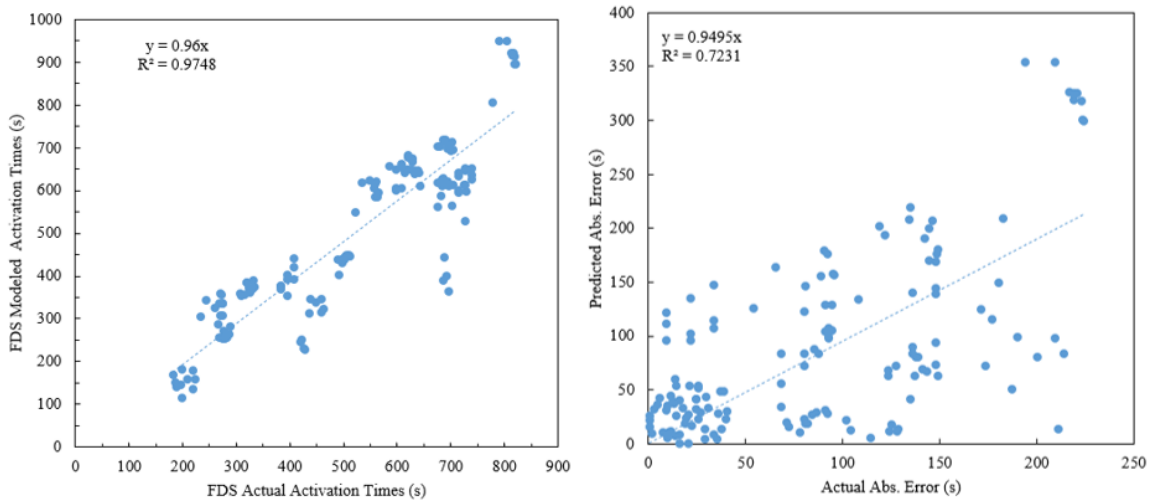
Figure 6-45: Predicted versus actual FDS (left) and abs. error (right) for model 2.

6.4.3: Model 3

This model took a different approach. Instead of trying to determine a linear regression between input parameters and FDS activation time, this model tried to establish a linear regression between input parameters and the error between FDS and CFAST. A total of five input parameters were selected for this model, with $k = 1, 2, 3, 4,$ and 5 for the room area, activation obscuration of the detector, ceiling height, CFAST detection time, and

radial distance from the smoke plume to the detector. For *n* number of detectors, the model is shown as

$$y_n = -0.069 \, x_{1n} + 28.03 \, x_{2n} - 8.883 \, x_{3n} + 0.701 \, x_{4n} - 1.54 \, x_{5n} + 1865.53 \quad \textbf{(6-5)}$$

From the predicted error time, the predicted FDS can be solved. Thus, the predicted FDS activation time from the model is plotted against the actual FDS time in Figure 6-46. A linear trendline with a slope of 0.9818 and an R^2 value of 0.9777 was obtained. Similarly, the actual error is plotted against the predicted error, resulting in a slope of 1.0593 and an R^2 value of 0.7543. Similar to model 1 and model 2, model 3 shows good agreement in the model for predicting FDS activation times. Although significantly better than model 1 and slightly better than model 2, model 3 shows some agreement when predicting the actual error between FDS and CFAST. The data points seem to be less sparse as model 1 and 2 and follows a somewhat linear shape, but still relatively collects within the origin area and spreads wider as the error increases.
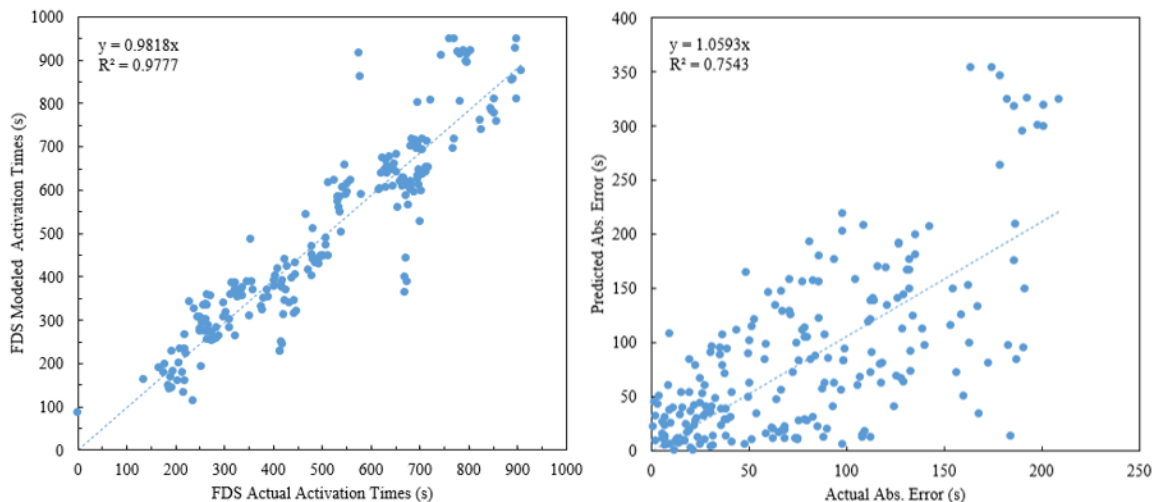

Figure 6-46: Predicted versus actual FDS (left) and abs. error (right) for model 3.

6.4.4: Conclusion on the Proposed Models

Overall, model 3 seems to provide the best agreement and prediction in both FDS activation time and absolute error between FDS and CFAST. Although, all three models predicted the FDS activation times well, as evidenced by their trendline slopes close to 1, there may be biases present. The biases come from the large number of detectors that do not lead to a large amount of error, thus the FDS prediction times fall close to that of CFAST. However, in few cases where large amount of error is present, such as high obscuration detectors and large doorways to compartment volume ratio, these errors are not correctly accounted for. Essentially, the models appear to be good predictors because the majority of detectors are not prone to large error conditions and the R^2 value may be artificially inflated because of that. However, when looking at the predicted versus the actual absolute error plots, the validity of the model does not hold up as well, except for model 3. It is important that the model can identify and predict cases that would lead to a large error between FDS and CFAST. However, models 1 and 2 fail to provide a reasonable prediction of the error between FDS and CFAST, as shown by the sparse and wide spread of data points. Model 3 provides the best correlation between CFAST and FDS, as well as a decent model in predicting error differences between CFAST and FDS. However, these models are mainly present for identifying a relationship between CFAST and FDS activation times, based on certain identified predictor variables. Under "non-ideal" or biased conditions, as identified in section 6.1: Aspect Ratio Compartment Variations to section 6.3: Ceiling Height Compartment Variations, these models should be used with caution since the error R^2 values for the three models ranges from 0.48 to 0.75.

Chapter 7: Conclusion and Future Work

There are a total of three main biases that were identified in causing differences between CFAST and FDS. These three biases are the volumetric compartment to doorway area ratio, the ceiling area of the compartment, and the thermally driven smoke layer presented in tall ceiling spaces.

The ratio between the doorway and the volumetric compartment was responsible for the divergence in soot yield and optical density between CFAST and FDS. The 24x36 ft and 36x36 ft compartments showed the best agreement in activation times, with a compartment volume ratio to doorway area of 216 m and 324 m respectively. A lower ratio, as exampled by the 8x16 ft and 16x36 ft compartments, were subjected to larger differences between CFAST and FDS.

The ceiling area also presented some slight differences between CFAST and FDS models. With larger ceilings, localized activation in FDS was more likely, as exampled by the 24x36 ft and 36x36 ft compartments. Smoke detectors along the wall and ceiling junction, as well as close to the detector were shown to activate quicker than the rest of the other detectors on the ceiling. Localized activation in FDS resulted in slight differences between FDS and CFAST. Although these differences were only between 5 to 60 seconds, larger area ceilings are more likely to result in larger differences for the affected areas.

Lastly, in tall ceiling spaces, where the ratio between the volume of the compartment and the doorway area is large, FDS was shown to activate slightly quicker than CFAST. This can be attributed to the thermally driven smoke layer that is accounted for in FDS, resulting in a larger percentage of the soot in the upper layer to accumulate

closer to the top of the ceiling. Additionally, the fire scenario itself could have contributed to the large biases shown between CFAST and FDS for the tall ceiling spaces. When using such a low HRR and slow ramp time, the smoke layer itself is prone to be inherently thermally driven. Therefore, using other fire scenarios and testing if the same differences between FDS and CFAST would indicate if the differences shown in this research are due to the actual ceiling height or the low HRR fire.

Overall, based on the given fire scenario for differing room, high obscuration detectors were shown to have the largest differences between CFAST and FDS. For tall ceiling spaces neither FDS nor CFAST, respectively. Therefore, for high obscuration detectors, caution with large doorway area to compartment volumes should be considered since the differences between CFAST and FDS occurred largest in those type of compartments. For tall ceiling areas, since neither high obscuration detectors activated within CFAST and FDS for the small fire scenario, there may be no need to even consider modeling them in tall ceiling spaces with low HRR fires.

A total of three models were proposed. A *t*-test was performed for each parameter, such that the dimensions of the model can be reduced, and the most statistically optimal models were found. The difference in R^2 coefficients for the actual versus predicted FDS times did not differ between the three models. However, model 3 had the largest R^2 coefficient for the error plots. Thus, it is statistically the best model for predicting the error between CFAST and FDS. However, despite the error plots' R^2 value being relatively high, the data points are widespread which can be an indication of overfitting. Therefore, these models should only be used in cases where the biases presented previously, or other known large biases between CFAST and FDS, are not present.

As a result, future work pertaining to relating CFAST and FDS models to each other can include exploring the biases presented in this research further. The major scope of this research was to identify general room configuration that affect detector activation in FDS and CFAST. Further research focused on collecting data and identifying the underlying mechanisms responsible for the biased doorway area configurations could provide more detailed insight into quantifying these parameters. Furthermore, exploration into the modeling biases for ceiling shapes, such as beamed, sloped, peak, and shed ceilings, could provide useful insight for modelers. Although only one fire scenario was prescribed for this project, considering different fire growth models in biased room configurations could provide modelers a way to expect model biases for a larger range of fire design scenarios and provide verification for the ceiling height configurations. Additionally, only a multivariable linear regression model was fitted to the data. Other regression models may fit better overall. Furthermore, t-testing was used as the sole method for reducing parameters for each model. Other methods for dimension reduction should be considered for developing future models that can better quantify the error difference between CFAST and FDS.

Bibliography

[1]   B. Meacham, "The evolution of performance-based codes and fire safty design methods, NIST-GCR-98-761," *Nat. Inst. Stand. Technol., USA*, Jan. 1998.

[2]   *Performance-Based Standard for Fire Protection for Light Water Reactor Electric Generating Plants, 2001*. One Batterymarch Park Quincy, MA: National Fire Protection Association, 2001. [Online]. Available: https://www.nfpa.org/codes-and-standards/all-codes-and-standards/list-of-codes-and-standards/detail?code=805&tab=research

[3]   "§ 50.48 Fire protection.," *NRC Web*. https://www.nrc.gov/reading-rm/doc-collections/cfr/part050/part050-0048.html (accessed Jan. 11, 2022).

[4]   "Verification and Validation of Selected Fire Models for Nuclear Power Plant Applications Volume 1: Main Report," U.S. Nuclear Regulatory Commission Office of Nuclear Regulatory Research, Two White Flint North, 11545 Rockville Pike Rockville, MD. [Online]. Available: https://www.nrc.gov/reading-rm/doc-collections/nuregs/staff/sr1824/index.html

[5]   "Verification and Validation of Selected Fire Models for Nuclear Power Plant Applications - Supplement 1," U.S. Nuclear Regulatory Commission, Office of Nuclear Regulatory Research (RES), Washington, D.C. Accessed: Jan. 11, 2022. [Online]. Available: https://www.nrc.gov/reading-rm/doc-collections/nuregs/staff/sr1824/s1/index.html

[6]   R. P. Schifiliti, R. L. P. Custer, and B. J. Meacham, *SFPE Handbook of Fire Protection Engineering, chapter Design of Detection Systems*, Fifth. New York, NY: Springer New York, 2016. doi: 10.1007/978-1-4939-2565-0.

[7]   K. B. McGrattan, "Fire dynamics simulator (version 4) :: technical reference guide,"
       National Institute of Standards and Technology, Gaithersburg, MD, NIST SP 1018,
       2006. doi: 10.6028/NIST.SP.1018.

[8]   *National Fire Alarm and Signaling Code, 2019*. National Fire Protection
       Association, 2018.

[9]   R. A. Jr and D. Martin, "Smoke Detector Spacing for High Ceiling Spaces," Fire
       Protection Research Foundation, Oct. 2017. [Online]. Available:
       https://www.nfpa.org/News-and-Research/Data-research-and-tools/Detection-and-
       Signaling/Smoke-Detector-Spacing-for-High-Ceiling-Spaces

[10]   R. Chagger and Building Research Establishment, *Smoke detection in high ceiling
       spaces*. Watford: IHS BRE Press, 2012.

[11]   W. D. Davis and K. A. Notarianni, "NASA Fire Detection Study - NISTIR 5798,"
       NIST, Mar. 1996. Accessed: Feb. 08, 2022. [Online]. Available:
       https://nvlpubs.nist.gov/nistpubs/Legacy/IR/nistir5798.pdf

[12]   "Smoke detection in buildings with high ceilings."
       https://5dok.org/document/lq5313wz-smoke-detection-in-buildings-with-high-
       ceilings.html (accessed Feb. 08, 2022).

[13]   W. Kuffner and G. Hadjisophocleous, "Method of Determining Smoke Detector
       Spacing in High Ceiling Applications," *Fire Technology*, vol. 50, pp. 1–22, May
       2010, doi: 10.1007/s10694-010-0141-5.

[14] J. A. Milke, F. W. Mowrer, and P. Gandhi, "Validation of a Smoke Detection
Performance Prediction Methodology Volume 3. Evaluation of Smoke Detector
Performance," p. 73.

[15] W. D. Davis, K. A. Notarianni, and K. B. McGrattan, "Comparison of Fire Model
Predictions With Experiments Conducted in a Hangar With a 15 Meter Ceiling.,"
Dec. 1996, Accessed: Feb. 08, 2022. [Online]. Available:
https://www.nist.gov/publications/comparison-fire-model-predictions-experiments-
conducted-hangar-15-meter-ceiling

[16] J. D. Averill *et al.*, "Performance of home smoke alarms :: analysis of the response
of several available technologies in residential fire setting," National Bureau of
Standards, Gaithersburg, MD, NBS TN 1455, 2007. doi: 10.6028/NIST.TN.1455.

[17] T. Cleary and G. Taylor, "Evaluation of Empirical Evidence Against Zone Models
for Smoke Detector Activation Prediction," *Fire Technol*, Nov. 2020, doi:
10.1007/s10694-020-01061-2.

[18] R. D. Peacock, P. A. Reneke, and G. P. Forney, "CFAST – Consolidated Model of
Fire Growth and Smoke Transport (Version 7) Volume 2: User's Guide," National
Institute of Standards and Technology, Dec. 2015. doi: 10.6028/NIST.TN.1889v2.

[19] "UL Standard for Safety for Smoke Detectors for Fire Alarm Systems, UL 268."
2016 Underwriters Laboratories Inc, Jan. 11, 2016. [Online]. Available:
https://standardscatalog.ul.com/ProductDetail.aspx?productId=UL268

[20] K. B. McGrattan and G. P. Forney, "Fire dynamics simulator (version 4) :: user's guide," National Institute of Standards and Technology, Gaithersburg, MD, NIST SP 1019, 2004. doi: 10.6028/NIST.SP.1019.

[21] T. Cleary, A. Mensch, and G. Taylor, "Validation Study for Smoke Detector Response in FDS," p. 8. [Online]. Available: https://www.nfpa.org/2021aubesupdetpapers

[22] C. L. Beyler and P. J. DiNenno, "Letter to the editor-Fire Technology," Aug. 1991.

[23] M. H. Salley and N. Iqbal, "NUREG-1805 'Fire Dynamics Tools (FDTs): Quantitative Fire Hazard Analysis Methods for the U.S. Nuclear Regulatory Commission Fire Protection Inspection Program' (Final Report).," Division of System Safety and Analysis Office of Nuclear Reactor Regulation U.S. Nuclear Regulatory Commission, Washington, DC, Dec. 2004.

[24] R. L. Alpert, "Calculation of response time of ceiling-mounted fire detectors," *Fire Technol*, vol. 8, no. 3, pp. 181–195, Aug. 1972, doi: 10.1007/BF02590543.

[25] R. W. Bukowski and J. D. Averill, "Methods for Predicting Smoke Detector Activation.," National Inst. of Standards and Technology (BFRL), Gaithersburg, MD. Fire Safety Engineering Div., PB99148140, 1998. Accessed: Jan. 17, 2022. [Online]. Available: https://ntrl.ntis.gov/NTRL/dashboard/searchResults/titleDetail/PB99148140.xhtml

[26] R. D. Peacock, P. A. Reneke, and G. P. Forney, "CFAST – Consolidated Model of Fire Growth and Smoke Transport (Version 7) Volume 1: Technical Reference

Guide," National Institute of Standards and Technology, Dec. 2015. doi: 10.6028/NIST.TN.1889v1.

[27] E. K. Budnick, D. D. Evans, and H. Nelson, "Simplified Fire Growth Calculations," vol. 18th Edition, no. NPFA FPH 1897, p. 11/97-107, Dec. 1997.

[28] F. W. Mowrer, "Lag times associated with fire detection and suppression," *Fire Technol*, vol. 26, no. 3, pp. 244–265, Aug. 1990, doi: 10.1007/BF01040111.

[29] J. A. Milke, "Smoke management for covered malls and atria," *Fire Technol*, vol. 26, no. 3, pp. 223–243, Aug. 1990, doi: 10.1007/BF01040110.

[30] "NFPA 92B: Standard for Smoke Management Systems in Malls, Atria, and Large Spaces," 2005. https://www.nfpa.org/codes-and-standards/all-codes-and-standards/list-of-codes-and-standards/detail?code=92B&year=2005 (accessed Jan. 20, 2022).

[31] J. G. Quintiere and C. A. Wade, *SFPE Handbook of Fire Protection Engineering, chapter Compartment Fire Modeling*, Fifth. New York, NY: Springer New York, 2016. doi: 10.1007/978-1-4939-2565-0.

[32] F. W. Mowrer, *SFPE Handbook of Fire Protection Engineering, chapter Enclosure Smoke Filling and Fire-Generated Environmental Conditions*, Fifth. New York, NY: Springer New York, 2016. doi: 10.1007/978-1-4939-2565-0.

[33] J. H. Klote, *SFPE Handbook of Fire Protection Engineering, chapter Smoke Control*, Fifth. New York, NY: Springer New York, 2016. doi: 10.1007/978-1-4939-2565-0.

[34] T. G. Cleary, A. A. Chernovsky, W. L. Grosshandler, and M. D. Anderson, "Particulate Entry Lag in Spot-Type Smoke Detectors," *International Association for Fire Safety Science*, vol. Fire Safety Science – Proceedings of the Sixth International Symposium, pp. 779–790, Jul. 1999.

[35] R. E. Walpole, R. H. Myers, S. L. Myers, and K. Ye, *Probability & statistics for engineers & scientists: MyStatLab update*. 2017. Accessed: Jan. 11, 2022. [Online]. Available: http://www.myilibrary.com?id=947904

[36] R. D. Peacock, S. Davis, and B. T. Lee, "Experimental Data Set for the Accuracy Assessment of Room Fire Models (NBSIR 88-3752)," Apr. 1988, Accessed: Jan. 26, 2022. [Online]. Available: https://www.nist.gov/publications/experimental-data-set-accuracy-assessment-room-fire-models-nbsir-88-3752

[37] C. L. Beyler, *SFPE Handbook of Fire Protection Engineering, chapter Fire Hazard Calculations for Large, Open Hydrocarbon Fires*. New York, NY: Springer New York, 2016. doi: 10.1007/978-1-4939-2565-0.

[38] T. A. Brzustowski and E. C. Sommer, *Predicting Radiant Heating from Flares*. 1973. [Online]. Available: https://books.google.com/books?id=crNAQwAACAAJ

[39] D. D. Drysdale, *SFPE Handbook of Fire Protection Engineering, chapter Ignition of Liquids*. New York, NY: Springer New York, 2016. doi: 10.1007/978-1-4939-2565-0.